ADVANCED STEEL CONSTRUCTION

An International Journal

Volume 3 Number 3

September 2007

CONTENTS

Technical Papers

Design Method for Light-Gauge Steel Shear Walls Sheathed with Flat Steel Plates
L.A. Fülöp and I. Hakola

FE Simulation of Space Steel Frames in Fire with Warping Effect
Zhan-Fei Huang and Kang-Hai Tan

Numerical Simulation of Hollow and Concrete-Filled Steel Columns
Shengbin Gao and Hanbin Ge

Dynamic Stability Analysis of Beam String Structures under Earthquake Loads
Qinghua Han, Chenyin Ma, Jingyu Zhang

MINLP Optimization of Steel Frames
Uroš Klanšek, Tomaž Žula, Zdravko Kravanja and Stojan Kravanja

ISSN 1816-112X

Website: *http://www.hkisc.org/*

ADVANCED STEEL CONSTRUCTION

VOL.3, NO.3 (2007)

ADVANCED STEEL CONSTRUCTION

an International Journal

ISSN 1816-112X

Volume 3 Number 3 *September 2007*

ISSN 1816-112X

Advanced Steel Construction
an international journal

Cover: Full scale test for a pre-tensioned truss system under wind pressure. Courtesy of RED Consultant Limited

General Information
Advanced Steel Construction, an international journal

Aims and scope

The International Journal of Advanced Steel Construction provides a platform for the publication and rapid dissemination of original and up-to-date research and technological developments in steel construction, design and analysis. Scope of research papers published in this journal includes but is not limited to theoretical and experimental research on elements, assemblages, systems, material, design philosophy and codification, standards, fabrication, projects of innovative nature and computer techniques. The journal is specifically tailored to channel the exchange of technological know-how between researchers and practitioners. Contributions from all aspects related to the recent developments of advanced steel construction are welcome.

Instructions to authors

Submission of the manuscript. Authors may submit three double-spaced hard copies of manuscripts together with an electronic copy on a diskette or cd-rom in an editable format (MS Word is preferred). Manuscripts should be submitted to the regional editors as follows for arrangement of review.

Asian Pacific , African and organizing editor :	Professor S.L. Chan
American editor :	Professor W.F. Chen
European editor :	Professor R. Zandonini

All manuscripts submitted to the journal are highly recommended to accompany with a list of four potential reviewers suggested by the author(s). This list should include the complete name, address, telephone and fax numbers, email address, and at least five keywords that identify the expertise of each reviewer. This scheme will improve the process of review.

Style of manuscript

General. Author(s) should provide full postal and email addresses and fax number for correspondence. The manuscript including abstract, keywords, references, figures and tables should be in English with pages numbered and typed with double line spacing on single side of A4 or letter-sized paper. The front page of the article should contain:

a) a short title (reflecting the content of the paper);
b) all the name(s) and postal and email addresses of author(s) specifying the author to whom correspondence and proofs should be sent;
c) an abstract of 100-200 words; and
d) 5 to 8 keywords.

The paper must contain an introduction and a conclusion. The length of paper should not exceed 25 journal pages (approximately 15,000 words equivalents).

Tables and figures. Tables and figures including photographs should be typed, numbered consecutively in Arabic numerals and with short titles. They should be referred in the text as Figure 1, Table 2, etc. Originally drawn figures and photographs should be provided in a form suitable for photographic reproduction and reduction in the journal.

Mathematical expressions and units. The Systeme Internationale (SI) should be followed whenever possible. The numbers identifying the displayed mathematical expression should be referred to in the text as Eq. (1), Eq. (2).

References. References to published literature should be referred in the text, in the order of citation with Arabic numerals, by the last name(s) of the author(s) (e.g. Zandonini and Zanon [3]) or if more than three authors (e.g. Zandonini et al. [4]). References should be in English with occasional allowance of 1-2 exceptional references in local languages and reflect the current state-of-technology. Journal titles should be abbreviated in the style of the Word List of Scientific Periodicals. References should be cited in the following style [1, 2, 3].

Journal: [1] Chen, W.F. and Kishi, N., "Semi-rigid Steel Beam-to-column Connections, Data Base and Modelling", Journal of Structural Engineering, ASCE, 1989, Vol. 115, No. 1, pp. 105-119.

Book: [2] Chan, S.L. and Chui, P.P.T., "Non-linear Static and Cyclic Analysis of Semi-rigid Steel Frames", Elsevier Science, 2000.

Proceedings: [3] Zandonini, R. and Zanon, P., "Experimental Analysis of Steel Beams with Semi-rigid Joints", Proceedings of International Conference on Advances in Steel Structures, Hong Kong, 1996, Vol. 1, pp. 356-364.

Proofs. Proof will be sent to the corresponding author to correct any typesetting errors. Alternations to the original manuscript at this stage will not be accepted. Proofs should be returned within 48 hours of receipt by Express Mail, Fax or Email.

Copyright. Submission of an article to "Advanced Steel Construction" implies that it presents the original and unpublished work, and not under consideration for publication nor published elsewhere. On acceptance of a manuscript submitted, the copyright thereof is transferred to the publisher by the Transfer of Copyright Agreement and upon the acceptance of publication for the papers, the corresponding author must sign the form for Transfer of Copyright.

Permission. Quoting from this journal is granted provided that the customary acknowledgement is given to the source.

Page charge and Reprints. There will be no page charges if the length of paper is within the limit of 25 journal pages. A total of 30 free offprints will be supplied free of charge to the corresponding author. Purchasing orders for additional offprints can be made on order forms which will be sent to the authors. These instructions can be obtained at the Hong Kong Institute of Steel Construction, Journal website: http://www.hkisc.org

The International Journal of Advanced Steel Construction is published quarterly by non-profit making learnt society, The Hong Kong Institute of Steel Construction, c/o Department of Civil & Structural Engineering, The Hong Kong Polytechnic University, Hung Hom, Kowloon, Hong Kong.

Subscription inquiries and change of address. Address all subscription inquiries and correspondence to Member Records, IJASC. Notify an address change as soon as possible. All communications should include both old and new addresses with zip codes and be accompanied by a mailing label from a recent issue. Allow six weeks for all changes to become effective.

The Hong Kong Institute of Steel Construction
HKISC
c/o Department of Civil and Structural Engineering,
The Hong Kong Polytechnic University,
Hunghom, Kowloon, Hong Kong, China.
Tel: 852- 2766 6047 Fax: 852- 2334 6389
Email: *ceslchan@polyu.edu.hk* Website: *http://www.hkisc.org/*
ISSN 1816-112X

ISSN 1816-112X

Advanced Steel Construction
an international journal

VOLUME 3 NUMBER 3 SEPTEMBER 2007

Technical Papers

Design Method for Light-Gauge Steel Shear Walls Sheathed with Flat Steel Plates 628
L.A. Fülöp and I. Hakola

FE Simulation of Space Steel Frames in Fire with Warping Effect 652
Zhan-Fei Huang and Kang-Hai Tan

Numerical Simulation of Hollow and Concrete-Filled Steel Columns 668
Shengbin Gao and Hanbin Ge

Dynamic Stability Analysis of Beam String Structures under Earthquake Loads 679
Qinghua Han, Chenyin Ma, Jingyu Zhang

MINLP Optimization of Steel Frames 689
Uroš Klanšek, Tomaž Žula, Zdravko Kravanja and Stojan Kravanja

DESIGN METHOD FOR LIGHT-GAUGE STEEL SHEAR WALLS SHEATHED WITH FLAT STEEL PLATES

L.A. Fülöp[1,*] and I. Hakola

[1]*VTT - Technical Research Centre of Finland*
P.O. Box 1000, FI-02044 VTT
Tel. +358 20 722 111; Fax +358 20 722 7001
**(Corresponding author: E-mail: Ludovic.Fulop@vtt.fi ; Ilkka.Hakola@vtt.fi)*

Received: 8 January 2007; Revised: 19 March 2007; Accepted: 28 March 2007

ABSTRACT: Sheathed Light-Gauge Steel (LGS) shear walls are often used in structures as load bearing elements against wind and earthquake actions. The design of walls is often complicated by the lack of analytical methods for the evaluation of the strength and rigidity. Design by testing is a possibility if large numbers of identical walls are used; but in the usual case designers are limited by economic consideration to use configurations which were already tested. These limitations greatly reduce the potential of using LGS shear walls in practical applications. In this paper an analytical design procedure is presented for LGS shear walls sheathed with flat thin steel plates. The procedure, developed for the evaluation of the shear strength and rigidity of the walls, takes into account the fixing of the steel plate to the skeleton. The method is validated using both Finite Element Modelling (FEM) and experiments; comparisons show good accuracy when it comes to the evaluation of strength, but not satisfactory for the rigidity.

Keywords: Light-gauge steel, shear walls, lateral loading, design method, tension-field action

1. INTRODUCTION

In LGS structures the wall sheathing often contributes to the load bearing of the system. One of the sheathing solutions, used for such walls, is based on flat steel in which cases a thin steel sheath (t=0.6-1.2mm) is attached to one or both sides of the skeleton of the wall. The method can be used both in multi-storey applications and single family houses (Figure 1).

Figure 1. NORDICON Wall Elements with Flat Steel Sheath (As Oy - Arabian Kotiranta; Builder: Sato Rakennuttajat Oy; Architect: Ark Oy Kahri & Co.; Wall: Ruukki)

One of the particularly interesting applications, in housing, is the use of thin steel cassette sections, Davies [1]. Even if the cassette walls are slightly different from the classical sheathed solutions, the load bearing mechanism is similar. In the case of cassette walls, the connected flanges of the cassettes form the "stud", while the large webs act as the sheathing (Figure 2).

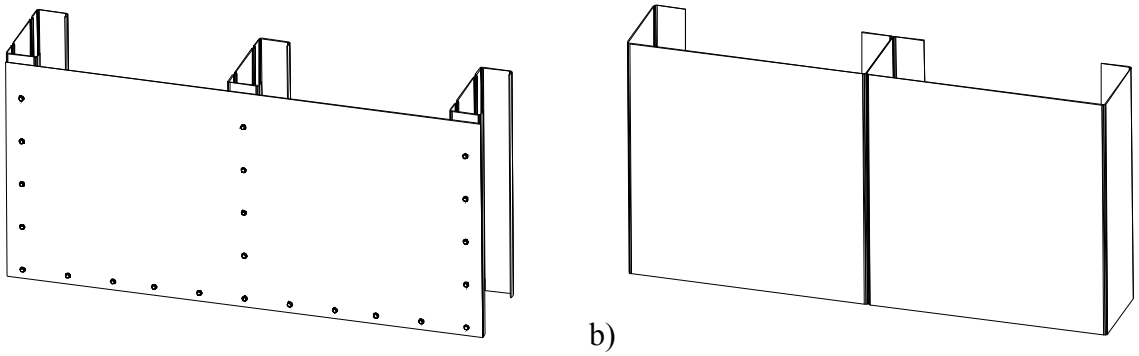

a) b)

Figure 2. (a) Steel Skeleton Walls with Flat Steel Sheathing and (b) Cassette Section Walls

Obviously, the sheathing provides a certain amount of stiffening for the wall, especially if the wall is loaded in shear. Such loading typically occurs in the wall when the structure is subjected to wind or earthquake action. In order to design a structure for these actions, the evaluation of the lateral load bearing capacity is required, with a significant part of the strength supplied by the sheathing. The main limitation in the design process comes from the lack of suitable analytical procedures for the calculation of the capacity and rigidity of the sheathed walls. Design assisted by testing is one possibility, but it is usually expensive and impractical, due to the diversity of configurations and dimensions of walls in everyday design.

In this paper an analytical design procedure is presented for the evaluation of the strength and rigidity of shear walls sheathed with flat steel plates. The procedure takes into account the strength and the rigidity of the connections between the plate and the frame of the wall, and proved to be sufficiently accurate for the evaluation of the strength of the walls, but less reliable for the evaluation of the stiffness. Several particularities of the behaviour of LGS shear walls, useful during the design process, are highlighted and critically discussed.

2. HISTORICAL DEVELOPMENT OF THE STEEL SHEAR WALLS

To some extent, the calculation methods for classical steel shear walls, used in heavy frame structures, can also be adopted for LGS walls. However, important differences also exist between the two typologies. These differences, and their consequences on the behaviour of the walls, are discussed in this section.

Flat steel plates with larger thickness ($t \approx 5$-10mm) are sometimes provided in bays of multi-storey steel frame structures in order to improve the earthquake performance. These shear plates increase the lateral rigidity and load bearing capacity of the structure, and also contribute to the energy dissipation during earthquake. [2].

Initially, in these classical applications, the intention was to avoid the elastic buckling of the plates. Until the 1980s, the design limit-state of steel plate shear walls, in North-America, was the out-of-plane buckling of the plate, resulting in the use of very robust walls [3]. Unquestionably, elastic buckling offers inferior performance as compared to plastic failure of the steel plate, especially in terms of dissipative capacity.

Plastic yielding of the plate was facilitated in practical applications by providing out-of-plane stiffeners. Besides the out-of-plane stiffeners, two other solutions were proposed with the aim of facilitating plastic failure instead of elastic buckling. The use of low-yield steel, as base material for the plates, was introduced in Japan [4]; and pure aluminium shear walls were proposed by DeMatteis [5]. In both cases the goal is to exploit the low yield capacity of the material in order to facilitate shear yielding.

Stiffened shear walls were used in most of the early applications in Japan and the USA [6], but this method became less popular as it requires large amount of labour for the welding of the stiffeners. An increasing number of recent applications, both in the USA and Canada, use non-stiffened steel plates [6]. In case of non-stiffened walls, elastic buckling is allowed to take place, and the load resisting mechanism is based on the development of tensile stresses in the already buckled plate, mechanism often referred as tension-field action.

The first tension-field theory concerning the post-buckling strength of shear panels was developed by Wagner [7]. Later theories incorporated the bending effect of the marginal beams and shear stresses in the plate [8]. A plastic design method for the classical steel shear walls was presented, for single-storey and multi-story frames, by Berman & Bruneau [3].

More recently, Elgaaly [2] proposed an analytical model for the calculation of the capacity of shear walls with both welded and bolted thin steel plates. The model is based on the concept of replacing the sheathing with a series of equivalent trusses. For the case of bolted steel plates Elgaaly [2] suggested, that the shear wall should be designed so that the yielding of the plate, and not the capacity of the end connections, should control the failure of the shear wall. It will be shown later in this paper, that this condition can hardly, if at all, be fulfilled with LGS shear walls.

In the case of LGS walls, it is also not possible to avoid the elastic buckling, due to the extreme thinness of the plate. If we would include LGS shear plates in the slenderness chart presented by Astaneh-Asl [6], they would form a group of “extremely slender” plates with very large width-to-thickness ratios (L/t≈600-1200, Figure 3). Therefore, the use of stiffeners or low-yield material is not feasible, and the storey shear has to be transmitted by the tension-field action only.

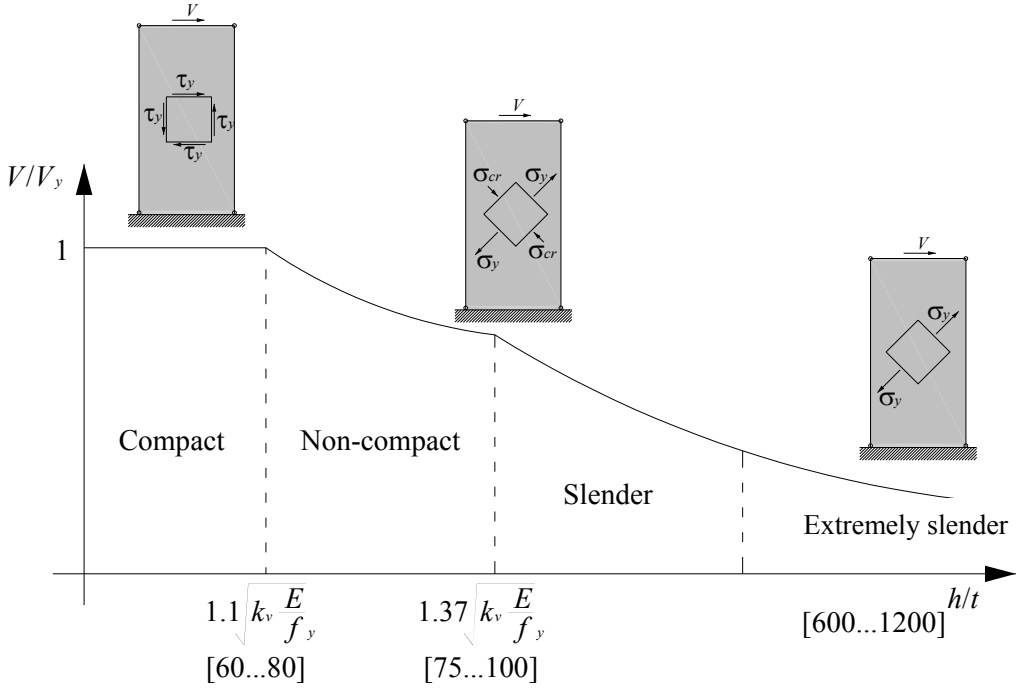

Figure 3. Behaviour of Steel Shear Walls (Adapted from Astaneh-Asl [6])

The other difference between classical and LGS walls, is that in the heavy steel applications the plates are usually continuously connected to the frame, most often by welding. But welding is rarely used in LGS structures, because of the damage it causes to the zinc coating of the elements, and the connection of the plate is usually in points, by screws or pins.

3. CALCULATION METHOD FOR WALLS WITH STEEL PLATES CONTINUOUSLY CONNECTED TO THE FRAME

3.1 Basic Assumptions

The calculation of shear walls, covered by thin steel sheathing, is based on the assumption that the shear is resisted by the tension-field action in the plate (Figure 3). Other assumptions include:

(i) The skeleton of the wall is pinned. This implies that the connections between studs and tracks do not transmit bending, and the frame effect of the wall skeleton is negligible.

(ii) The bending rigidity of studs and tracks is large, as compared to the rigidity of the thin plate. Therefore, the studs and tracks do not bend significantly during the deformation of the wall. This assumption may be doubtful when it comes to relatively long studs.

In the first step of the analysis, the wall panel is divided along the length into cells, which are sheathed with a single steel plate (Figure 4). If the cells are identical, they act in parallel and the shear loading of the wall is transmitted equally to each cell. Since the capacity and rigidity of the cells can be summed, the calculation method for these values has been developed for one cell.

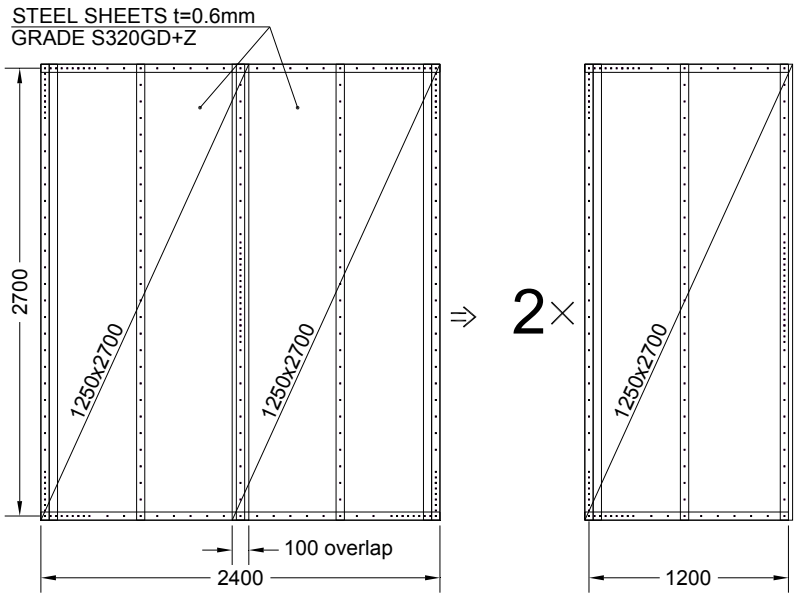

Figure 4. Division of Wall Panels into “Cells”

Buckling of the plate occurs in the very early stage, and at small forces, due to the very large width-to-thickness ratios ($L/t \approx 600$-1200). However, the buckling force does not represent the ultimate capacity of the wall, because the post-buckling path is stable, and the load can substantially increase due to tension-field action. An oblique tension stress pattern develops in the plate resembling a pattern of oblique strips subjected to tension (Figure 5.a). These strips yield gradually, leading to the loss of load bearing capacity of the cell, and of the entire wall.

For analytical purposes, the cells can be divided into finite strips running obliquely and forming an angle α with the vertical. The position of the current strip is defined by its distance from the corner of the cell (x), while its width is dx (Figure 5.a). The load bearing capacity of the cell is calculated by supposing that the only mechanism to resist the loading is the strips subjected to stretching.

As presented in Figure 5.a, the strips can have different characteristics (e.g. length, axial stiffness), depending on their position in the plate. Based on the geometry, several zones of strips can be defined. As shown later, the behaviour of strips in the same zone can be described by identical formulae. In the elastic stage, the structural scheme of this multi-strip model is staticallyindeterminate, but when all strips yielded classical plastic analysis apply. In the yielding stage the forces in every strip are known, and equal to the yield resistance of the strip.

Finite Element (FE) analyses and experimental evidence suggest that independent yield patterns develop for each cell of a wall, thus substantiating the assumption that the cells in a wall act independently.

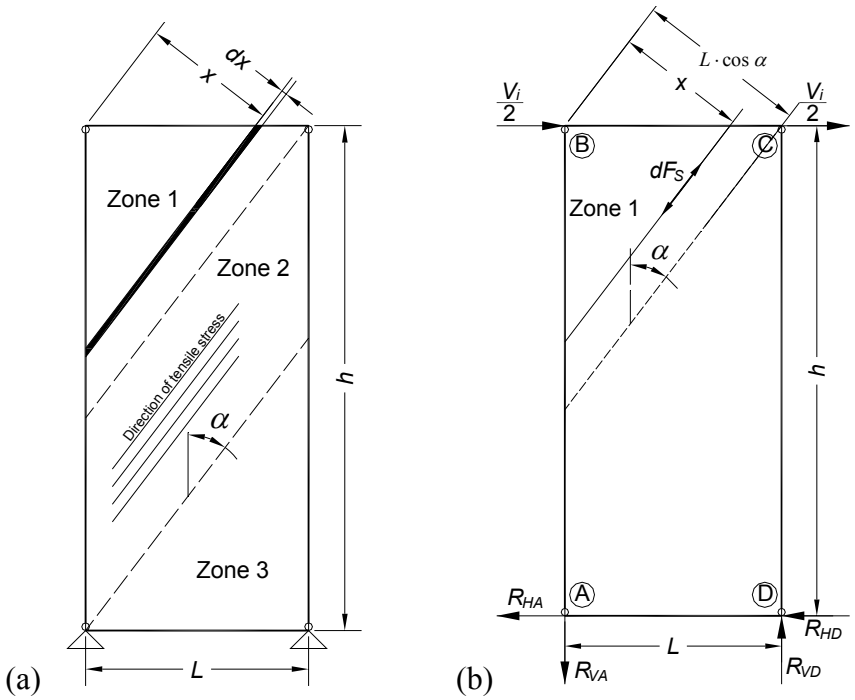

Figure 5. (a) Differential strips (dx) and Zones, (b) forces in strips from horizontal loads (V_i)

3.2 Evaluation of the Load Bearing Capacity

The relationship between the tensile force in the strip (dF_s) and the horizontal force (V_i) that causes it (Figure 5.b), can be written for strips in Zone 1 as:

$$V_i = \frac{dF_S \cdot x}{h} \tag{1}$$

If dF_S is interpreted as the resistance of the strip, then V_i will represent the contribution of the strip to the capacity of the cell. The total load bearing capacity contribution of strips in Zone 1 (V_i^{Zone1}) can be calculated by summing up the contributions of individual strips in the entire Zone 1:

$$V_i^{Zone1} = \int_{x=0}^{L\cdot\cos\alpha} \frac{dF_S \cdot x}{h} \tag{2}$$

Similarly the load bearing contributions of all strips in Zone 2 (V_i^{Zone2}) and Zone 3 (V_i^{Zone3}) are:

$$V_i^{Zone2} = \int_{x=L\cdot\cos\alpha}^{h\cdot\sin\alpha} \frac{dF_S \cdot L \cdot \cos\alpha}{h} \tag{3}$$

$$V_i^{Zone3} = \int_{x=h\cdot\sin\alpha}^{h\cdot\sin\alpha+L\cdot\cos\alpha} \frac{dF_S \cdot \left[(h\cdot\sin\alpha + L\cdot\cos\alpha) - x\right]}{h} \tag{4}$$

By simplifying Eq. (4) it can be shown that the contributions of strips in Zone 1 and Zone 3 are equal. Intuitively it can also be seen that the two zones are identical from the point of view of the load bearing. Therefore:

$$V_i^{Zone3} = \int_{x=0}^{L\cdot\cos\alpha} \frac{dF_S \cdot x}{h} = V_i^{Zone1} \tag{5}$$

The total horizontal load bearing capacity of the cell (V), in the stage when all strips yield, is the sum of the contributions of the three zones:

$$V = V_i^{Zone1} + V_i^{Zone2} + V_i^{Zone3} = 2\cdot V_i^{Zone1} + V_i^{Zone2} \tag{6}$$

As the yield resistance of all strips is equal to $dF_S = dA \cdot f_y = t \cdot dx \cdot f_y$, the total capacity expressed in Eq.6 can be calculated as:

$$\begin{aligned} V &= 2\cdot \int_{x=0}^{L\cdot\cos\alpha} \frac{dF_S \cdot x}{h} + \int_{x=L\cdot\cos\alpha}^{h\cdot\sin\alpha} \frac{dF_S \cdot L \cdot \cos\alpha}{h} = \\ &= 2\cdot \frac{t\cdot f_y}{h} \int_{x=0}^{L\cdot\cos\alpha} x\cdot dx + \frac{t\cdot f_y \cdot L\cdot\cos\alpha}{h} \int_{x=L\cdot\cos\alpha}^{h\cdot\sin\alpha} dx = \frac{1}{2}\cdot t\cdot f_y \cdot L\cdot\sin(2\alpha) \end{aligned} \tag{7}$$

The background of this expression was presented in more detail by Berman and Bruneau [3] for classical steel shear walls used in multi-storey frames.

3.3 Evaluation of the Rigidity

Based on the assumption that the frame is pinned, and made of very rigid bars that do not bend, it can be noticed that the deformed shape of the cell is geometrically determined (Figure 6). This means that the lengthening and the corresponding force in each strip can be calculated for any horizontal displacement of the top. Therefore, the rigidity of the cell can be evaluated.

A deformation Δ at the top of the cell causes the points 1 and 2 to displace with Δ_1 and Δ_2 (Figure 6). If the deformations are small, it can be accepted that the two points have only horizontal displacements.

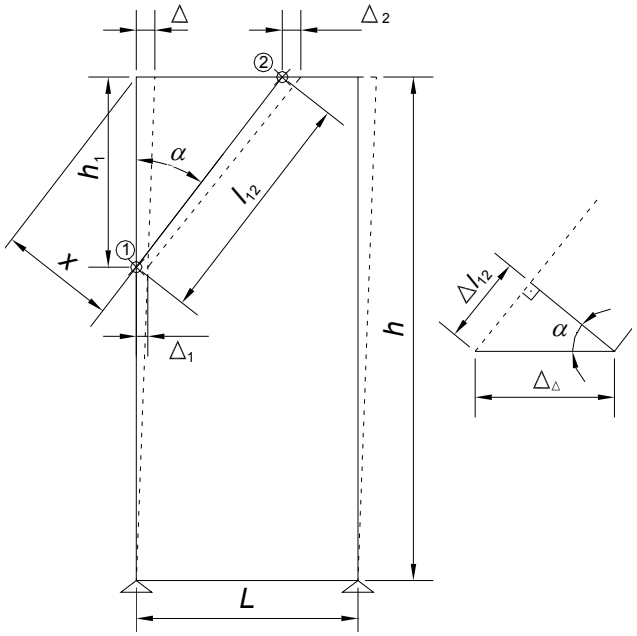

Figure 6. Strip in the Deformed Stage of the Cell (Zone 1)

The length ($l_{12,Z1}$) of a strip in Zone 1, at a distance x from the corner, is:

$$l_{12,Z1} = \frac{x}{\sin\alpha \cdot \cos\alpha} \tag{8}$$

The lengthening of the strip ($\Delta l_{12,Z1}$) corresponding to the top displacement of Δ can be expressed as:

$$\Delta l_{12,Z1} = \frac{\Delta \cdot x}{h} \tag{9}$$

The deformations $\Delta l_{12,Z1}$ and Δ can be expressed as a function of the strip force (dF_S) and the contribution of dF_S to the load bearing of the wall (V_i):

$$\frac{dF_S}{k_{s,Z1}} = \frac{x}{h} \cdot \frac{V_i}{dk_t^{Z1}} \tag{10}$$

Where $k_{s,Z1}$ is the axial rigidity of the current strip, and dk_t^{Z1} is the strips contribution to the shear rigidity of the cell.

Also, by using the formula of V_i (Eq. 1), the rigidity contribution of one strip in Zone 1 to the horizontal rigidity of the cell (dk_t^{Z1}) can be written:

$$dk_t^{Z1} = \frac{x^2}{h^2} \cdot k_{s,Z1} \tag{11}$$

Similarly, the length of a strip in Zone 2 ($l_{12,Z2}$) is:

$$l_{12,Z2} = \frac{L}{\sin\alpha} \tag{12}$$

The elongation of a strip in Zone 2 ($\Delta l_{12,Z2}$):

$$\Delta l_{12,Z2} = \Delta \cdot \frac{L \cdot \cos\alpha}{h} \tag{13}$$

And the contribution of a strip in Zone 2 (dk_t^{Z2}) to the rigidity of the wall reads:

$$dk_t^{Z2} = \frac{L^2 \cdot \cos^2\alpha}{h^2} \cdot k_{s,Z2} \tag{14}$$

The strips in Zone 3 are similar to the ones in Zone 1, their contribution to the rigidity of the cell being identical to the ones in Zone 1.

The combined rigidity contribution of the strips in Zone 1 to the rigidity of the wall (K^{Zone1}) is the summation of the rigidity contribution of each strip:

$$K^{Zone1} = \int_0^{L\cdot\cos\alpha} dk_t^{Z1} = \int_0^{L\cdot\cos\alpha} \frac{x^2}{h^2} \cdot k_{s,Z1} = \frac{E \cdot t \cdot L^2 \cdot \sin\alpha \cdot \cos^3\alpha}{2 \cdot h^2} \tag{15}$$

Where the rigidity of strips in Zone 1 ($k_{s,Z1}$) is:

$$k_{s,Z1} = \left(\frac{E \cdot A}{l_{12,Z1}}\right) = E \cdot t \cdot dx \cdot \frac{\sin\alpha \cdot \cos\alpha}{x} \tag{16}$$

Similarly for Zone 2:

$$\begin{aligned} K^{Zone2} &= \int_{L\cdot\cos\alpha}^{h\cdot\sin\alpha} dk_t^{Z2} = \int_{L\cdot\cos\alpha}^{h\cdot\sin\alpha} \frac{L^2 \cdot \cos^2\alpha}{h^2} \cdot k_{s,Z2} = \\ &= \frac{E \cdot t \cdot L \cdot \sin\alpha \cdot \cos^2\alpha}{h^2} \cdot \left(h \cdot \sin\alpha - L \cdot \cos\alpha\right) \end{aligned} \tag{17}$$

If the rigidity contributions of the strips in Zones 1, 2 and 3 are summed up, the total rigidity of the cell (K_{TOT}) is obtained as follows:

$$K_{TOT} = 2 \cdot K^{Zone1} + K^{Zone2} = \frac{1}{4} \cdot \frac{E \cdot t \cdot L}{h} \sin^2\left(2 \cdot \alpha\right) \tag{18}$$

3.4 Characteristics of the Plate Yielding

If we suppose that the strips behave in an elastic-plastic manner, it can be shown that all strips in the cell yield simultaneously at a lateral displacement of the wall Δ_y.

For strips in Zone 1 (and Zone 3) the yield elongation of any strip ($\Delta l_{12y,Z1}$) is (using Eq. 8):

$$\Delta l_{12y,Z1} = \varepsilon_y \cdot l_{12,Z1} = \frac{f_y}{E} \cdot \frac{x}{\sin\alpha \cdot \cos\alpha} \tag{19}$$

For the strips in Zone 2, $\Delta l_{12y,Z1}$ is (from Eq. 12):

$$\Delta l_{12y,Z2} = \varepsilon_y \cdot l_{12,Z2} = \frac{f_y}{E} \cdot \frac{L}{\sin\alpha} \tag{20}$$

Both of these elongations correspond to a top displacement that can be calculated by expressing Δ from Eq. (9) and (13), and by substituting into them $\Delta l_{12y,Z1}$ and $\Delta l_{12y,Z2}$ from Eq. (19) and (20), respectively:

$$\Delta_y = \left\{ \begin{array}{l} \frac{h}{x} \cdot \Delta l_{12y,Z1} \\ \frac{h}{L \cdot \cos\alpha} \cdot \Delta l_{12y,Z2} \end{array} \right\} = \frac{f_y \cdot h}{E} \cdot \frac{1}{\sin\alpha \cdot \cos\alpha} \tag{21}$$

Therefore, strips yield at the same top horizontal displacement Δ_y, given by Eq. (21), regardless of their position in the cell. Even the yield displacement of the variable length strips in Zone 1 does not depend on the position of the strip in the cell. Interesting to note that Δ_y is linearly dependent on the height of the cell (h), but not dependent on L.

In conclusion, Eq. (7), (18) and (21) express the load bearing capacity (V), the rigidity (K_{TOT}) and the yield displacement (Δ_y) of the wall-cell. The wall-cell, modelled with the strip model, has elastic-plastic behaviour, provided that the strips have elastic-plastic behaviour; and only two of the three equations are independent, while the third can always be expressed from the other two.

3.5 Evaluation of the Inclination Angle of the Strips (α)

As it can be observed in Eq. (7) and (18), in order to calculate the capacity and rigidity of a cell, one should previously determine the inclination of the strips α (Figure 5). Based on FE modelling, corresponding to usual dimensions of the walls, in this paper a proposal is made for the empirical evaluation of α.

For the sake of simplicity Elgaaly [2] suggested that the angle should be taken as α=45°, regardless of the dimensions of the wall. However, it can be observed that the use of α=45° in Eq. (7) leads to a maximisation of the expression and to an unsafe over-estimation of the design capacity.

On the other hand, as early as in Wagner's [7] work a formulation was presented for the evaluation of α, based on the minimisation of the strain energy accumulated during the deformation. The formula takes into account the strain energy due to the tension-field in the plate and due to the axial force in the frame members. Timler and Kulak [8] amended the formula of Wagner by including the bending effect of the frame members. They argued that the bending for members with plate on both sides (ex. intermediate studs in LGS walls) can be neglected, but for members with plate acting on one side it should be taken into account. This second case applies for marginal studs and tracks in LGS walls. Both proposals neglect the compression and shear stresses in the plate.

If the frame members are considered infinitely rigid, both under axial loading and in bending, the strain energy due to the tension-field action in the plate remains the only factor to be taken into account. In this case, the strain energy is minimum for α=45° independently of the dimensions of the plate.

However, experimental observations and preliminary FEM analyses, using rigid frame members, have shown that this is not the case. In reality α depends on the dimensions of the plate, probably due to the presence of the compression and shear stresses.

A series of FE models have been prepared for the evaluation of α, and for the verification of the capacity and the rigidity formulae (Eq. 7 & 18). The models, developed in ABAQUS 6.5, consisted of a perfectly pinned frame modelled as beams (Linear line type B31) with the thin steel plate modelled as shell (Quadratic quadrilateral type S8R).

The flatness of the plate was locally disturbed close to the midpoint, by a self-balancing pair of small out-of-plane bending moments, before applying lateral loading at the top. Then the cell was subjected to steadily increasing lateral load at the top, and the yield pattern was left to develop without further disturbance. The analysis was performed with displacement control, and the model included both geometrical and material non-linearity.

In the first stage, the h/L ratio ranged from 1.42 to 6.17 (Table 1). The behaviour of the plate material was elastic-plastic with f_y=210N/mm^2 (E=210000N/mm^2) and no limitation on the plastic strain. The thickness of the plate was t=0.6mm, the plate being continuously connected to the frame. The inclination angles, evaluated using the FE models, are summarized in Table 1.

Table 1. Cases of Cells Calculated with FEM and Analytically

Model	h	L	h/L	α_{FEM}	V(Eq.7)	K_{TOT}(Eq.18)
	mm	mm		deg	N	N/mm
2_1	1700	600	2.83	39.0	36801	10538
2_2	2200	600	3.67	34.9	35697	7662
2_3	2700	600	4.50	32.3	34202	5731
2_4	3200	600	5.33	30.3	32333	4321
2_5	3700	600	6.17	25.0	30109	3241
3_1	1700	900	1.89	39.8	55906	16213
3_2	2200	900	2.44	37.8	54611	11954
3_3	2700	900	3.00	35.6	52718	9077
3_4	3200	900	3.56	31.1	50248	6958
3_5	3700	900	4.11	27.7	47227	5316
4_1	1700	1200	1.42	42.1	75186	21992
4_2	2200	1200	1.83	40.3	73948	16439
4_3	2700	1200	2.25	37.8	71900	12663
4_4	3200	1200	2.67	34.2	69064	9858
4_5	3700	1200	3.08	30.6	65472	7662

In a second stage, further FE models were developed in order to improve the prediction for the angle. Cells with length of L=600, 900, 1200, 1600mm; width of h=1400, 1800, 2200, 2600, 3000, 3400mm, and plate thicknesses of t=0.4; 0.6; 0.8 and 1.2 have been analysed. The yield stress of f_y=350N/mm^2 has been used for the steel plate.

Based on the first set of data the following empirical formulation was proposed by Fülöp [10] for the evaluation of α:

$$\alpha_{DEG} = 45 - 0.006 \cdot (h - L) \tag{22}$$

The results of the second set of FE modelling highlighted that the thickness of the sheathing plate also influences the inclination angle. Consequently, an improved form of the equation is proposed, which includes the effect of the plate thickness:

$$\alpha_{DEG} = 45 - (0.0035 \cdot t + 0.00263) \cdot (h - L) \tag{23}$$

The reliability of Eq. 22 and 23 has been evaluated using *ER*, the average absolute value calculated from the relative error of the predictions, based on the data from the two stages of the analysis. *ER* and its standard deviation σ_{ER} are presented in Table 2. A comparison plot of the angles given by the proposed expression (Eq. 23) and the angles evaluated using the FEM is shown in Figure 7.

Table 2. Reliability of the Proposed Formula for α (Eq. 22 and 23)

Analysis stage	Plate thickness (t)	Formula	*ER* (%)	σ_{ER} (%)
1	All	Eq. 22	2.06	1.37
		Eq. 23	6.03	5.03
2	All	Eq. 23	2.66	2.62
	t=0.4mm		2.20	1.52
	t=0.6mm		1.74	7.39
	t=0.8mm		2.54	2.70
	t=1.2mm		4.16	3.55
1+2	All	Eq. 23	3.12	3.27

It can be noticed in Table 2 that, the values of the error *ER* are larger for the thicker plates (ex. t=1.2mm). This highlights the fact that, for larger thicknesses, the effect of compression and shear stresses become important, and the behaviour can be less and less accurately described by the tension strip model.

It is also notable that the angles evaluated with the first set of FE models (t=0.6mm, f_y=210N/mm^2) show good fit with Eq. 23 only for some cases (Figure 7). The difference becomes more significant as the h/L ratio increases, as it can be seen also from the larger errors *ER* and σ_{ER} (Table 2). This may point to the yield stress having an effect on α. However, in practical applications, the range of the yield stress of the plate is quite narrow and the resulting variation of the angle not significant.

It is important to note again that Eq. 23 is empirical, based on the evaluation of the angle from FEM, so its accuracy may be uncertain. However, it was judged that this accuracy is enough for the evaluation of the angle in practical cases, especially because α in the expressions for strength (Eq. 7) and stiffness (Eq. 18) is used in trigonometrical functions that reduce the variability in the vicinity of 45°.

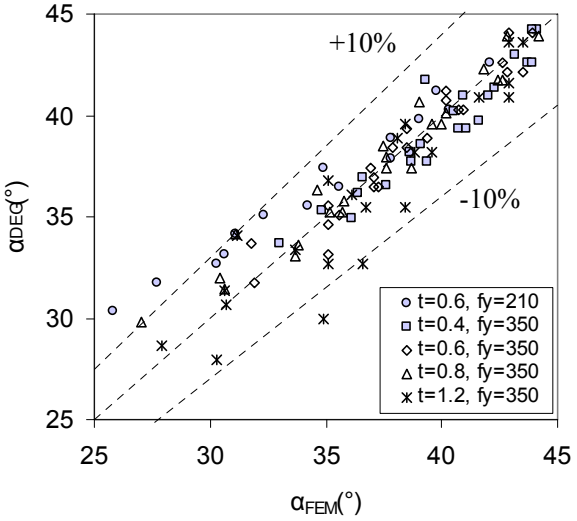

Figure 7. Comparison of the Angle α Values. FEM vs. Eq. (23)

3.6 Validation of the Strength and Rigidity Formulas

The previously presented FE models were also used for the checking of the accuracy of the analytical formulas for strength (Eq. 7) and rigidity (Eq. 18). The strength (V) and rigidity (K_{TOT}) of the cells have been calculated by using Eq. (7) and (18), for the cases corresponding to the first step of the FE study, and have been compared to the characteristic curves obtained by FEM (Table 1). For example, the nonlinear FEM characteristic curves for the cells with L=1200mm are compared in Figure 8 with the equivalent elastic-plastic line, based on the analytical rigidity and capacity from Table 1.

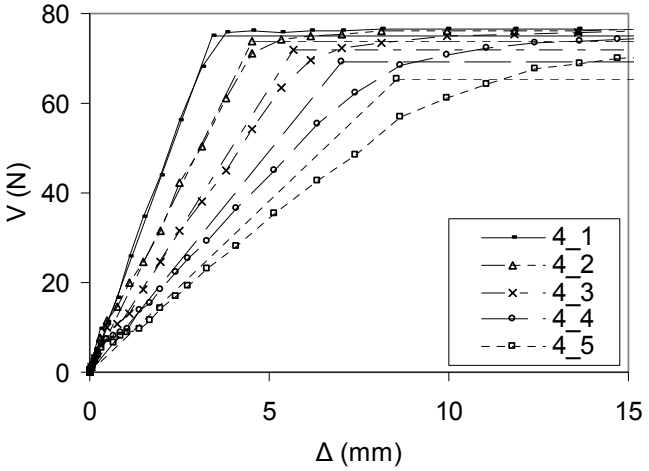

Figure 8. Analytical vs. FEM Curves for Walls with L=1200mm

A bump, corresponding to the buckling of the plate, can be observed at the beginning of each characteristic curve obtained by FEM. It can be noticed that the rigidity is higher at the very beginning of the curves; but once the plate buckles the rigidity decreases, the response stabilizes, and the rest of the curve is purely due to the tension-field action.

According to the analytical formulation (Eq. 21) all strips in the equivalent strip model should yield at the same lateral displacement Δ_y. The tendency to have a distinct yield point can also be observed on the characteristic curves obtained by FEM (Figure 8). The effect is more obvious for lower h/L ratios and tends to be attenuated for very high ones.

In some cases the prediction of the rigidity is less accurate. The results suggest that the accuracy of the strip model decreases as the h/L ratio increases, but the difference between the FEM result and Eq. (18) was not more than 20% for the cases presented in Table 1. Of course, very large h/L ratios are not feasible, and for practical applications the upper limit of $h/L \approx 5$ is suggested.

The rigidity determined by FEM is always bigger than the one calculated analytically. This is due to the fact that the analytical calculation ignores secondary load transmission by compression or shear stresses in the plate.

Overall, both V and K_{TOT} are well predicted by the analytical formulation, suggesting that the strip model is adequate to describe the behaviour of the thin plate.

4. CALCULATION METHOD FOR WALLS WITH PLATE CONNECTED TO THE FRAME IN POINTS

The expressions presented in the previous chapters are valid only as long as the yielding capacity of each individual strips is equal. This is true if the steel plate is connected to the frame continuously. However, if the plate is connected to the frame in points, several failure modes of the plate can develop, like: (1) the yielding of the plate, (2) the failure of the connections on the vertical edge, (3) net-section failure of the plate in the vertical connection line, (4) failure of the connections on the horizontal edge, and (5) net-section failure of the plate in the horizontal connection line. Each of these failure modes, and the behaviour of the components causing them, has to be taken into account in terms of both capacity and rigidity.

4.1 Evaluation of the Load Bearing Capacity

The effect of the failure modes can be incorporated in the strength calculation, by assigning, at the strip level, a characteristic resistance to each mode. The smallest of these characteristic resistances will point to the governing failure mode of the strip and will determine its tensile capacity, dF_S in Eq (1). The practical way to take into account the failure modes is to operate with stresses instead of forces. In case of each strip, an equivalent yield stress ($f_{y,ech}$) will correspond to each failure mode, and the smallest of these yield stresses will be the basis for the calculation of the strip resistance ($dF_S = \min(f_{y,ech,1}, f_{y,ech,2}...) \cdot t \cdot dx$). Similar procedure was proposed by Elgaaly [2].

All five enumerated failure modes influence the capacity in the case of strips from Zone 1 and 3; but in the case of strips in Zone 2, only the first three modes exist.

The equivalent yield stresses corresponding to each failure mode are:

(i) The yielding of the strip at force $dF_S = f_y \cdot t \cdot dx$ is the basic case. The yield stress is f_y.

(ii) The equivalent stress corresponding to the capacity of the vertically placed connectors can be expressed as:

$$f_{y,ech,s}^{V} = \frac{F_{BS}}{S \cdot t} \cdot \frac{1}{\sin\alpha} \tag{24}$$

Where, the capacity of one connector is F_{BS} and the spacing of the connectors is S (Figure 9).

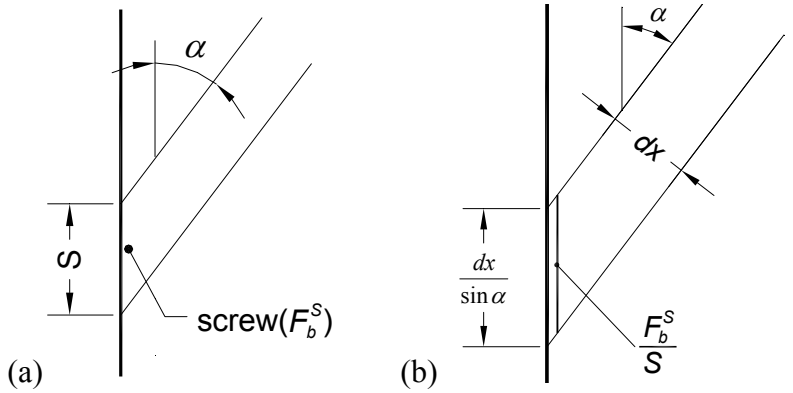

Figure 9. (a) One Screw in the Vertical Row and (b) Characteristics of the Screw Reduced to *dx*

If the connectors are self-tapping screws, the bearing capacity of a screw is $F_{BS} = \alpha_{EC3} \cdot f_u \cdot d \cdot t$, according to prEN-1993-1-3 [11], and Eq. 24 becomes:

$$f_{y,ech,s}^{V} = \frac{\alpha_{EC3} \cdot f_u \cdot d}{S \cdot \sin\alpha} \tag{25}$$

It should be noted that only bearing failure of the screws is acceptable, because this failure mode ensures ductile behaviour of the wall. Bearing failure is easily obtained as the thickness of the plate is considerably smaller than that of the profiles of the skeleton. Therefore, the joint is a typical thin-to-thick sheath connection that usually fails by bearing, if the end distances are adequate.

(iii) The equivalent stress for net-section failure in the vertical connection line, can be calculated, using the definition of net-section area given in prEN-1993-1-1 [12], when both normal and tangential stresses act on the net-section surface:

$$A_{net} = A_{gross} - t \cdot \left(n \cdot d - \sum \frac{s^2}{4 \cdot p} \right) \tag{26}$$

The net-section area expression can be adapted for the oblique strips having a width of S (Figure 10):

$$A_{net} = t \cdot (S - d) + \frac{t \cdot S}{4} \cdot \frac{\cos^2\alpha}{\sin\alpha} \tag{27}$$

Therefore, based on net-section failure, and reduced to *dx* width, the capacity of the strip (F^{V}_{net}) is:

$$F_{net}^{V} = f_u \cdot A_{net,dx}^{V} = f_u \cdot t \cdot dx \cdot \left[\frac{1 - d/S}{\sin\alpha} + \frac{t}{4} \cdot \frac{1}{\tan^2\alpha} \right] \tag{28}$$

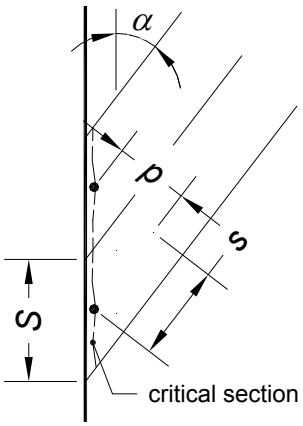

Figure 10. Net-section Failure of the Vertical Screw Line

And the corresponding equivalent yield stress reads:

$$f_{y,ech,net}^{V} = f_u \cdot \left[\frac{1-d/S}{\sin\alpha} + \frac{t}{4} \cdot \frac{1}{\tan^2\alpha} \right] \tag{29}$$

(iv) The equivalent yield stress corresponding to the capacity of horizontally placed connectors is:

$$f_{y,ech,s}^{H} = \frac{F_{BS}}{S \cdot t} \cdot \frac{1}{\cos\alpha} \tag{30}$$

Or, based on the bearing capacity of the self-tapping screws [11]:

$$f_{y,ech,s}^{H} = \frac{\alpha_{EC3} \cdot f_u \cdot d}{S \cdot \cos\alpha} \tag{31}$$

(v) The equivalent yield stress for net-section failure of the horizontal connector line reads:

$$f_{y,ech,net}^{H} = f_u \cdot \left[\frac{1-d/S}{\cos\alpha} + \frac{t}{4} \cdot \tan^2\alpha \right] \tag{32}$$

The equivalent yield-stresses for a strip in Zone 1 or 3 ($f_{y,1,3}$) and Zone 2 ($f_{y,2}$) can be expressed using Eq. (24) or (25), (29), (30) or (31) and (32), as:

$$f_{y,1,3} = \min(f_y, f_{y,ech,s}^{V}, f_{y,ech,net}^{V}, f_{y,ech,s}^{H}, f_{y,ech,net}^{H}) \tag{33}$$

$$f_{y,2} = \min(f_y, f_{y,ech,s}^{V}, f_{y,ech,net}^{V}) \tag{34}$$

The capacity of a wall-cell with steel plate, connected on every edge by using a uniform scheme of connectors, can be written in similar form as in Eq. (7), but using the equivalent yield stresses derived above:

$$V = 2 \cdot \int_{x=0}^{L \cdot \cos\alpha} \frac{dF_{S,1,3} \cdot x}{h} + \int_{x=L \cdot \cos\alpha}^{h \cdot \sin\alpha} \frac{dF_{S,2} \cdot L \cdot \cos\alpha}{h} =$$
$$= \frac{t \cdot L}{h} \cdot \left[f_{y,1,3} \cdot L \cdot \cos^2\alpha + f_{y,2} \cdot \cos\alpha \cdot (h \cdot \sin\alpha - L \cdot \cos\alpha) \right] \quad (35)$$

If the connector distance S is not constant on the perimeter of the steel plate, the already defined three zones can be further divided in sub-zones that are homogeneous from the point of view of equivalent yield stress. The capacity expression, for one cell, can be derived by summing up the individual contributions on intervals corresponding to these sub-zones, similarly to Eq. (6).

4.2 Priority of the Failure Modes

In the expression of the equivalent yield stresses (Eq. 24, 29, 30, 32), the angle α should be evaluated using Eq. 23, valid for the dimensions L≈600…1600 mm, h≈1400…3700 mm, t≈0.4…1.2mm. It can be observed that, the angle is in the range of α≈25…65°, for the walls in the above range of dimensions, corresponding to the practical configurations. This property of α can be used to limit the value of the trigonometric functions in the expressions of the yield stresses. Also, it can be shown that the bearing failure of the screws is the most probable failure mode, if self-tapping screws are used as connectors between the plate and the frame of the wall.

The five possible failure modes, discussed in the calculation procedure, resulted in five equivalent stress values: f_y and the ones from Eq. (24), (29), (30), and (32).

In order to have bearing failure of the connections before yielding of the plate, the following condition of the equivalent yield stresses should be fulfilled, based on Eq. (24) and (30):

$$\left.\begin{aligned} f_{y,ech,s}^{V} &= \frac{F_{BS}}{S \cdot t} \cdot \frac{1}{\sin\alpha} \\ f_{y,ech,s}^{H} &= \frac{F_{BS}}{S \cdot t} \cdot \frac{1}{\cos\alpha} \end{aligned}\right\} < f_y \Rightarrow F_{BS} < \begin{cases} S \cdot t \cdot f_y \cdot \sin\alpha \\ S \cdot t \cdot f_y \cdot \cos\alpha \end{cases} \quad (36)$$

The limitation 25º<α<65º leads to $\{\sin\alpha, \cos\alpha\} > 0.422$. If the connectors are self-tapping screws, we have $F_{BS} = \alpha_{EC3} \cdot d \cdot t \cdot f_u$, where $\max(\alpha_{EC3}) = 2.1$ and $f_u / f_y \approx 1.2$ [11]; and the condition from Eq. (36) becomes:

$$\alpha_{EC3} \cdot d \cdot t \cdot f_u < 0.422 \cdot S \cdot t \cdot f_y \Rightarrow S > 5.97 \cdot d \quad (37)$$

For the usual self-tapping screw diameters (d=4.2, 4.8, 5.5 mm) this leads to S≈33 mm, and the screw spacing will be probably larger in practical applications.

Net-section failure can take place when connections are placed closely. In order to avoid it, a minimum S can be calculated by comparing the equivalent yield stresses from Eq. (24), (29), (30) and (32):

$$\begin{cases} f_{y,ech,s}^{V} < f_{y,ech,net}^{V} \\ f_{y,ech,s}^{H} < f_{y,ech,net}^{H} \end{cases} \Rightarrow \begin{cases} F_{BS} < S \cdot t \cdot f_u \cdot \left[1 - \frac{d}{S} + \frac{t}{4} \cdot \frac{\cos^2\alpha}{\sin\alpha} \right] \\ F_{BS} < S \cdot t \cdot f_u \cdot \left[1 - \frac{d}{S} + \frac{t}{4} \cdot \frac{\sin^2\alpha}{\cos\alpha} \right] \end{cases} \quad (38)$$

The trigonometric functions can be minimized based on the limits for the angle ($25º<\alpha<65º$), $\min\left\{\frac{\sin^2\alpha}{\cos\alpha}, \frac{\cos^2\alpha}{\sin\alpha}\right\} = 0.197 \approx 0.2$; and the condition to avoid net-section failure rewritten as:

$$F_{BS} < S \cdot t \cdot f_u \cdot \left[1 - \frac{d}{S} + 0.05 \cdot t\right] \tag{39}$$

If the connectors are self-tapping screws with bearing capacity $F_{BS} = \alpha_{EC3} \cdot d \cdot t \cdot f_u$, with $\max(\alpha_{EC3}) = 2.1$ [11], the condition becomes:

$$S > \frac{3.1 \cdot d}{1 + 0.05 \cdot t} \tag{40}$$

Hence, in the extreme case of t=0, $S > 3.1 \cdot d$ is the condition for net-section failure to be avoided. Therefore, for usual wall dimensions, and when self-tapping screws are used as connectors between the steel plate and the frame of the wall, the bearing of the screws should be the main failure mode, based on the simplified formulae from prEN-1993-1-3 [11], and if $S > 6 \cdot d$. Such screw spacing is the usual case in practical applications.

4.3 Evaluation of the Rigidity

The influence of the connections can be included in the rigidity formulation, similarly as in the case of capacity (Eq. 35). At the level of one strip, the connection plays a role due to their rigidity, transforming the strip in a series of three springs: (1) a spring representing the effect of the connection with the vertical edge, (2) one corresponding to the steel strip itself, and (3) one representing the connections with the horizontal edge (Figure 11). The rigidity of the spring system can be expressed based on these three components for strips in Zone 1, 3 and strips in Zone 2 as:

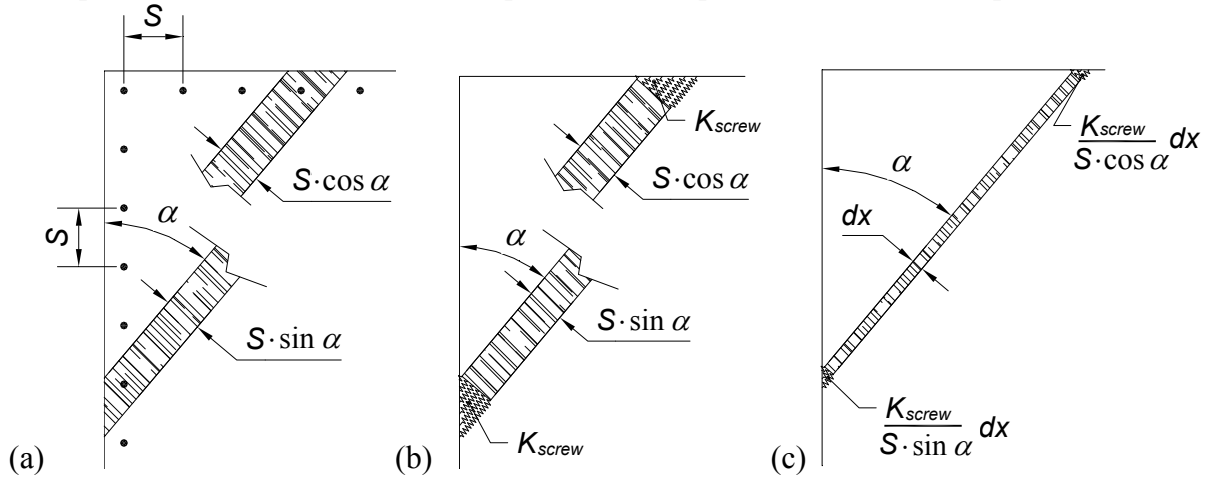

Figure 11. Rigidity of a Strip: (a) Real Arrangement, (b) Projected and (c) Reduced to *dx*

$$\frac{1}{k_{s,Z1}} = \frac{1}{k_V} + \frac{1}{k_{st}} + \frac{1}{k_H} \quad \text{and} \quad \frac{1}{k_{s,Z2}} = \frac{1}{2 \cdot k_V} + \frac{1}{k_{st}} \tag{41}$$

Where $k_{s,Z1}$ and $k_{s,Z2}$ are the rigidity of a strip as in Eq. (11) and (14), and the components corresponding to the screws can be expressed as follows (Figure 11.c.):

$$k_V = \frac{k_{screw}}{S \cdot \sin\alpha} \cdot dx \quad \text{and} \quad k_H = \frac{k_{screw}}{S \cdot \cos\alpha} \cdot dx \tag{42}$$

By substituting the expressions above in the Eq. (41), the rigidities of strips $k_{s,Z1}$ and $k_{s,Z2}$ become:

$$k_{s,Z1} = \frac{1}{\frac{S \cdot (\sin\alpha + \cos\alpha)}{k_{screw}} + \frac{x}{t \cdot E \sin\alpha \cdot \cos\alpha}} \cdot dx \tag{43}$$

$$k_{s,Z2} = \frac{1}{\frac{2 \cdot S \cdot \sin\alpha}{k_{screw}} + \frac{L}{t \cdot E \cdot \sin\alpha}} \cdot dx \tag{44}$$

If the expressions from Eq. (43) and (44) are introduced in the corresponding Eq. (15) for Zone 1 and (17) for Zone 2, the rigidity contribution of all strips in Zone 1 or 3 (K^{Zone1}) and in Zone 2 (K^{Zone2}) become:

$$K^{Zone1} = K^{Zone3} = \int_0^{L\cdot\cos\alpha} \frac{1}{C1 + C2 \cdot x} \cdot \frac{x^2}{h^2} \cdot dx =$$

$$= -\frac{C1}{C2^2} \cdot \frac{L \cdot \cos\alpha}{h^2} + \frac{1}{2 \cdot C2} \cdot \frac{L^2 \cdot \cos^2\alpha}{h^2} + \frac{C1^2}{C2^3 \cdot h^2} \cdot \left[\ln(C1 + C2 \cdot L \cdot \cos\alpha) - \ln(C1)\right] \tag{45}$$

And,

$$K^{Zone2} = \int_{h\cdot\cos\alpha}^{L\cdot\sin\alpha} \frac{L^2 \cdot \cos^2\alpha}{h^2} \cdot C3 \cdot dx = C3 \cdot \frac{L^2 \cdot \cos^2\alpha}{h^2} \cdot (h \cdot \sin\alpha - L \cdot \cos\alpha) \tag{46}$$

Where:

$$C1 = \frac{S \cdot (\sin\alpha + \cos\alpha)}{k_{screw}}; \quad C2 = \frac{1}{t \cdot E \cdot \sin\alpha \cdot \cos\alpha} \quad \text{and} \quad C3 = \frac{1}{\frac{2 \cdot S \cdot \sin\alpha}{k_{screw}} + \frac{L}{t \cdot E \cdot \sin\alpha}}$$

It can be observed that Eq. (45) and (46) are equivalent to Eq. (15) and (17), and they show the rigidity contributions of strips in Zone 1, 3 and Zone 2, but now include also the effect of the connections. To calculate the total rigidity of the cell, the effects of the strips in Zone 1, Zone 2 and Zone 3 have to be added:

$$K_{TOT} = 2 \cdot K^{Zone1} + K^{Zone2} \tag{47}$$

These expressions are too complex and have limited applicability. Moreover, the elongation of the strips in Zones 1 and 3 (Eq. 43) is not any more linearly dependent on x, as in the case of continuous connections (Eq. 9). For this reason, the strips in Zone 1 and 3 do not yield simultaneously as in the case of continuously connected plates. The expression for V (Eq. 35) is valid when all strips are yielded, and the one for K_{TOT} (Eq. 47) is accurate as long as the rigidity of the connections is high, as compared to that of the thin plate.

5. EXPERIMENTAL AND FEM VALIDATION

In order to check the validity of the method, proposed for walls with steel plates connected to the frame in points, a simple configuration was tested and modelled by FE (Figure 12). The configuration is characterized by: h=2700mm, L=1200mm, t=0.715mm, f_y=420N/mm^2, f_u=510N/mm^2, S=100mm, d=4.8mm and F_{BS}=4.14kN [13].

Figure 12. Plate Deformation: (a) Experiment and (b) FEM

The main components defining the capacity of the wall are the screws between the plate and the frame. The capacity of these connections has been determined by lap-joint tests. The test specimens were single screw lap-joints in compliance with ECCS-21 [14], made of the same basic materials as the panel, and using the same screws. Therefore, all material properties for the lap-joints were identical to the ones used in the panel test.

The experimental force displacement curves, for the 5 lap-joint tests, are presented with dashed lines in Figure 13, together with the design resistance prediction of ENV-1993-1-3 [15] and prEN-1-3 [11]. The design resistances were calculated without safety factors, and by using measured material properties and dimensions. Interesting to note, that the resistances, predicted by the two versions of the code, significantly differ: $F_{b,Rd}$=2162N [11] and $F_{b,Rd}$=3676N [15].

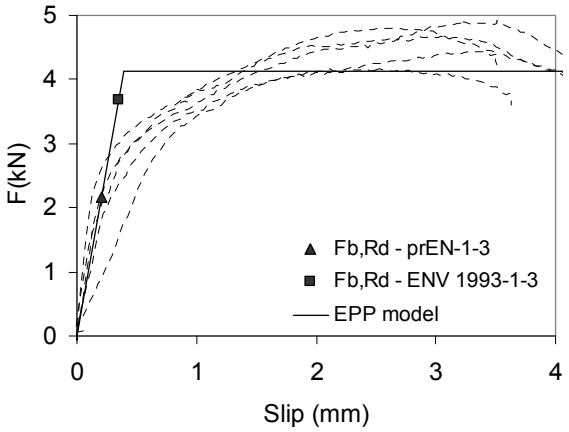

Figure 13. Experimental Curves for Lap-joints

Based on the tests, the rigidity of the connection (k_{screw}) was calculated as secant rigidity up to the force of $0.4 \cdot F_{max}$, and the yield force (F_y) was defined at $0.9 \cdot F_{max}$. The average values of these characteristics are: k_{screw}=10.63kN/mm, F_{max}=4.59kN and F_y=4.14kN. The resulting equivalent elastic-plastic curve is also presented in Figure 13.

The load bearing capacity, and rigidity of the wall, have been calculated, by the proposed analytical procedure (Eq. 35, 47), and by FEM, using for the screws: (i) elastic-plastic model with F_{BS}=F_y=4.14kN (FEM-EPP) or (ii) full non-linear model based on the lap-joint test (FEM-Non). The results of the modelling are compared to the ones obtained from the full scale wall test, in Table 3 and Figure 14.

Table 3. Properties of the Wall in Figure 12

Analytical		FEM-EPP		Experimental	
V (N)	K_{TOT} (N/mm)	V_{FEM} (N)	K_{FEM} (N/mm)	V_{EXP} (N)	K_{EXP} (N/mm)
33469	6869	32857	6488	34183	1329

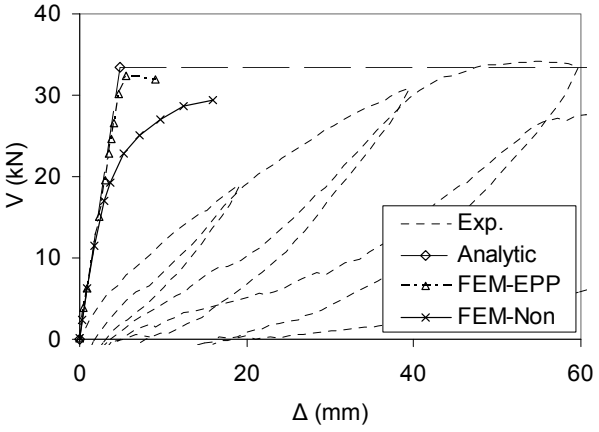

Figure 14. Predicted Behaviour of the Wall

The strength (V) formulation is validated by both the FEM and experimental results (Figure 14), but in order to be accurate, the calculation method of the rigidity should take into account additional sources of flexibility (e.g. corner flexibility). The rigidity obtained analytically (K_{TOT}) still compares well with the FEM results, which means that the analytical model correctly predicts the rigidity, at least in regard to the phenomena incorporated in the model.

6. CONCLUSIONS

An analytical calculation method has been developed for the evaluation of the capacity and the rigidity of LGS wall panels sheathed with thin steel plates. The method is based on the assumptions that: (i) the elements of the skeleton are rigid but hinged at the ends, and (ii) the steel plate transmits the load only by tension-field action. The oblique tension stress pattern, developing within the steel plate, is replaced for the calculation by strips that are subject only to tension.

The rigidity (K_{TOT}) and the capacity (V), of the wall panels, are predicted with good accuracy in the case of a continuous connection of the steel plate to the frame. For this case, the analytical calculations have been compared to FEM results.

An empirical formula is proposed for the evaluation of the angle by which the yield pattern develops (α). The formula is based on extensive FEM analysis, and is valid for the most usual wall dimensions in practical applications.

The effects of the connection between the frame and the steel plate have been incorporated into the analytical model, proposing formulas for the calculation of the capacity (Eq. 35) and rigidity (Eq. 47) of such walls. The strength formula was found to be sufficiently accurate, when compared to FE modelling and test results.

When self-tapping screws are used to connect the steel plate to the frame, it was shown that the failure mode of the wall will be governed by the bearing of the screws. This conclusion is based on design expressions from prEN 1993-1-3 [11], and applies for usual geometric configurations. This observation can be used for further simplification of the procedure.

ACKNOWLEDGEMENT

The material contained in this paper is based on the work supported by the European Community's Sixth Framework Program, Marie Curie project MEIF- CT-2005-009448. This support is gratefully acknowledged. All opinions, findings, conclusions or recommendations expressed in this material are those of the writers. The European Community is not liable for any use of the information contained in this paper.

REFFERENCES

[1] Davies, J.M., "The Use of Cassette Sections in Prefabricated Low Rise Construction. In D. Dubina, I. Vayas & V. Ungureanu (eds.)", New Technologies and Structures in Civil Engineering, Case Studies on Remarkable Constructions, 1999, Timisoara.

[2] Elgaaly, M., "Thin Steel Plate Shear Walls Behavior and Analysis", Thin Walled Structures, 1998, Vol. 32, pp. 151-180.

[3] Berman, J. & Bruneau, M., "Plastic Analysis and Design of Steel Plate Shear Walls", Journal of Structural Engineering, 2003, Vol. 129, No. 11, pp. 1448-1456.

[4] Nakashima, M. et al., "Energy Dissipation Behavior of Shear Panels Made of Low Yield Steel", Earthquake Engineering and Structural Dynamics, 1994, Vol. 23, pp. 1299-1313.

[5] De Matteis, G., Mazzolani, F.M., Panico, S., "Pure Aluminium Shear Panels as Passive Control System for Seismic Protection of Steel Moment Resisting Frames", Proc. of the 4th International Conference STESSA 2003, Mazzolani F.M. Editor, A.A. Naples, 2003, 9–12 June, Rotterdam: Balkema.

[6] Astaneh-Asl, A., "Seismic Behavior and Design of Steel Shear Walls", Structural Steel Educational Council, 2001, Moraga, California.

[7] Wagner, H., "Flat Sheet Metal Girder with Very Thin Metal Web. Part 1. General Theories and Assumptions", Technical Memorandum No. 2662, 1931, Washington DC: NACA.

[8] Timler, P.A. & Kulak G.L., "Experimental Study of Steel Plate Shear Walls, Structural Engineering Report No. 114, 1983, Department of Civil Engineering, University of Alberta, Edmonton Alberta.

[9] Kuhn, P., "Stresses in aircraft structures", New York: McGraw-Hill, 1955.

[10] Fulop, L.A, Hakola, I., "Design of Light-gauge Steel Shear Walls Sheathed with Thin Steel Plates", Proceedings of the International Conference in Metal Structures "Steel – A New and Traditional Material for Buildings", 20-22 IX 2006, Poiana Brasov, Romania, ISBN 0415408172.

[11] prEN-1-3, "General Rules. Supplementary Rules for Cold-formed Members and Sheeting", Brussels, 2004.

[12] prEN 1993-1-1, "Design of Steel Structures – Part 1-1: General Rules and Rules for Buildings", Brussels, 2003.

[13] E0012, "Seismic Tests of Shear Walls. Part 2. Report to ECSC, Document PR377/WP3/E0012. Version 1", Helsinki: VTT- Building and Transport, 2005.

[14] ECCS-21, "Recommendations for Steel Construction: The Design and Testing of Connections in Steel Sheeting and Section", Brussels: ECCS Committee TC7. WG 7.2, 1983.

[15] ENV 1993-1-3, "General Rules, Supplementary Rules for Cold-formed Members and Sheeting, Brussels, 1996.

NOTATIONS

A_{net} net-section in a connection according to prEN-1993-1-1
A_{gross} gross cross section
d diameter of bolt or screw
dA cross section area of one calculation strip
dF_S tensile capacity of a calculation strip
$dF_{S,1,3}$ equivalent capacity of a strip in Zone 1 and Zone3 ($dF_{S,1,3}=dx\cdot t\cdot f_{y,1,3}$)
$dF_{S,2}$ equivalent capacity of a strip in Zone 2 ($dF_{S,2}=dx\cdot t\cdot f_{y,2}$)
dk_t^{Z1} contribution of the current strip in Zone1 to the horizontal rigidity of the cell
dk_t^{Z2} contribution of the current strip in Zone2 to the horizontal rigidity of the cell
dx differential width of the calculation strip
E elastic modulus (of steel)
ER average of the absolute values of the relative error for the prediction of α
$f^H_{y,ech,s}$ equivalent yield stress corresponding to the failure of the screws on a horizontal edge
$f^H_{y,ech,net}$ equivalent yield stress corresponding to the net-section failure of a horizontal connection line
f_u ultimate strength
$f^V_{y,ech,s}$ equivalent yield stress corresponding to failure of the screws on a vertical edge
$f^V_{y,ech,net}$ equivalent yield stress corresponding to net-section failure of a vertical connection line
f_y yield stress of the flat steel plate
$f_{y,1,3}$ equivalent yield stress of strips in Zone 1 or Zone3
$f_{y,2}$ equivalent yield stress of strips in Zone 2
$f_{y,ech}$ equivalent yield stress of a strip
F_{BS} bearing failure of one screw
F^V_{net} capacity of a strip corresponding to the net-section failure of the vertical connection line
h height of the wall
k_H equivalent distributed rigidity from connections on the horizontal edge
$k_{s,Z1}$ axial rigidity of the current strip in Zone1
$k_{s,Z2}$ axial rigidity of the current strip in Zone2
k_{screw} rigidity of one connection
k_{st} tension rigidity of the strip
k_V equivalent distributed rigidity from connections on the vertical edge
K_{TOT} total shear rigidity of one cell
K^{Zone1} shear rigidity of the wall due to all strips in Zone1
K^{Zone2} shear rigidity of the wall due to all strips in Zone2
K^{Zone3} shear rigidity of the wall due to all strips in Zone3
$l_{12,Z1}$ length of the current strip in Zone1
$l_{12,Z2}$ length of the current strip in Zone2
L length of a sheathing cell
n number of holes in any diagonal or zig-zag line progressively across the section
p distance between bolts perpendicular on the loading direction
s distance between bolts parallel to the loading direction
S distance between screws
t thickness of the flat steel plate
V total shear capacity of one cell
V_y shear yield capacity of the wall panel
V_i contribution of one strip to the shear capacity of the cell
V_i^{Zone1} contribution of all strips in Zone1 to the shear capacity of the cell

V_i^{Zone2} contribution of all strips in Zone2 to the shear capacity of the cell
V_i^{Zone3} contribution of all strips in Zone3 to the shear capacity of the cell
x oblique coordinate of the current calculation strip
α angle of the principle tensile stress (yield angle of the strip model)
α_{EC3} α coefficient form Table 8.2 of ENV-1993-1-3 (or prEN-1993-1-3)
ε_y yield strain of the steel of the plate
σ_{ER} standard deviation of the error measure ER
Δ horizontal displacement of the top of the wall
$\Delta l_{12,Z1}$ elongation of a current strip in Zone1 due to a Δ horizontal top displacement
$\Delta l_{12,Z2}$ elongation of a current strip in Zone2 due to a Δ horizontal top displacement
$\Delta l_{12y,Z1}$ yield elongation of a current strip in Zone1
$\Delta l_{12y,Z2}$ yield elongation of a current strip in Zone2
Δ_y top horizontal displacement corresponding to the yielding of all strips

FE SIMULATION OF SPACE STEEL FRAMES IN FIRE WITH WARPING EFFECT

Zhan-Fei Huang[1,*] and Kang-Hai Tan[2]

[1]*Research Fellow, School of Civil and Environmental Engineering, College of Engineering, Nanyang Technological University, 50 Nanyang Avenue, Singapore 639798*
[2]*Assoc. Professor, School of Civil and Environmental Engineering, College of Engineering, Nanyang Technological University, 50 Nanyang Avenue, Singapore 639798*
**(Corresponding author: E-mail: czfhuang@gmail.com)*

Received: 8 January 2007; Revised: 19 March 2007; Accepted: 28 March 2007

ABSTRACT: Most structural fire resistance analyses are confined to 2-D frames. To gain a more in-depth understanding of the response of a steel frame at elevated temperatures, 3-D simulations are necessary. This paper outlines the formulation of a two-noded 3-D beam-column to study the response of a steel frame in fire. The program is capable of small-strain large deformation analysis. Warping effect, a significant phenomenon in thin-walled members, is considered in the formulation. Degradation of steel mechanical properties at elevated temperatures is also considered, while thermal gradient is considered by slicing a cross-section into discrete segments. Creep can be either implicitly or explicitly taken into account. Several widely-used beam-to-column connections are approximated as zero-length semi-rigid springs. Their nonlinear moment-rotation relationships at elevated temperature are incorporated into the program. Unloading of both material stress-strain curve and moment-rotation characteristics of a connection are accounted for. The Newton-Raphson method is employed for nonlinear solving procedure. At the latter part of this paper, the program is verified against benchmark tests. All of them demonstrate the accuracy and reliability of the program.

Keywords: Finite element analysis, 3-D beam element, warping, fire, steel frame, creep

1. INTRODUCTION

In recent years, there is growing awareness in the understanding of the structural behaviour of a steel frame subjected to fire attack. This is partially owing to a series of tests conducted at Cardington, UK, which demonstrate the resilience of steel frames under fire conditions. Although a fairly extensive number of structural fire resistance experiments have been conducted, it was found these tests contained inherent limitations such as:

- Specimen boundary conditions are simplified as pined, roller or fully fixed, which are at variance with the much more complicated realistic boundary condition for a beam or column within an actual frame.
- Columns are tested as non-sway members in the test rig. In reality, even in a non-sway frame, columns may experience large sway during a compartment fire (Huang and Tan [1]).
- Interactions among structural components can hardly be simulated by experiments.
- Column post-buckling behaviour, slab membrane action as well as beam catenary actions cannot be captured by experiments.
- Fire resistance tests are extremely expensive.

Thus, researchers and engineers now resort more often to numerical analysis which is more versatile than purely analytical approaches such as Rankine method (Zeng et al. [2]; Huang and Tan [3,4]). Traditionally, 2-D finite element (FE) analyses have been carried to study the behaviour of steel frames in fire for decades. However, actual steel frames behave quite differently compared to 2-D simulation. For instance, steel columns are in reality subjected to biaxial bending and torque in addition to axial compression. Besides, warping effects is significant in thin-walled members. Therefore, in the past decade, more and more 3-D programs have been developed to achieve more accurate simulations (Wang et al. [5], Najjar and Burgess [6], Song et al. [7], Iu and Chan [9], Iu et al. [10], Ma and Liew [11]), the pace hastened by the rapid development of

computer technology. These programs allow structural fire engineers to analyse a structure in a more holistic way through 3D full-frame analysis.

Iu and Ma's works differ to those of others in their plastic-hinge approach, which will be discussed herein.

In 2004, Iu and Chan extended Chan's program GMNAF to predict the behaviour of steel frames in fire. Both material and geometric nonlinearities were taken into account, while beam-to-column connections were simulated as semi-rigid springs. Material yielding is modelled by plastic hinges at both ends of an element. Limited by the nature of formulation, the actual yielding process of a beam was over-simplified although this formulation is famous for its high convergence rate due to simplicity in stiffness matrix formulation. The program was later used to investigate the behaviour of a steel frame during cooling stage which is essential for a full-history simulation of a frame in a real fire condition (Iu et al. [10]).

In Singapore, Ma and Liew [11] also developed a 3-D FE program for simulating steel frame in fire. Their approach was based on plastic hinge formulation, whereby the yielding of a steel cross-section is approximated by two nested 3-D stress-resultant surfaces by considering the softening effect of steel at elevated temperature. Such a model actually evolved from conventional single-surface plasticity model which is computationally efficient with compromise of prediction accuracy.

There are more works on traditional beam approach, where the plastification of a beam is monitored at discrete segments within a cross-section on integration points. In the UK, Najjar and Burgess [6] developed 3-D program 3DFIRE for unprotected steel frame simulation at elevated temperature. Warping effect is taken into account. The program was further refined by Bailey [8] with incorporation of functions such as semi-rigid spring, shear deformation as well as continuous floor slab of uniform temperature. Nevertheless, creep effect was not considered and degree of freedom (hereafter, DOF) to torsion was treated as scalar in the beam formulation.

This paper outlines the 3-D beam simulation work extended from on Bailey's work, so that creep strain is explicitly incorporated while torsion DOF is treated as a vector. A layered membrane reinforced concrete slab, which allows for uneven thermal distribution along the slab thickness direction, is being developed. Nonetheless, this to-be-incorporated slab will not be discussed herein. That is, this paper focuses on the formulation of the revised 3-D beam-column element.

2. 3-D STEEL BEAM FORMULATION

The adopted 3-D steel beam element is extended from Bailey's work [8]. At each node of the beam, there are 8 DOFs in local coordinates which are transformed into 10 DOFs in global coordinates (Figure 1). In the formulations, it is assumed that:

- Only bi-symmetric sections (such as I-, rectangular and circular ones) are considered. As such, shear center coincides with the centroid of section.
- Element is straight and prismatic.
- Bernoulli-Euler hypothesis: a transverse plane remains plane and normal to the beam longitudinal axis.
- Shear strain is unconsidered, while strain unloading is taken into account.
- Cross-sectional area of a beam is undistorted under applied load and thermal effect.

- Terms higher than 4th-order are neglected in the formulation. Under elevated temperature, steel frames may experience large deformation (Huang and Tan [1]), thus retaining high order terms is necessary for an accurate prediction.
- Warping effect is considered only for open thin-wall sections.
- Unlike translation and rotation, warping $\partial\theta_z/\partial z$ (Figure 1) is treated as a scalar.
- External loads are treated as conservative, i.e., they are independent of structural deformation.

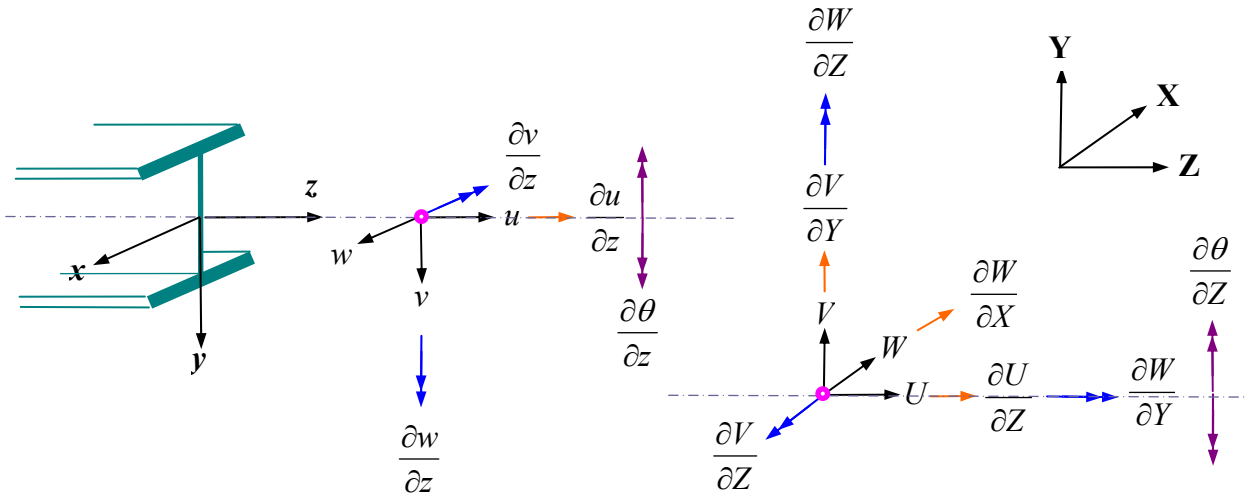

(a) Local coordinate (8 DOFs) (b) Global coordinate (10 DOFs)

Figure 1. Definition of Degree of Freedoms at a Beam Node

The formulation of beam is based on Total Lagrangian description, which specifies the displacement of a point within a cross-section with regard to its initial position at the beginning of heating or loading. Under local coordinate system, x- and y-axis are referred to the symmetric axes passing through the centroid of a cross section, while z-axis is the longitudinal axis of an element. Traditional cubic shape function $\langle N \rangle$ (Bathe [12]) is adopted to calculate the displacements at integration points along a beam as:

$$u_0 = \langle N \rangle \{\bar{u}\} \qquad v_0 = \langle N \rangle \{\bar{v}\} \qquad w_0 = \langle N \rangle \{\bar{w}\} \qquad \theta_z = \langle N \rangle \{\bar{\theta}_z'\} \tag{1}$$

where

$$\{\bar{u}\} = \begin{Bmatrix} u_i \\ \left(\frac{\partial u}{\partial z}\right)_i \\ u_j \\ \left(\frac{\partial u}{\partial z}\right)_j \end{Bmatrix}, \quad \{\bar{v}\} = \begin{Bmatrix} v_i \\ \left(\frac{\partial v}{\partial z}\right)_i \\ v_j \\ \left(\frac{\partial v}{\partial z}\right)_j \end{Bmatrix}, \quad \{\bar{w}\} = \begin{Bmatrix} w_i \\ \left(\frac{\partial w}{\partial z}\right)_i \\ w_j \\ \left(\frac{\partial w}{\partial z}\right)_j \end{Bmatrix}, \quad \{\bar{\theta}_z\} = \begin{Bmatrix} (\theta_z)_i \\ (\theta_z')_i \\ (\theta_z)_j \\ (\theta_z')_j \end{Bmatrix} \tag{2}$$

In Eq. (1), terms u_0, v_0, w_0 are translations in z-, y- and x-axes, and θ_z is the twist angle along the beam axis. The subscript '*0*' denotes at an integration point and 'z' is the longitudinal axis (i.e., z- axis). In Eq. (2), vectors $\{\bar{u}\}$, $\{\bar{v}\}$, $\{\bar{w}\}$ and $\{\bar{\theta}_z'\}$ denotes 16 DOFs at the respective nodes i and j of a beam as shown in Figure 1.

A cross section is sliced into 64 segments to incorporate the temperature difference and the spreading of plasticity (Figure 2). Each segment has a central sampling point where its displacements are defined.

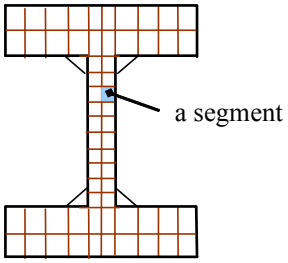

Figure 2. Segments of a Cross-section

Once the displacement at the centroid of a cross section is obtained, the associated 3 translations at any other point in this section can be calculated as (Figure 3):

$$u = u_0 - \left(y \cdot \sin\theta_y + x \cdot \sin\theta_x \right) + \omega\theta_z' \tag{3}$$

$$v = v_0 - y + \left(y\cos\theta_y \cos\theta_z + x\cos\theta_x \sin\theta_z \right) \tag{4}$$

$$w = w_0 - x + \left(x\cos\theta_x \cos\theta_z - y\cos\theta_y \sin\theta_z \right) \tag{5}$$

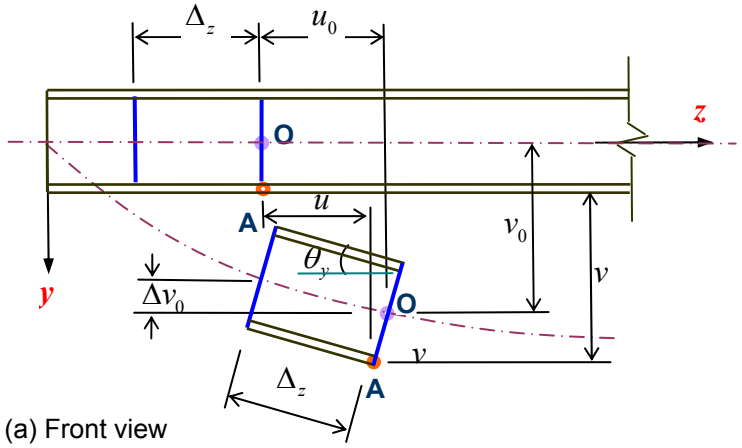

(a) Front view

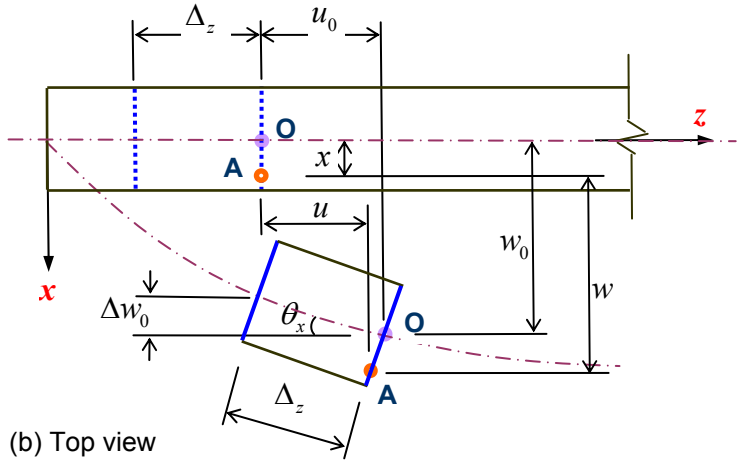

(b) Top view

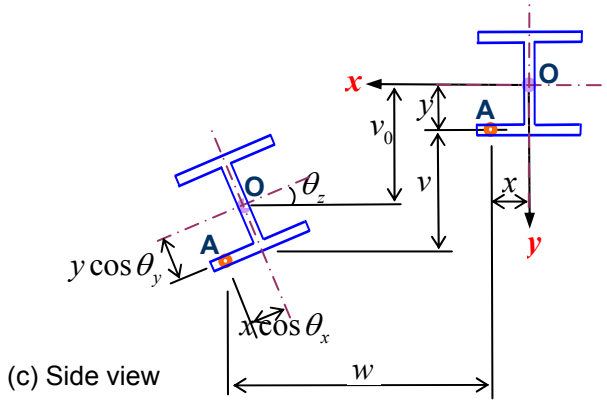

Figure 3. Definition of Space Displacements of a General Point within a Cross-section

in which ω is the normalized sectional coordinate for a particular point (Kohnke, [13]).
The associated slope of the deflected element in y - and x - axis can be respectively approximated as (Figure 3):

$$v_0' = \tan\theta_y \approx \sin\theta_y \tag{6}$$

$$w_0' = \tan\theta_x \approx \sin\theta_x \tag{7}$$

Further differentiating Eqs. (5) and (6) results in

$$v_0'' = \cos\theta_y \frac{d\theta_y}{dz} \tag{8}$$

$$w_0'' = \cos\theta_x \frac{d\theta_x}{dz} \tag{9}$$

Based on small rotation assumption, one obtains (Figure 3):

$$\cos\theta_y = \sqrt{1-(v_0')^2} \tag{10}$$

$$\cos\theta_x = \sqrt{1-(w_0')^2} \tag{11}$$

Thus, Eqs. (8) and (9) can be rewritten as:

$$\frac{d\theta_y}{dz} = \frac{v_0''}{\cos\theta_y} = \frac{v_0''}{\sqrt{1-(v_0')^2}} \tag{12}$$

$$\frac{d\theta_x}{dz} = \frac{w_0''}{\cos\theta_x} = \frac{w_0''}{\sqrt{1-(w_0')^2}} \tag{13}$$

Differentiating Eqs. (3) to (5) will produce:

$$u' = u_0' - \left(y \cdot v_0'' + x w_0''\right) + \omega\theta_z'' \tag{14}$$

$$v' = v_0' - y\frac{v_0' v_0''}{\sqrt{1-(v_0')^2}} + x\theta_z'\sqrt{1-(w_0')^2} \tag{15}$$

$$w' = w_0' - x\frac{w_0' w_0''}{\sqrt{1-(w_0')^2}} - y\theta_z'\sqrt{1-(v_0')^2} \tag{16}$$

By substituting Eqs. (14) to (15) into Green strain expression $\varepsilon_z = u' + \frac{1}{2}\left[(u')^2 + (v')^2 + (w')^2\right]$, one has

$$\varepsilon_z = u_0' - y v_0'' - x w_0'' + \omega\theta_z'' + \frac{1}{2}(u_0')^2 - y u_0' v_0'' \; - x u_0' w_0'' + \omega u_0'\theta_z'' + \frac{1}{2}y^2(v_0'')^2 + \frac{1}{2}x^2(w_0'')^2 \tag{17}$$

$$+\frac{1}{2}\left(w_0'\right)^2-x\frac{\left(w_0'\right)^2 w_0''}{\sqrt{1-\left(w_0'\right)^2}}-y\theta_z' w_0'\sqrt{1-\left(v_0'\right)^2}+\frac{1}{2}x^2\frac{\left(w_0' w_0''\right)^2}{1-\left(w_0'\right)^2}+\frac{1}{2}y^2\left(\theta_z'\right)^2\left[1-\left(v_0'\right)^2\right]$$

$$+\frac{1}{2}\left(v_0'\right)^2-y\frac{\left(v_0'\right)^2 v_0''}{\sqrt{1-\left(v_0'\right)^2}}+x\theta_z' v_0'\sqrt{1-\left(w_0'\right)^2}+\frac{1}{2}y^2\frac{\left(v_0' v_0''\right)^2}{1-\left(v_0'\right)^2}+\frac{1}{2}x^2\left(\theta_z'\right)^2\left[1-\left(w_0'\right)^2\right]$$

Warping of an I-section is considered with reference to ANSYS (Kohnke, [13]).
Once the axial strains are obtained, the Principle of Virtual Work can be applied:

$$\delta W=\int_V \sigma_z\delta\varepsilon_z dV-\langle Q\rangle\{\delta q\}=0 \tag{18}$$

in which σ_z denotes axial stress, $\langle Q\rangle$ external load vector, V total volume of an element and $\{\delta q\}$ incremental displacements.

Following the standard nonlinear FE procedure, the incremental equilibrium equations are formulated at the global structural level:

$$\left[\mathbf{K_T}\right]\cdot\{\mathbf{\Delta q}\}=\{\mathbf{\Delta Q}\} \tag{19}$$

where $\left[\mathbf{K_T}\right]$ denotes global tangent stiffness matrix, $\{\mathbf{\Delta q}\}$ global incremental displacements and $\{\mathbf{\Delta Q}\}$ out-of-balance forces. Traditional Newton-Raphson method is used to solve Eq. (19). To improve the convergence rate and to ensure a monotonic convergence, potential-energy-based line search method is employed in conjunction with N-R method.

Steel material modelling, which takes unloading into account, is in line with Tan et al. [18].

As mentioned, our formulation differs from Bailey's [8] algorithm at three points.

(1) Firstly, the nodal torsion parameter θ_z is treated as a vector and thus it can be decomposed into three global rotations $\partial W/\partial Y$, $\partial W/\partial Z$ and $\partial V/\partial Z$ after coordinate transformation (Figure 1). Bailey treated θ_z as a scalar which is an independent DOF. Obviously, the new approach is more rational and one less DOF is needed under global coordinate system.

(2) Secondly, creep strain is incorporated explicitly into the program. Although creep strain is implicitly considered by some widely-used stress-strain models like EC3 Pt.1.2 [14] when heating rate falls into the range of 2 to 50°C/min, theoretically, creep strain should be treated explicitly due to its transient nature. Numerous studies have shown the importance of incorporating creep strain explicitly into numerical simulation (Harmathy [15], Cheng [17], Furumura and Shimohara [16], Tan et al. [18], Zeng et al. [2], Huang et al. [19]).

Generally, when the temperature increases beyond 450 to 500°C, which commonly take place under a real fire, steel creep strain becomes significant. This study adopts Harmathy's creep model [20], which is based on a concept put forward by Dorn [21] in which the effect of variable temperature is considered. Dorn [21] proposed a temperature-compensated time θ which is expressed as:

$$\theta=\int e^{-\frac{Q}{RT'}}dt \tag{20}$$

where Q is the activation energy of creep (J/mol), R is the gas constant (J/mol·K), and T' is the absolute temperature.

Harmathy [20] derived an analytical expression of creep strain rate $\dot{\varepsilon}_{cr}$ for ASTM A36 structural steel:

$$\dot{\varepsilon}_{cr} = Z \exp\left(\frac{-Q}{RT'}\right) \coth^2 \left[\frac{3tZ \exp\left(\frac{-Q}{RT'}\right)}{\varepsilon_{cr,0}} \right]^{1/3} \quad \text{(time hardening)} \tag{21}$$

$$\dot{\varepsilon}_{cr} = Z \exp\left(\frac{-Q}{RT'}\right) \coth^2 \left[\frac{\varepsilon^*_{cr}}{\varepsilon_{cr,0}} \right] \quad \text{(strain hardening)} \tag{22}$$

in which $Z = 0.026S^{4.7}$, when $S \le 15{,}000$ (psi),

$Z = 1.23 \times 10^{16} \exp(0.0003S)$, when $15{,}000 < S \le 45{,}000$ (psi);

where S is the second Kirchhoff stress;

$\varepsilon_{cr,0} = 1.7 \times 10^{-10} S^{1.75}$;

$\frac{Q}{R} = 70{,}000^\circ$ Rankine;

$T' =$ degrees Fahrenheit + 459.67 (Rankine);

$t =$ time (hr);

$\varepsilon^*_{cr} = \sum \left| \dot{\varepsilon}_{cr} \right| \cdot \Delta t$, compounded creep strain (Harmathy [15]).

Both strain-hardening rule and time-hardening rule are incorporated into FEMFAN3D. Predictor and corrector technique is applied in calculating the creep strain ε_{cr} at a faster convergence rate (Levy [22]).

(3) Thirdly, the approach differs from Bailey's [8] in that we do not adopt subdivision technique on each member. In Bailey's [8] formulation, each member was subdivided into three elements with the central one being 80 percent of member length. This was to cater for a better reflection of spread of material yielding in the proximity at nodal area. However, this purpose was achieved with greater CPU time. In our approach, Newton-Cotes scheme is employed and there are two integration points on element boundary (Bathe [12]).

In addition, elastic unloading of stress-strain relationship is also considered in line with Tan et al. [18]. To model the beam-to-column connections, a two-noded zero length semi-rigid spring element is employed. Under local coordinate system, this spring element has two DOFs, namely, rotations about x and y axes (Figure 1). The other six nodal DOFs on a beam end are assumed to be rigidly connected to the others. At the present time, there is very little experimental data for joint characteristics at elevated temperatures although data for the in-plane rotational characteristics of steel beam-to-column connection at ambient temperature abound. Thus, only El-Ramawi's model [23] using Ramberg-Osgood expression to establish the relationship between the connection bending moment M^T_{con} and its relative rotation θ^T_{con} is incorporated into the program. Unloading of $M^T_{con} - \theta^T_{con}$ curve is modelled in line with El-Rimawi et al [24]'s work.

3. NUMERICAL VERIFICATION

The program has been validated against a fairly number of benchmark tests numerically and experimentally. Following shows the most representative ones.

3.1 Deflection of a Flat Arch Subject to a Lateral Loading at Ambient Temperature

This benchmark test is used to validate the large deformation analytical capability of program FEMFAN3D. A flat arch that supports a monotonically increasing point load at its mid-span (Figure 4a, from ABAQUS [25] is chosen for this purpose. Creep is not included in the simulation. Due to symmetry, only half of the arch is modelled, with a rigid vertical roller at 'A'. A vertical load of $N/2$ is applied at 'A'. The arch is pin-connected at the end 'B' (Figure 4a) and it consists of a rectangular section with 1 inch width and 2 inch height. The arch is divided into 20 linear elements for a better simulation of flat arch. Displacement control is adopted to trace the snap-through phenomenon of flat arch. Figure 4b illustrates clearly that the vertical deflection v predicted from FEMFAN3D compares very well with ABAQUS results [25]. The large-displacement capability of FEMFAN3D is verified.

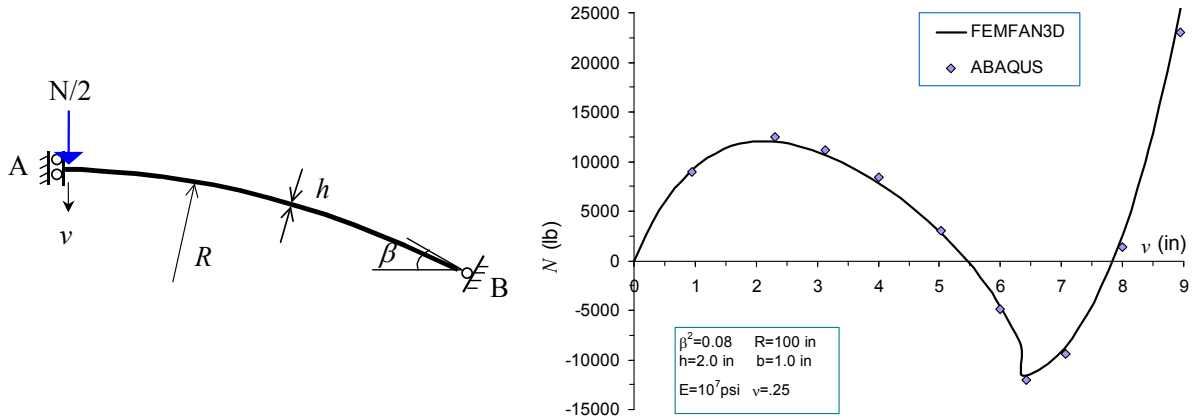

(a) (b)

Figure 4. (a) Loading and Dimension of Flat-arch with Pinned Ends, (b) Mid-span Deflection

3.2 Deflection of a Subframe under Fire Condition with Creep Considered

This benchmark test is used to validate the creep effect on the structural behaviour of a steel frame under fire conditions.

Furumura and Shimohara [16] developed a F.E. elastic-plastic creep analysis for 2D steel frames in fire. Based on the same example, Najjar [26] validated his program 3DFIRE using Furumura and Shimohara's work. There is no publication on the simulation by using Bailey's formulation. It should be mentioned that in Najjar's original beam formulation, upon which Bailey's work extended, shear strain and strain unloading were not taken into account.

Some of assumptions adopted by Furumura and Shimohara are listed below:

(1) The thermal strain of steel ε_{th} is calculated as:

$$\varepsilon_{th} = 5.04 \times 10^{-9} T^2 + 1.13 \times 10^{-5} T \tag{23}$$

where T is in °C.

(2) The stress-strain relationship of SM50 steel is shown in Figure 5. where

$$E_0^T / E_0^{20} = -8.75 \times 10^{-7} T^2 - 3.87 \times 10^{-4} T + 1.008 \quad (24)$$

In this equation, E_0^T and E_0^{20} are the elastic modulus at temperature T and 20°C, respectively. The material descriptions also include the behaviour during unloading, in tension or, temperature variation. Kinematic hardening rule is applied as unloading occurs.

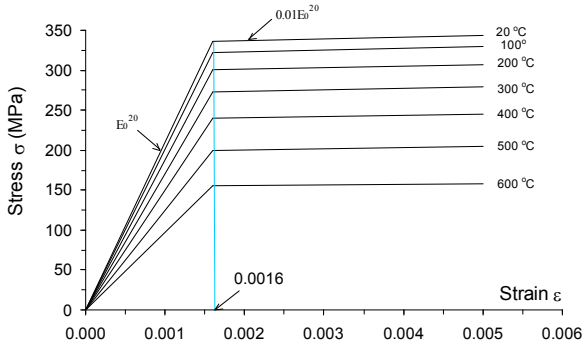

Figure 5. Stress-strain Relationship of Steel SM50 at Elevated Temperature (Furumura and Shimohara [16])

(3) To evaluate the creep deformation, it is assumed that the creep strain increment $\dot{\varepsilon}_{cr}$ for SM50 steel during the time increment dt, is related to time t, absolute temperature T, and current stress σ in the following form:

$$\dot{\varepsilon}_{cr} = 10^{(c-\frac{a}{2.3}\cdot\frac{1}{T})\frac{1}{n}} \cdot \left(\frac{2.37\times|\sigma|}{3.4}\right)^{\left(\frac{b}{2.3}\cdot\frac{1}{T}+\alpha\right)\frac{1}{n}} \cdot n^{\frac{n-1}{n}} \cdot \left(\int_0^{\varepsilon_c}\left|\frac{d\varepsilon_{cr}}{dt}\right|dt\right)^{\frac{n-1}{n}} \cdot dt \cdot \operatorname{sgn}\sigma \quad (25)$$

where c=20.53, α=-7.25, n=0.35, a=4.5x10^4, b=1.9x10^4, T: absolute temperature, t: time (min.), σ: stress (kg/mm^2), ε_{cr}: creep strain (%).

Strain-hardening rule is applied for the calculation of the non-stationary creep deformation.

(4) The concrete slabs do not interact with the steel frame system or contribute to its stiffness.

(5) The stress and strain states of the element are uniaxial and are evaluated only at both ends of the element. The stress state within the element is interpolated by using the values at both ends of each element.

(6) The deformations of members by axial force and bending moment are considered, but the shearing and local deformations are ignored.

A total of three beam-columns have been analysed by Furumura and Shimohara [16], with different end conditions. Limited by the paper length, only sub-frame2a is presented here. Figure 6a shows the geometry and loading of the frame, which is a simplified structural model suggested by Furumura and Shimohara [16] to represent a multi-storey frame. The concentrated loads at the column top represent loadings transferred from top storeys. The developments of cross-sectional temperatures profile is shown in Figure 6b, where significant thermal gradient is presented throughout the heating.

In this paper, the numerical results from Furumura and Shimohara, Najjar and us are compared. All works adopt Furumura and Shimohara's material model, except that Najjar's did not take creep into account limited by the nature of his program 3DFIRE. To illustrate creep effect, the

prediction of FEMFAN3D excluding creep effect is also shown. In our simulation, the beam is divided into ten elements of even length, while each column is divided into four elements.

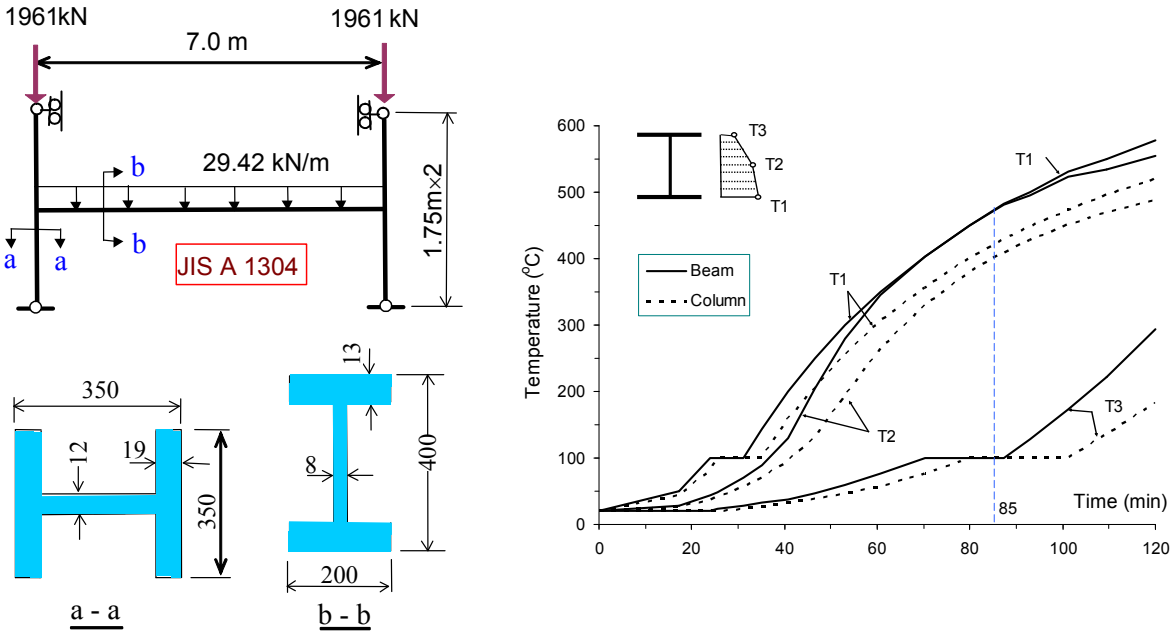

(a) Dimension and Loading (b) Temperature Development within Members

Figure 6. Subframe-2a Subjected to Fire Standard JIS A 1304 Fire

Figure 7 compares the results predicted by all parties. Figure 7a shows the development of horizontal displacement at beam end u, as well as mid-span deflection v_{mid}, whereas Figure 7b shows the progress of beam internal axial force P. In general, (1) current analysis with creep effect yields good agreement with Furumura and Shimohara's prediction within the full heating history albeit some discrepancies exist; (2) since creep effect was excluded from Najjar's simulation, his result somewhat contains discrepancy towards the end of heating when creep becomes significant.

These deformations and internal force should be analysed in detail.

In terms of mid-span deflection v_{mid} (Figure 7a), both Furumura et al. and FEMFAN3D analyses give nearly the same result throughout the heating, while 3DFIRE agrees well with the other two only before 85 min. Beyond 85 minutes, due to the negligence of creep strain, 3DFIRE predicts much smaller v_{mid} compared to the others. At 85 minutes, the corresponding temperatures at the bottom flange and web of steel sections ($T1$ and $T2$ in Figure 6b) attain about 450°C and 400°C, respectively. It is acknowledged that creep starts to affect the behaviour of a steel structure beyond around 450°C. At the end of heating, that is at t=120 min. while $T1 = 580\,°C$ and $T2 = 505\,°C$ in the beam, the magnitude of v_{mid} predicted by FEMFAN3D (or Furumura and Shimohara) is almost twice that of 3DFIRE. By the same reasoning, FEMFAN3D prediction without creep effect differs much from that with creep effect beyond 85 min.

With respect to beam end horizontal movement u, all predictions follow closely with each other before 85 min. The predictions differ from each other beyond 85 min when the temperature rises above 450°C and creep effect becomes significant.

It is also interesting to check the progress of beam internal axial force P under the rising temperature. Figure 7b shows that difference among three analyses starts after 40 minutes of heating. Both 3DFIRE and FEMFAN3D predict slightly higher P than Furumura and Shimohara. It is reasonable that the 3DFIRE analysis overestimated P which is induced by the thermal expansion of beam — the absence of creep effect stiffens the adjoining columns. Besides, FEMFAN3D prediction is still slightly greater than Najjar's beyond 40 minutes, when P begins to decrease due to rapid development of beam lateral deflection. This is mainly due to the fact that elastic unloading of $\sigma - \varepsilon$ model which is considered in this approach, was not considered by Najjar who adopted tangent modulus unloading scheme. A decrease of P engenders unloading at the top fibers of heated beam. The significant effect of unloading in the numerical simulation has been discussed by Franssen [27].

Beyond 85 minutes, the presence of significant creep strain leads to a faster decreasing P by both Furumura et al. and FEMFAN3D than that of Najjar's result.

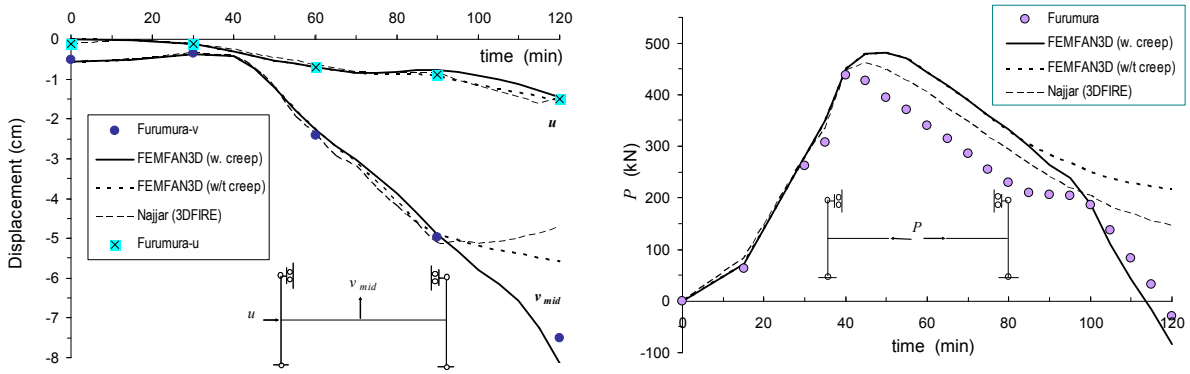

(a) displacement (b) beam internal axial force

Figure 7. Comparison of Predictions on Frame Deformation and Internal Force

3.3 A 2-Storey Space Frame at Ambient Temperature

This comparison is carried out to verify the 3D analysis capability. In 1971, Morino and Lu reported two second-order elastic-plastic analyses of two space frames, which are also analysed by program FEMFAN3D. Limited by the paper length, only the comparison on the 2-storey one is presented here. The frame is subjected to monotonically increasing load at room temperature until it fails. Creep is not included in the simulation. Figure 8 shows the frame geometry and the load-deflection curves at node '5' of the frame. All members are of 14W43 I-section and with slenderness ratio l/r_W =60, in which r_W denotes radius of gyration about the weak axis. Numbers on the Morino and Lu's curve show the sequence of plastic hinge formations in the frame.

Clearly, the predictions agree well with Morino and Lu's results up to the point when the cross-section of the first predicted plastic hinge starts to yield. Beyond that point, the prediction of external load N is slightly greater than theirs corresponding to the same horizontal movement U. This is mainly due to the different approaches adopted. The approach considers the spread of plasticity across a member under increasing N, while Morino and Lu assumes fully elastic behaviour of a section before it becomes fully plastic. In their analysis, once a plastic hinge forms, a mechanical hinge will be inserted on the element and the analysis continues until the whole frame turns into a mechanism.

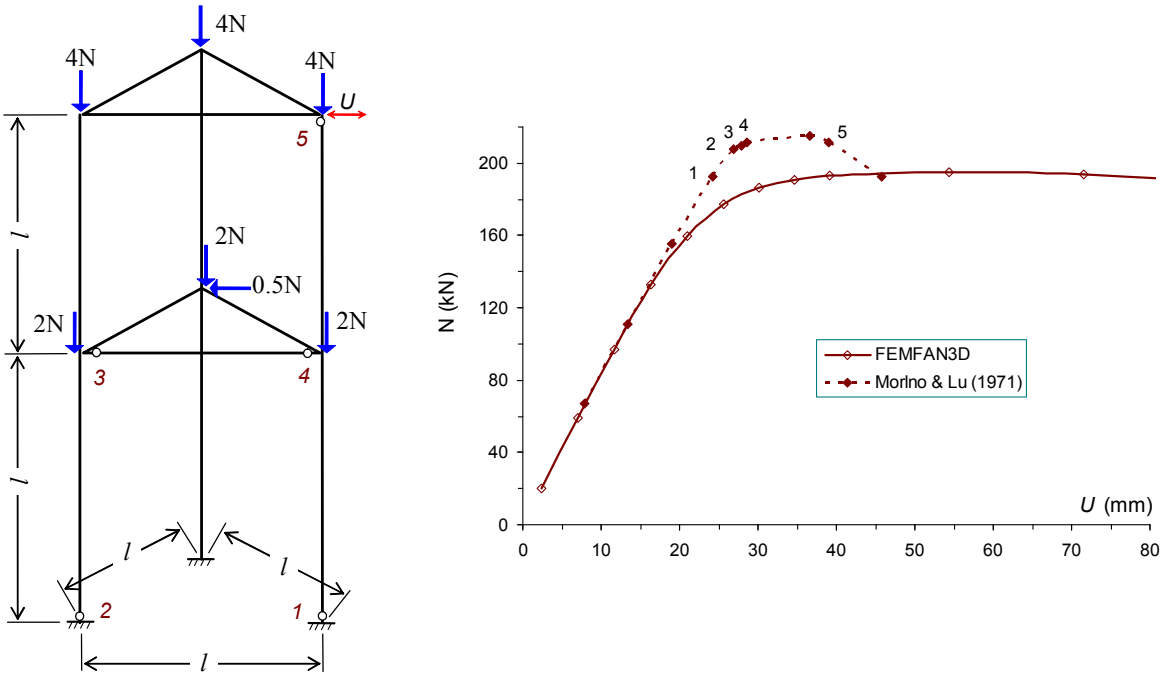

(a) Dimension and Loading (b) Horizontal Movement at Point-5

Figure 8. Collapse Process of a Two-storey Space Frame (Morino and Lu [28])

3.4 Response of Semi-rigid Connected Beams in Fire

Bailey [8] studied the influence of semi-rigid connections on a pin-roller steel beam subjected to fire as shown in Figure 9a. The beam is of 305×165UB40 section and grade 43 steel. Three constant concentrated loads act at the quarter points of beam, corresponding to a load ratio of 0.6 (according to BSI [29]). Different end restraints are considered, viz. 25%, 50%, 75% and 100% scaling of both the stiffness and strength of the extended end-plate characteristics as proposed by El-Ramawi et al. [30]. Temperature is uniformly distributed along the beam length as well as across the section. The connection temperature takes 70% of the beam temperature. Since the Ramberg-Osgood stress-strain model (BSI [29]) adopted by Bailey is not incorporated in program FEMFAN3D, in this analysis, EC3 model (CEC [14]) is used. Thus, explicit creep is not included in the FEA.

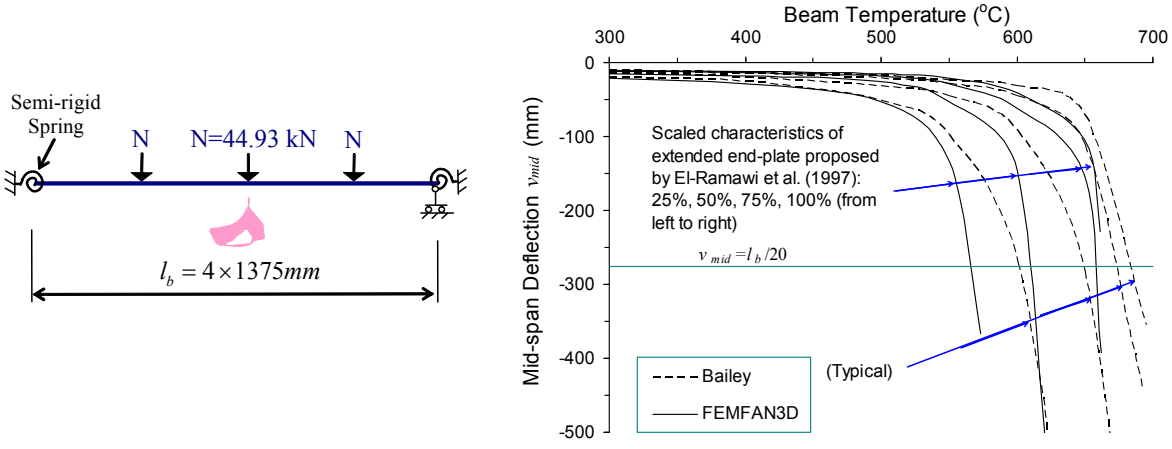

Figure 9. Collapse Process of a Heated Steel Beam with Semi-rigid Connection (Bailey [8])

The mid-span deflection v_{mid} predicted by FEMFAN3D and Bailey is presented in Figure 9b. Adopting $v_{mid} = l_b/20$ as the beam critical state, Figure 9b illustrates that the critical temperature is increased significantly by incorporating the semi-rigid connections. There is very little difference between the predictions pertaining to 75% and 100% connection rigidities. Nonetheless, Figure 9b demonstrates that for the entire four cases, FEMFAN3D predicts smaller critical temperatures than Bailey's results. This is because beyond 500°C, with the plastic zone spreading from the mid-span towards the two ends, EC3 model with no strain-hardening assumes infinitesimal value for tangent modulus E_T^T beyond the yield strength, while Ramberg-Osgood model with strain hardening gives much greater values for E_T^T.

3.5 Experimental Validation

Finally, the program is validated against a plane fire frame test reported by Franssen et al. [31] under fire conditions as few experimental results are available for the behaviour of a space skeletal steel frame in fire. This portal frame consists of two 203×203UC52 columns and one 406×178UB54 beam, all of which are made of grade 43A steel. No test was carried out to measure the actual mechanical properties of steel. Thus, in the first FE analysis, steel yield strength at ambient temperature f_y^{20} is first assumed to be 275 MPa. The frame was analysed using the temperature profiles measured at different parts of the frame.

The development of mid-span defection of the beam v_{mid} is shown in Figure 10. Obviously, the FE analysis slightly overestimates v_{mid} and this is due to: (1) f_y^{20} might be underestimated, and (2) strain-hardening is not considered by EC3 Pt.1.2 stress-strain model. Simply increasing f_y^{20} to 305 MPa will yield a relatively accurate prediction compared to test result (Figure 10).

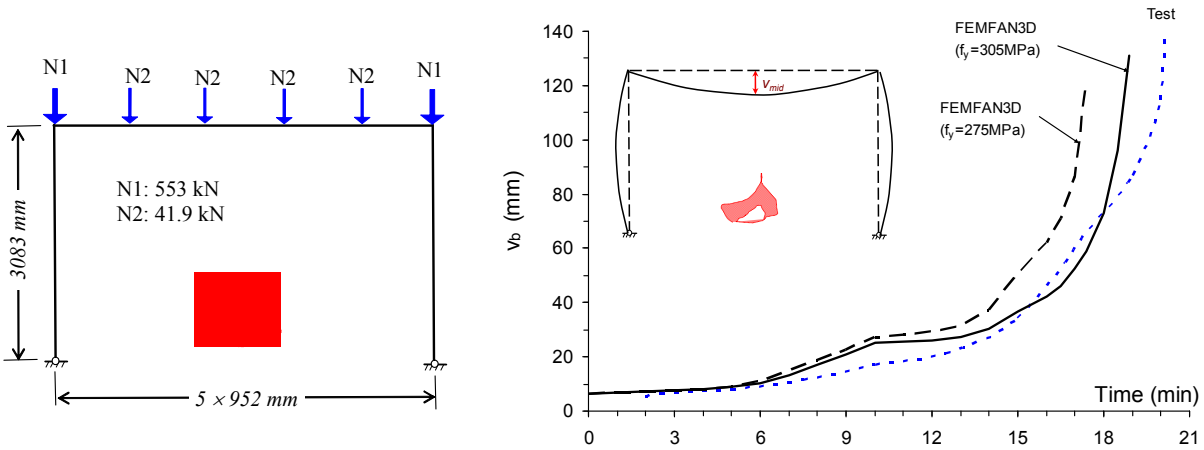

(a) Dimension and Loading (b) Beam Mid-span Deflection

Figure 10. Collapse Process a Portal Frame in an Actual Fire (Franssen [31])

4. CONCLUSIONS

This paper outlines the formulations of a 3D small-strain large-deformation beam-column element being used to simulate the structural response of a skeletal steel frame under fire conditions. The cross-section of a beam-column is divided into segments to simulate the uneven temperature distribution under fire conditions. Creep strain can be included explicitly. Beam-to-column

connections are simulated as semi-rigid springs in the formulation. Five benchmark tests are carried out to verify different aspects of the program, viz., large deformation, creep, effect of semi-rigid connection on the deflection of a heated beam, full collapse process of a space frame at room temperature, and deformation of a plane frame under elevated temperature. In general, good agreement is obtained between numerical predictions and the published results. Unfortunately, validation for space skeletal steel frames in fire was not performed due to the lack of test data. Apart from demonstrating the capability and reliability of the FE program, these verifications also illustrate that response of a structural member in fire is substantially influenced by the interactions among adjoining members.

Development of RC and composite slab element, which is requisite for more accurate simulation of an actual structure, is currently being carried out.

5. ACKNOWLEDGEMENTS

The authors would like to thank Nanyang Technological University for the research grant RGM 28/03 as well as Ministry of Education grant ARC 5/03, without which the conduct of this research will not be possible.

REFERENCES

[1] Huang, Z.F. and Tan, K.H., "Fire Resistance of Compartments within a High-rise Steel Frames: New Sub-frame and Isolated Member Models", J Construct. Steel Res., 2006, Vol. 62, No. 10, pp. 974-986.

[2] Zeng, J.L., Tan, K.H. and Huang, Z.F., "Primary Creep Buckling of Steel Columns in Fire", J. Constuct. Steel Res., 2003, Vol. 59, No. 8, pp. 951-970.

[3] Huang, Z.F. and Tan, K.H., "Analytical Fire Resistance of Axially Restrained Steel Columns", J. Struct. Engng. ASCE, 2003a, Vol. 129, No. 11, pp. 1531-1537.

[4] Huang, Z.F. and Tan, K.H., "Rankine Approach for Fire Resistance of Axially-and-flexurally Restrained Steel Columns", J. Construct. Steel Res., 2003b, Vol. 59, No. 12, pp. 1553-1571.

[5] Wang, Y.C., Lennon, T. and Moore, D.B., "The Behaviour of Steel Frames Subjected to Fire", J. Construct. Steel Res., 1995, Vol. 35, pp. 291-322.

[6] Najjar, S.R. and Burgess, I.W., "A Nonlinear Analysis for Three-dimensional Steel Frames in Fire Conditions", Engng Struct., 1996, Vol. 18, No. 1, pp. 77-89.

[7] Song, L., Izzuddin, B.A., Elnashai, A.S. and Dowling, P.J., "An Integrated Adaptive Environment for Fire and Explosion Analysis of Steel Frames – Part I: Analytical Models", J. Construct. Steel Res., 2000, Vol. 53, pp. 63-85.

[8] Bailey, C.G., "Development of Computer Software to Simulate the Structural Behaviour of Steel-framed Buildings in Fire", Comput & Struct., 1998, Vol. 67, pp. 421-438.

[9] Iu, C.K. and Chan, S.L., "A Simulation-based Large Deflection and Inelastic Analysis of Steel Frames Under Fire", J. Construct. Steel Res., 2004, Vol. 60, pp. 1495-1524.

[10] Iu, C.K., Chan, S.L. and Xiao, X.Z., "Nonlinear Pre-fire and Post-fire Analysis of Steel Frames", Engng Struct., 2005, Vol. 27, pp. 1689-1702.

[11] Ma, K.Y. and Liew, J.Y.R., "Nonlinear Plastic Hinge Analysis of Three-dimensional Steel Frames in Fire", J. Struct. Engng., ASCE, 2004, Vol. 130, No. 7, pp. 981-990.

[12] Bathe, K.J., "Finite Element Procedures", Prentice Hall, Inc., 1996.

[13] Kohnke, P., "ANSYS User's Manual for Revision 5.0, Vol. IV, Theory", Swanson Analysis Systems, Inc., Houston, USA, 1992.

[14] Commission of European Communities(CEC), "Design of Steel Structures: Part 1.2: General Rules – Structural Fire Design (EC3 Pt.1.2", Eurocode 3, Brussels, Belgium, 1995.
[15] Harmathy, T.Z., "Creep Deflection of Metal Beams in Transient Heating Processes, with Particular Reference to Fire", Can. J. Civ. Eng., 1976, Vol. 3, No. 2, pp. 219-228.
[16] Furumura, F. and Shimohara, Y., "Inelastic Behavior of Protected Steel Beams and Frames in Fire", Report of the Research Laboratory of Engineering Materials, 1978, No.3, pp. 1-14, Tokyo Institute of Technology, Japan.
[17] Cheng, W.C., "Theory and Application on the Behaviour of Steel Structures at Elevated Temperatures", Comput & Struct., 1983, Vol. 16, No. 1-4, pp. 27-35.
[18] Tan, K.H., Ting, S.K. and Huang, Z.F., "Visco-Elasto-Plastic Analysis of Steel Frames in Fire", J. Struct. Engng, ASCE, 2002, Vol. 128, No. 1, pp. 105-114.
[19] Huang, Z.F,, Tan, K.H. and Ting, S.K., "Heating Rate and Boundary Restraint Effects on Fire Resistance of Steel Columns with Creep", Engng Struct., 2006, Vol. 28, No. 6, pp. 805-817.
[20] Harmathy, T.Z., "A Comprehensive Creep Model", J. Basic Engng Trans., ASME, 1967, Vol. 89, pp. 469-502.
[21] Dorn, J.E., "Some Fundamental Experiments on High Temperature Creep", J. Mech. & Phys Solids, 1954, Vol. 3, pp. 85-116.
[22] Levy, A., "High-Temperature Inelastic Analysis", Comput & Struct., 1984, Vol. 13, pp. 249-256.
[23] El-Rimawi, J.A., Burgess, I.W. and Plank, R.J., "The Influence of Connection Stiffness on the Behaviour of Steel Beams in Fire", J. Construct. Steel Res., 1997, Vol. 43, No. 1-3, pp. 1-15.
[24] El-Rimawi, J.A., Burgess, I.W. and Plank, R.J., "The Treatment of Strain Reversal in Structural Members During the Cooling Phase of a Fire", J. Construct. Steel Res., 1996, Vol. 37, No. 2, pp. 115-135.
[25] ABAQUS, "Standard Verification Manual, Version 5.5", Hibbitt, Karlsson & Sorensen, Inc., 1995.
[26] Najjar, S.R., Three-Dimensional Analysis of Steel Frames and Subframes in Fire, Ph.D. thesis, Sheffield University, U.K, 1994.
[27] Franssen, J.M., "The Unloading of Building Materials Submitted to Fire", Fire Saf. J., 1990, Vol. 16, pp. 213-227.
[28] Morino, S. and Lu, L.W., "Analysis of Space Frames", Fritz Engineering Laboratory, Report No. 331.13., 1971.
[29] BSI, "Code of Practice for Fire Resistant Design: Structural Use of steelwork in Building, Part 8, BS5950", London, UK, 1990.
[30] EI-Rimawi, J.A., Burgess, I.W. and Plank, R.J., "The Influence of Connection Stiffness on the Behaviour of Steel Beams in Fire", J. Construct. Steel Res., 1997, Vol. 43, No. 1-3, pp. 1-15.
[31] Franssen, J.M., Cooke, G.M.E. and Latham, D.J., "Numerical Simulation of a Full Scale Fire Test on a Loaded Steel Framework", J. Construct. Steel Res., 1995, Vol. 35, pp. 377-408.

Nomenclature

A=	Area (m^2);
E_0=	Elastic modulus at ambient temperature (MPa);
E_0^T=	Elastic modulus at elevated temperature T;
E_T^T=	Tangent modulus at elevated temperature T;
f_y^{20} =	Yield strength at ambient temperature (MPa);
f_y^T=	Yield strength at elevated temperature T (MPa);
$\mathbf{K_T}$=	Frame global tangent stiffness matrix;
l=	Length of a beam/column (m);
N=	External load (N);
P=	Applied axial load (N);
r_S=	radius of gyration about strong axis;
R=	Gas Constant (J/mol·K) or, utilization factor (CEC 1995);
S=	Second Kirchhoff stress;
t=	Time;
T=	Temperature (°C);
T'=	Absolute temperature (Rankine);
u_0, v_0, w_0 =	Translations at centroid of a cross-section;
u, v, w =	Translations at a specific point within a cross-section;
v_{mid} =	Mid-span deflection on a beam (m);
θ=	Temperature compensated time (hr);
ε_{cr}^* =	Compounded creep strain (Harmathy, 1976);
$\dot{\varepsilon}_{cr}$ =	Creep strain rate;
ε_y^T=	Yielding strain at elevated temperature T;
λ=	Slenderness ratio;
$\mathbf{\Delta Q}$=	Vector of out-of-balance forces (kN);
$\mathbf{\Delta q}$=	Vector of increments displacements (m);
Subscript	
0	At centroid of a section;
z	Longitudinal coordinate.

NUMERICAL SIMULATION OF HOLLOW AND CONCRETE-FILLED STEEL COLUMNS

Shengbin Gao[1] and Hanbin Ge[2,*]

[1] *Associate Professor, Department of Civil Engineering, Shanghai Jiao Tong University, Shanghai 200240, China*
[2] *Associate Professor, Department of Civil Engineering, Nagoya University, Nagoya 464-8603, Japan*
(Corresponding author: E-mail: ge@civil.nagoya-u.ac.jp)

Received: 5 September 2006; Revised: 30 March 2007; Accepted: 4 April 2007

ABSTRACT: This paper aims to predict the inelastic behavior of thin-walled steel and composite structures, such as hollow and concrete-filled steel columns. For this purpose, a three-dimensional (3D) elasto-plastic finite element analysis methodology has been presented for both thin-walled steel columns with pipe and box-shaped sections, and concrete-filled steel box columns. By comparing with experimental result, it is concluded that the proposed analytical method can give an accurate prediction to the experimental results of both steel and composite structures.

Keywords: Steel column; concrete-filled steel column; interface element; cyclic loading; elasto-plastic behavior; buckling mode

1. INTRODUCTION

Cantilever steel hollow and concrete-filled columns (CFT) have been widely designed and used as bridge piers in many countries. Such cantilever type bridge piers occupy less space and thus allow the free traffic flow in the roads below the highways. Moreover, concrete-filled steel columns can provide excellent seismic resistant behavior, such as high strength, high ductility, and large energy absorption capacity. As a result, various researches on these types of structures have been conducted in recent years (Gao et al. [1]; Ge and Usami [2, 3]; Ge et al. [4, 5]; Morino [6]; Schneider [7]; Susantha et al. [8, 9]; Hu et al. [10]). Figure 1 shows a view of steel box-section bridge pier damaged during Hyogoken-nanbu earthquake near Kobe city in Japan on January 17, 1995.

Figure 1. Steel Box Section Bridge Pier Damaged During Hyogoken-nanbu Earthquake Near Kobe City in Japan on January 17, 1995

A clear understanding of inelastic behavior is very important in developing a seismic design methodology for these structures. To this end, the load-displacement curves of the structures play a very important role. To date, fiber model analysis is usually considered as an effective and convenient approach for capacity prediction of structures (Susantha et al. [8, 9]). However, this concept without considering local buckling of steel members or interaction between steel-concrete interfaces of composite members needs an additional criterion to determine the ultimate state. On the other hand, three dimensional approaches are very limited because of time-consuming of such analyses and complicated modeling in the case of composite structures. As the rapid development of computers and the spread of use of structural analysis software packages, the 3D analysis will be widely used to better understand inelastic behavior of complicated structures.

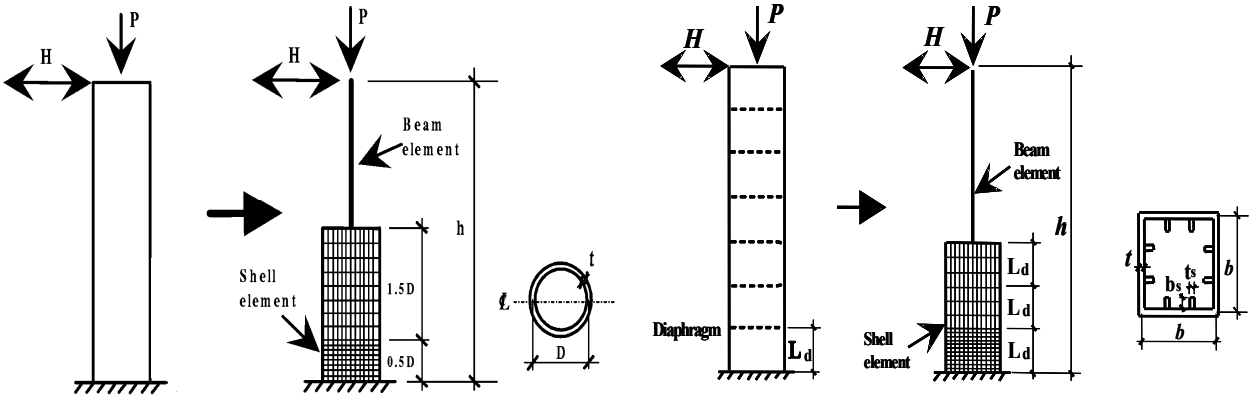

(a) Pipe Section Column (Pl) (b) Box Section Column (KD-5)

Figure 2. Analytical Models of Steel Columns

This paper presents a three-dimensional finite element analysis methodology for determining the load-displacement relation of steel and composite structures under either monotonic or cyclic loading. For this purpose, a software package DIANA [11] is employed. The structures analyzed are hollow steel columns with pipe and box sections, as well as concrete-filled steel box columns. The results of the analysis are compared with those of the experiments. It is found that the presented analysis methodology can give an accurate prediction to the experimental results in cases of both steel and concrete-filled steel box columns.

2. CYCLIC BEHAVIOR OF HOLLOW STEEL COLUMNS

2.1 Analytical Model

Two kinds of steel columns (Nakamura et al. [12]; Nishikawa et al. [13]), as shown in Figure 2 are adopted in this analysis. For thin-walled steel columns of uniform pipe-sections and box-sections subjected to constant axial load and cyclic lateral displacement, local buckling generally occurs near the base of the columns. Therefore, shell elements that can consider local buckling are employed for the lower part of the column. The upper part of the column is modeled using beam-column elements. For the beam-column elements, the spread of plasticity is accounted for both through the cross-section and along the member length. The element type is 3-node open section beam element (CL18B).

For the shell elements, the spread of plasticity is considered through the thickness and the plane of the element. The element type is a four-node curved shell element (Q20SH) that has four integration points within the plane and five integration points across the thickness.

Half of the column is modeled due to the symmetry of both geometry and loading. With respect to the mesh division of column P1, the length from the base which equals to the radius of the column is divided into 15 segments, while the following length of 3 times of the radius is only subdivided into 10 segments along the column length. In the circumferential direction, both are divided into 16 segments. For the beam-column elements, it is divided into 10 segments. Therefore, the analytical model of column P1 consists of 400 shell elements and 10 beam-column elements. In addition, a stiff plate with infinite bending stiffness is assumed in the interface between the beam-column elements and shell elements. A similar mesh division method is applied to the steel box-sectional column KD-5. It is noted here that the longitudinal stiffener should be divided into more than 3 meshes in width direction in order to consider its buckling behavior.

The modified Newton iteration technique coupled with the displacement control method is used in the analysis. The energy convergence criterion is adopted in the analysis and the convergence tolerance is taken as 10^{-5}. The initial geometrical deflections and residual stresses are not taken into consideration.

2.2 Geometrical and Material Properties

The tested specimen P1 has a slenderness ratio parameter of $\bar{\lambda}$ = 0.26 and radius-thickness ratio parameter of R_t = 0.11 (Nishikawa et al. [13]; Gao et al. [1]). The main dimensions and material properties are: h = column height = 3403 mm; r = radius of gyration of cross section = 315 mm; σ_y = yield stress = 289.6 MPa; E = Young's modulus = 206 GPa; υ = Poisson's ratio = 0.3; D = diameter of the column = 891 mm; and t = thickness = 9 mm. During the test, the column is subjected to a constant axial load of P/P_y = 0.12 and cyclic horizontal displacement at the tip. Here, P_y denotes the squash load.

The tested specimen KD-5 has a flange plate width-thickness ratio parameter of R_f =0.45 and column slenderness ratio parameter of $\bar{\lambda}$ =0.30 (Nakamura et al. [12]; Ge et al. [5]). The dimensions of column KD-5 are: h=3303mm; flange and web width b=738mm; flange and web thickness t=12mm; stiffener width b_s=90mm; stiffener thickness t_s=9mm. The material properties are: σ_y = 350.2 MPa; E = 206 GPa; υ = 0.3. Moreover, P/P_y = 0.166.

The kinematic hardening constitutive model is employed in this analysis. The hardening rates of the employed bi-linear stress-strain relation are assumed as E'/E = 1/100, which approximately equals to the slope of the line joining the initial yield point to the loading point corresponding to 5% axial strain.

2.3 Comparison of Hysteretic Curves

The curves of nondimensionalized horizontal load, H/H_y, versus horizontal displacement, δ/δ_y, from both the experiment and analysis are shown in Figure 3. The notations, H_y and δ_y, represent

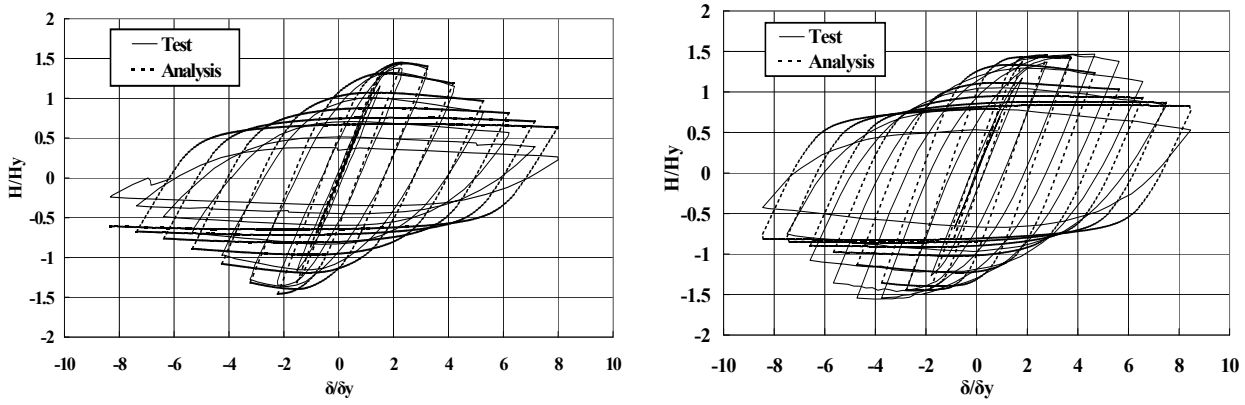

(a) Pipe Section Column (Pl) (b) Box Section Column (KD-5)

Figure 3. Comparison of Load - Displacement Relation of Steel Columns

respectively the yield load and yield displacement considering the effect of axial load (Gao et al. [1]).

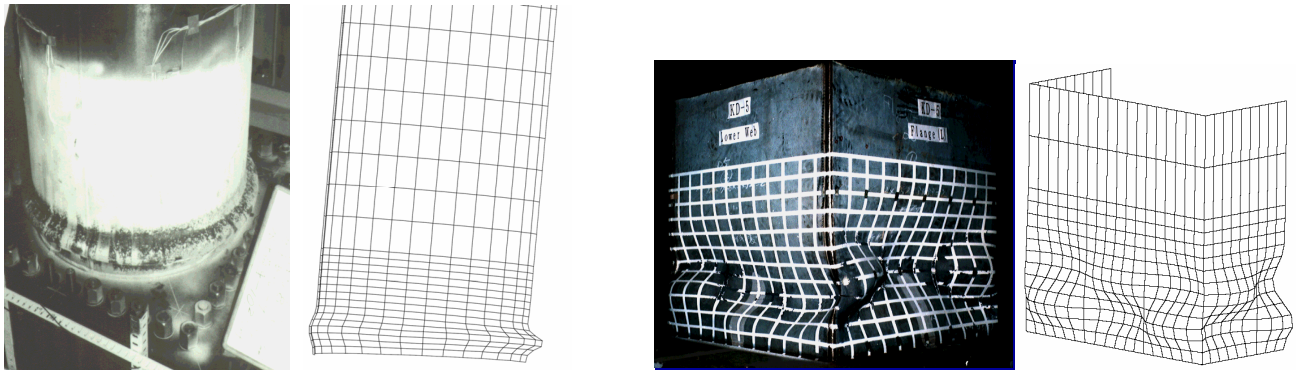

Experiment Analysis Experiment Analysis

(a) Pipe section Column (Pl) (b) Box Section Column (KD-5)

Figure 4. Comparisons of Buckling Modes of Steel Columns

Figure 3(a) shows the comparison of hysteretic curves between the present analysis and the experimental result of column P1. It is observed that the shape of the hysteretic loops and the ultimate strength obtained from the present analysis is in good agreement with the experimental result. Comparison of hysteretic curves of the column KD-5 is shown in Figure 3(b). The ultimate strength of the present analysis coincides well with the experiment although the post-buckling strength of the analysis is a little lower than the experiment. This indicates that the developed FEM formulation can accurately predict the cyclic behavior of such steel structures.

2.4 Comparison of Local Buckling Modes

Figure 4 shows the local buckling modes obtained from both the experiment and analysis, respectively. It is observed that the buckling mode of either the column P1 or column KD-5 is almost the same as that of the corresponding test specimen. The part near the base of the pipe column P1 bulged outward and a half sine-wave is formed, while in the box column KD-5, the outward and inward buckling mode for both flange and web plates similar to that of the experiment is well simulated.

3. PURE COMPRESSION BEHAVIOR OF CONCRETE-FILLED STEEL COLUMN

3.1 Analytical Model

The analytical model shown in Figure 5 is a concrete-filled thin-walled steel stub-column of box shape (Ge and Usami [2]). Due to its symmetry, one-eighth of the column is taken for the analysis. The mesh division is shown in Figure 5(b). 8×8 meshes are employed across the cross section and 10 divisions are made along the axial direction. In the analytical model, eight-node linear solid element is employed to model concrete part. Four-node isoparametric shell element is used for steel plate panel. The position of the shell element is set at the center line of the steel plate panel.

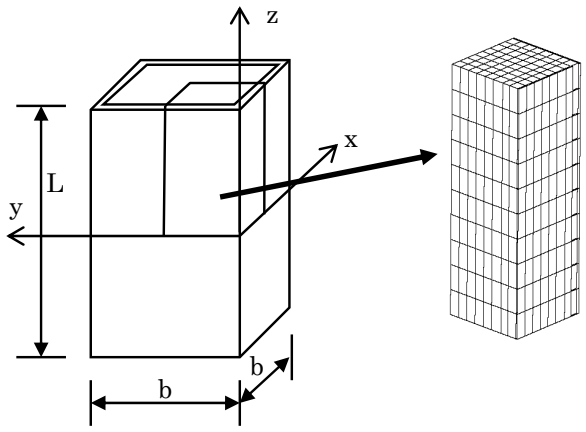

(a) Specimen U12-C (b) Mesh Division

Figure 5. Analytical Model of Concrete-filled Steel Column under Pure Compression

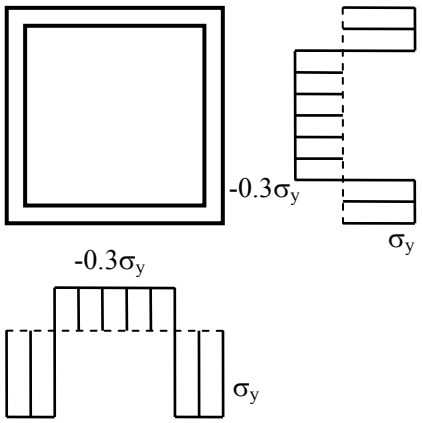

Figure 6. Distribution of Residual Stresses of Specimen U12-C due to Welding

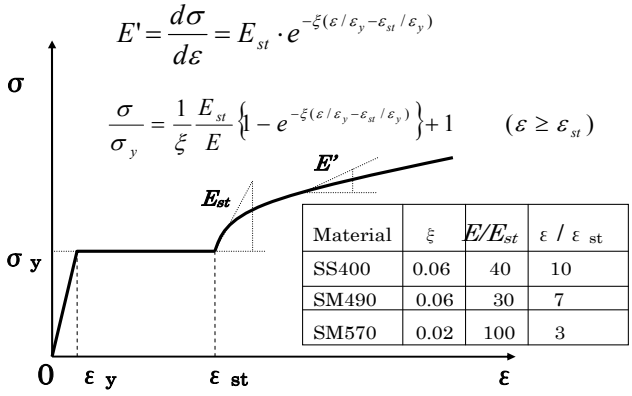

Figure 7. Uniaxial Stress-strain Relation for Steel

Plane interface element is used to model the interaction between steel and concrete. The plane interface element is an isoparametric element between two planes in a three-dimensional configuration, with which the interface surface and directions are evaluated automatically from the geometry of the element itself. In this analysis, the initial out-of-flatness is not taken into consideration due to its negligible effect on the ultimate strength (Ge and Usami [2]). An idealized form of residual stresses pattern of the plate panel due to welding is employed, as shown in Figure 6 (Chen and Ross [14]).

3.2 Material Properties

The von Mises yield criterion is adopted to consider the material property of the steel plate. As shown in Figure 7, strain hardening of the steel is taken into consideration (Usami and Ge [15]), 1998). A nonlinear elastic constitutive law of the interface element is employed to model the interaction behavior between the steel plate and the concrete. It is assumed here that the interface element behaves elastically in compressive regime, but it can not resist shear stresses as well as tensile stresses.

The Drucker-Prager type yield surface with 10 degree of friction angle is used for concrete. To investigate the effect of the lateral confinement on concrete, two types of uniaxial stress versus strain relations of concrete (i.e., unconfined and confined concrete) are employed. The uniaxial stress-strain relation of the unconfined concrete ("Concrete Standard Specification" [16]) is shown in Figure 8(a). Here, fc denotes the uniaxial strength and ε_c is the corresponding strain of the unconfined concrete. When concrete is subjected to laterally confining pressure, both the uniaxial strength f_{cc} and the corresponding strain ε_{cc} will be larger than those of unconfined concrete. The relations between f_{cc}, f_c and between ε_{cc}, ε_c are proposed by Mander et al. [17] and Hu et al. [10] as follows (Figure 8(a)).

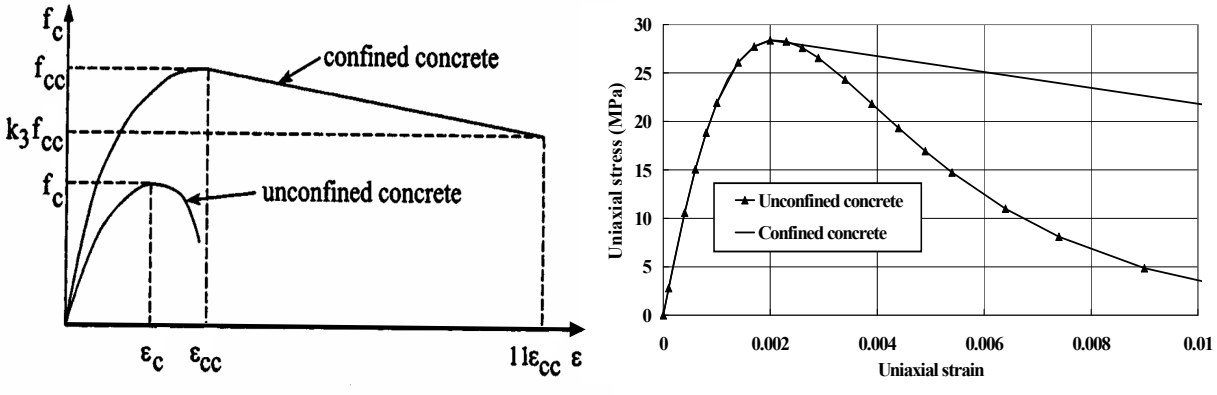

(a) Sketch (b) Input Curve

Figure 8. Uniaxial Stress Versus Strain Relations for Concrete

$$f_{cc} = f_c + k_1 f_l \tag{1}$$

$$\varepsilon_{cc} = \varepsilon_c (1 + k_2 \frac{f_l}{f_c}) \tag{2}$$

$$f_l / \sigma_y = 0.055048 - 0.001885 \ (b/t) \qquad (17 \le b/t \le 29.2) \tag{3}$$

$$= 0.0 \qquad (29.2 \le b/t \le 150)$$

Here, f_l represents the confining pressure around the concrete core. k_1 and k_2 are constants which were set as 4.1 and 20.5 based on the study of Richart et al. [18]. b denotes the flange width and t is the flange thickness. When the strain is larger than peak strain ε_{cc}, a linear descending line is used to model the softening behavior of concrete. The strength degradation parameter corresponding to $11\varepsilon_{cc}$ for CFT columns with box-section is calculated as follows.

$$k_3 = 0.000178 \ (b/t)^2 - 0.02492 \ (b/t) + 1.2722 \qquad (17 \le b/t \le 70) \tag{4}$$

$$= \quad 0.4 \qquad (70 \le b/t \le 150)$$

According to the above formula, the uniaxial stress- strain curve of confined concrete is shown in Figure 8(b). Because the value of *b/t* of Specimen U12-C is 58.3 (Here, flange width *b*=263mm; plate thickness *t*=4.51mm), the peak stress of confined concrete has the same value as that of unconfined concrete. The main difference between confined concrete and unconfined concrete lies in that the stress deterioration slope of confined concrete is much larger than that of unconfined concrete, as stated in Eqn. 4 and Figure 8(b).

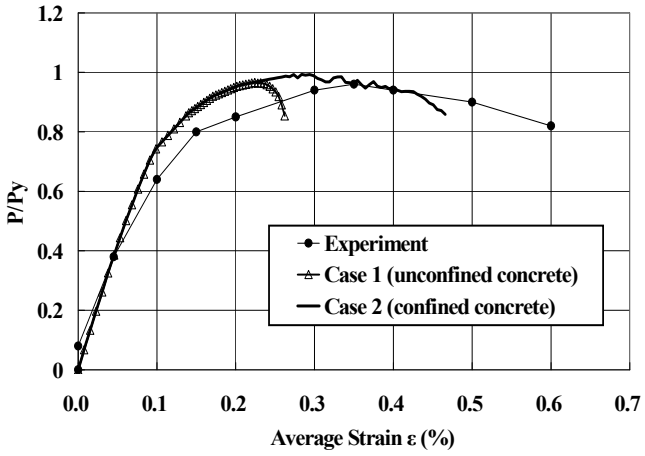

Figure 9. Computed Load-average Strain Curves of Concrete-filled Steel Column under Compression

3.3 Analytical Results

The analytical results of nondimensionized axial load, P/P_y, versus average strain are shown in Figure 9. Here, P_y is the squash load of concrete-filled columns (Ge and Usami [2]). It is observed

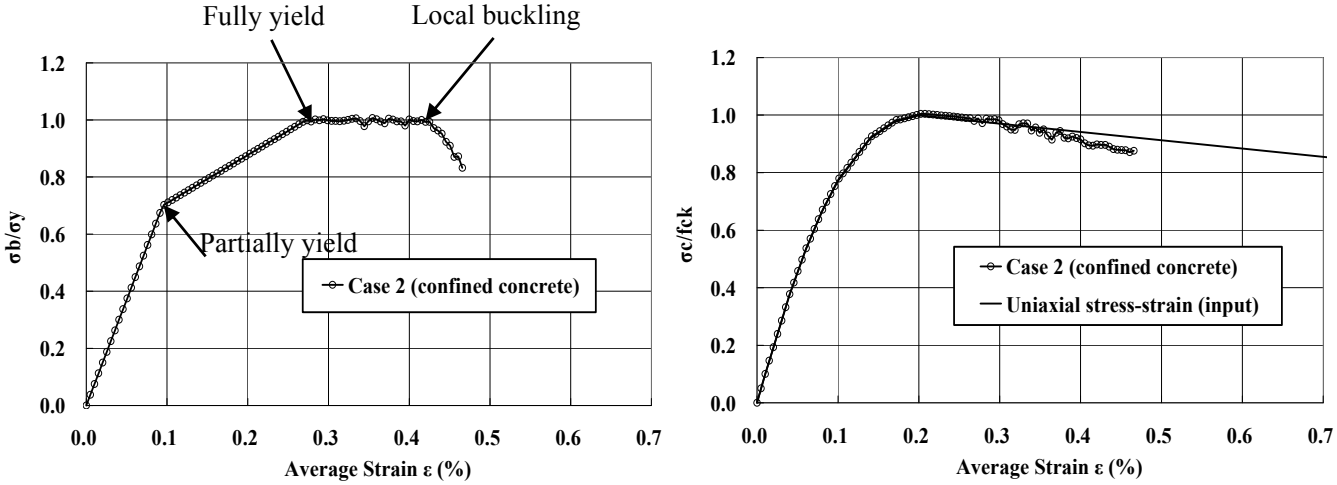

(a) Steel (b) Concrete

Figure 10. Computed Average Stress -Average Strain Curves of Steel and Concrete member

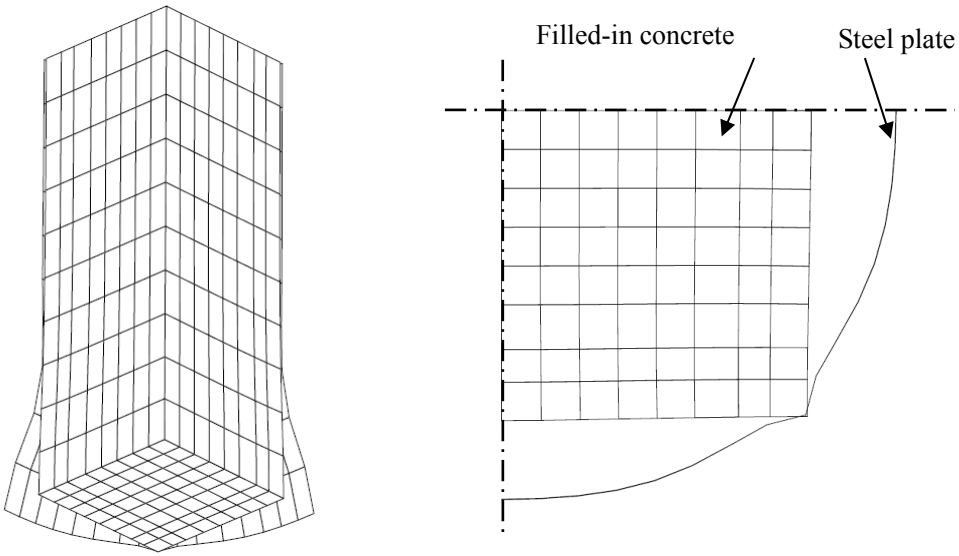

(a) Elevation View (b) Plane View

Figure 11. Local Buckling Mode of Case 2 at Final Step (Opening of Interface Element)

that both the analyses of Case 1 and Case 2 well predict the ultimate strength of the experiment. However, the post-peak strength decreases rapidly in the analysis of Case 1. On the contrary, the analytical result of Case 2 shows a gentle strength deterioration behavior at post-peak stage, which coincides well with the experimental result. Comparisons of computed load-average strain curves between Case 1 and Case 2 indicate that the lateral confinement pressure of steel plate have a large influence on the post-peak behavior of the concrete-filled steel column.

Figure 10 shows the computed average stress-average strain curves of steel and concrete members, respectively. Figure 10(a) clearly illustrates 3 stages of the steel members, that is, partially yield stage, fully yield stage, and finally the stage of local buckling. It is noted that partially yield stage appears only when the residual stresses are accounted for in the analysis. The local buckling

mode of Case 2 at final step is shown in Figure 11 (Deformation scale is 3.0). It is observed that local buckling arises at the mid-span of the compressed column.

4. BENDING BEHAVIOR OF PARTIALLY CONCRETE-FILLED STEEL COLUMN

4.1 Analytical Model

The analytical model of a concrete-filled steel column with box shape UC70-25-3[0] (Ge et al. [4]; Ge and Usami [3]) is shown in Figure 12. Due to its symmetry, half of the column is modeled. The same element types as those stated in previous section are employed to model the concrete part (solid element), steel part (shell element), as well as the interaction behavior between steel and concrete (interface element). Moreover, the filled-in concrete is also possible to detach from the base plate and diaphragm. Nonlinear interface elements are set up between the concrete and base plate, diaphragm.

4.2 Geometrical and Material Properties

The main geometrical properties of this specimen are: R_f=0.75, $\bar{\lambda}$=0.276, flange width B=738mm, web width D=157mm, flange and web thickness t=5.87mm, column length h=788mm, length of filled-in concrete from the base l_c=236mm. The uniaxial stress-strain relations for steel (see Figure 7) and confined concrete (see Figure 8(b)) are adopted, with the following material properties: σ_y = 308 MPa; E = 211 GPa; υ = 0.27, E_{st}= 5.83GPa, and ε_{st}=2.01% for steel, f_c = 36.4 MPa; E = 24.2 GPa; υ = 0.158 for concrete. Moreover, the applied axial load ratio P/P_y is 0.20.

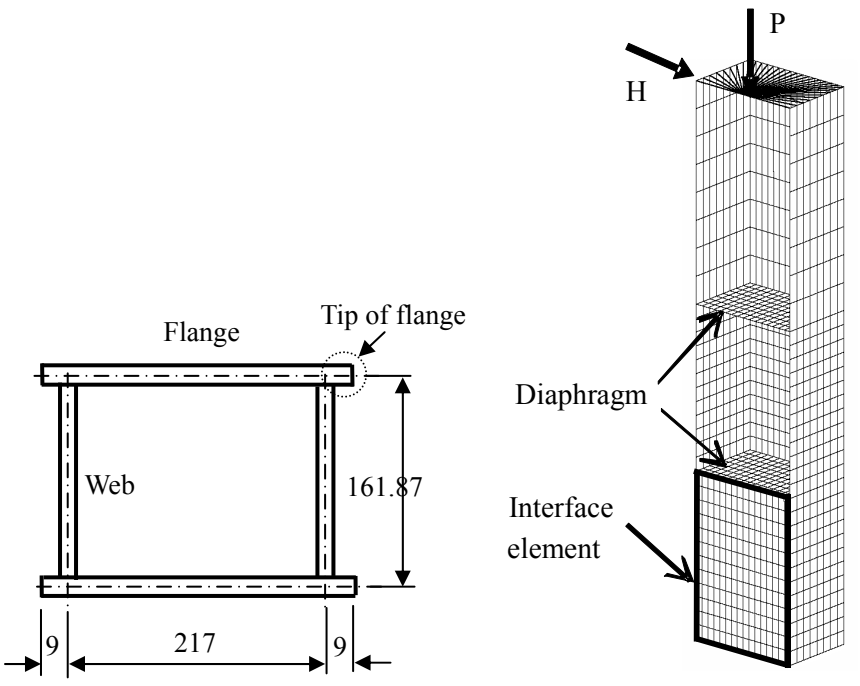

(a) Cross Section (b) Analytical Model

Figure 12. Analytical Model of Partially Concrete-filled Specimen UC70-25-3[0] under Combined Compression and Bending

As given in Table 1, three cases are considered in the analysis. The steel column without filled-in concrete is analyzed in Case 1. The difference between Case 2 and Case 3 is the material behavior of interface element. The interface element in Case 2 can only resist compressive stress. The interface element will open (that is to say, the stress becomes zero) as soon as tensile stress arises. The elastic compressive and tension behavior of the interface element is assumed in Case 3.

Table 1. Analytical Cases

Case No.	Interface Behavior	Remarks
Case 1	—	Only steel part is considered.
Case 2	Only compressive stresses can be transferred in the interface element	—
Case 3	Both compressive and tensile stresses can be transferred in the interface element	—

4.3 Analytical Results

Comparison of nondimensionalized horizontal load versus horizontal displacement relation is shown in Figure 13. It is observed that Case 1 reaches peak load (H/H_y =1.06) at $\delta / \delta y$=1.9. The local buckling occurred at the column base, as shown in Figure 14(a). Compared with Case 1, Case 2 predicts a higher ultimate strength of H/H_y=1.45. Due to the existence of concrete, the inward local buckling at the column base is prevented at Case 2. The flange plate above the concrete-filled part deforms inwards (see Figure 14(b)). The ultimate strength predicted by Case 2 coincides well with the experiment. However, Case 2 diverges at the moment when the analysis enters the post-peak regime. The divergence reason is due to the lateral detachment of steel part from concrete part, as shown in Figure 14(c).

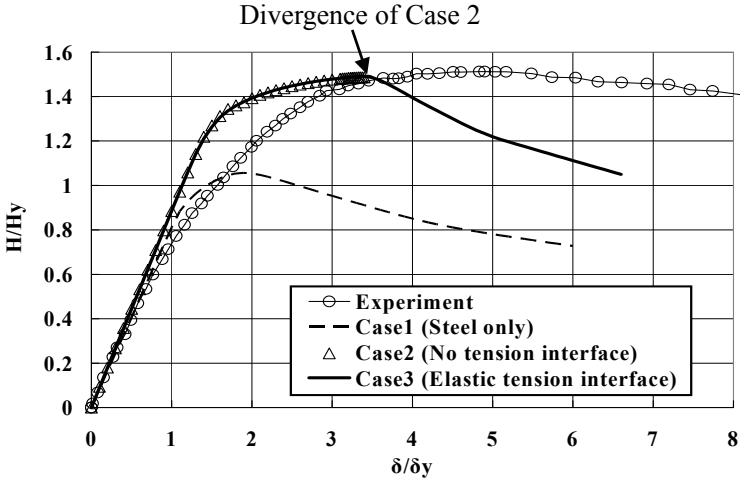

Figure 13. Comparison of Load-displacement Relation of Partially Concrete-filled Specimen UC70-25-3[0] under Combined Compression and Bending

Case 3 successfully predicts both the ultimate strength and post-peak behavior although the predicted post-peak strength is a little lower than that of the experiment. The possible reason is due to the simplification of the assumed elastic compressive and tension behavior in modeling the interface element. The buckling mode of Case 3 coincides well with the experiment (see Figure 15). The local buckling occurs at the position just above the concrete-filled part. Comparison of Case 2 with Case 3 demonstrates that the material property of interface element is a key point in predicting the post-peak behavior of concrete filled-in steel column. Further research is needed to focus on the evaluation of tensile stress that the interface element can really resist.

5. CONCLUSIONS

This paper addresses an elasto-plastic large deformation formulation of hollow and concrete-filled steel columns. Based on the analytical results, the following conclusions can be drawn.

1. The predicted hysteretic curve and buckling mode of steel structures such as the pipe specimen P1 and box specimen KD-5 coincide well with the experimental results.

2. The present analysis gives accurate predictions to the ultimate strength of concrete-filled steel structures. The lateral confinement pressure can not be neglected in predicting the post-peak behavior of axial compressed concrete filled-in steel column.
3. The interaction treatment between the steel and concrete is very important in predicting the post-buckling behavior of partially concrete filled-in steel column subjected to combined compression and bending.

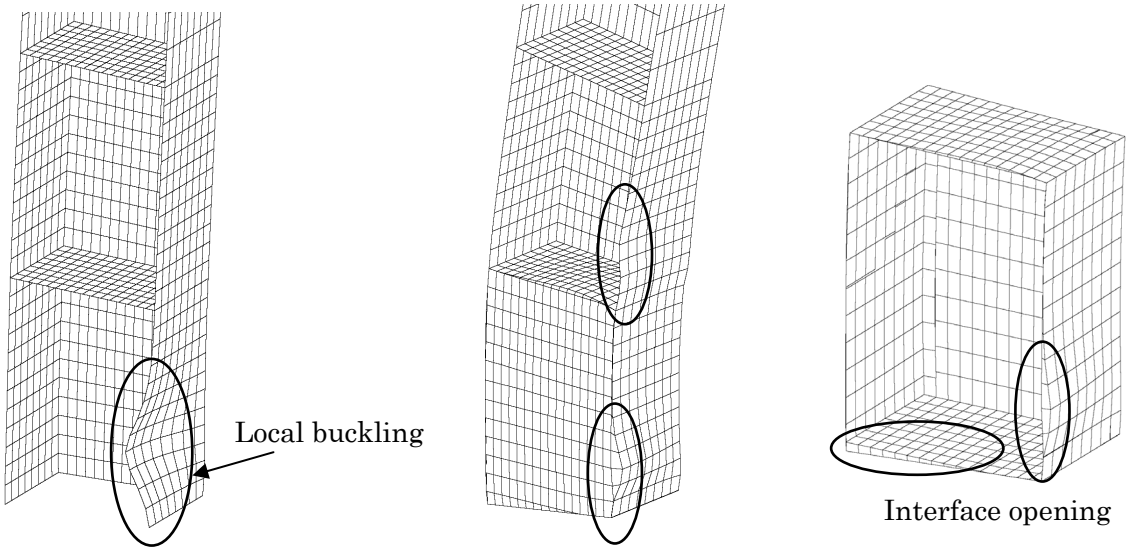

(a) Buckling Mode of Case 1 (b) Total Deformation of Case 2 (c) Interface Opening of Case 2

Figure 14. Comparison of Deformation Mode of Partially Concrete-filled Specimen UC70-25-3[0] under Combined Compression and Bending

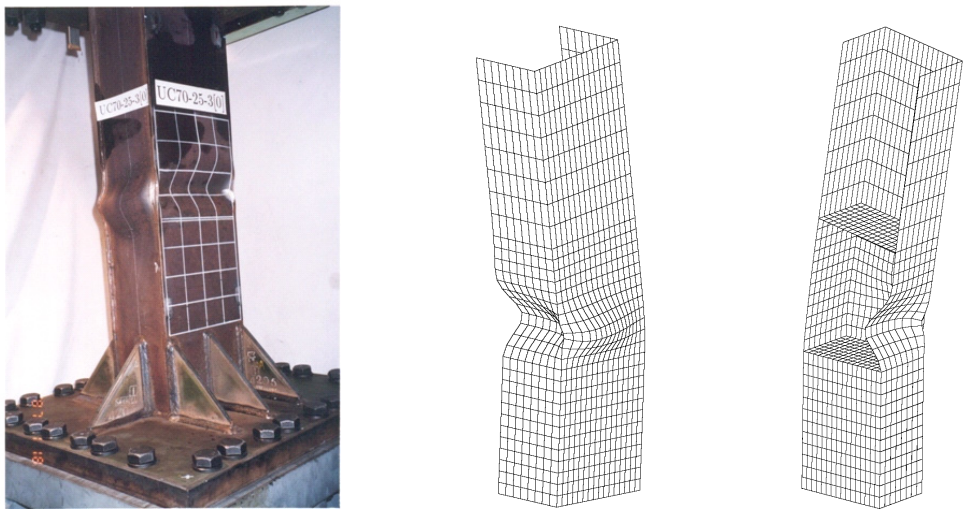

(a) Experiment (b) Analysis

Figure 15. Comparison of Buckling Mode between Experiment and Case 3

Further researches are needed to focus on the evaluation of tensile stress that the interface element can really resist, as well as a series of parametric studies to evaluate the ultimate strength and ductility behavior of such concrete filled-in steel columns.

REFERENCES

[1] Gao, S.B., Usami, T. and Ge, H.B., "Ductility Evaluation of Steel Bridge Piers with Pipe-sections", Journal of Engineering Mechanics, ASCE, 1998, Vol. 124, No. 3, pp. 260-267.

[2] Ge, H.B. and Usami, T., "Strength Analysis of Concrete-filled Thin-walled Steel Box Columns", Journal of Construction Steel Research, 1994, Vol. 30, pp. 259-281.

[3] Ge, H.B. and Usami, T., "Cyclic Tests of Concrete-filled Steel Box Columns", Journal of Structural Engineering, ASCE, 1996, Vol. 122, No. 10, pp. 1169-1177.

[4] Ge, H.B., Usami, T. and Toya, K., "A Study on Strength and Deformation Capacity of Concrete-filled Steel Columns under Cyclic Loading", Journal of Structural Engineering, JSCE, 1994, 40A, pp.163-176. (in Japanese)

[5] Ge, H.B., Gao, S.B. and Usami, T., "Stiffened Steel Box Columns. Part 1: Cyclic Behavior", Earthquake Engineering and Structural Dynamics, 2000, Vol. 29, pp. 1691-1706.

[6] Morino, S., "Recent Developments in Hybrid Structures in Japan—Research, Design, and Construction", Engineering Structures, 1998, Vol. 20, No. 4-6, pp. 336-346.

[7] Schneider, S.P., "Axial Loaded Concrete-filled Steel Tubes", Journal of Structural Engineering, ASCE, 1998, Vol. 124, No. 10, pp. 1125-1138.

[8] Susantha, K.A.S., Ge, H.B. and Usami, T., "A Capacity Prediction Procedure for Concrete-filled Steel Columns", Journal of Earthquake Engineering, 2001, Vol. 5, No. 4, pp.483-520.

[9] Susantha, K.A.S., Ge, H.B. and Usami, T., "Cyclic Analysis and Capacity Prediction of Concrete-filled Steel Box Columns", Earthquake Engineering and Structural Dynamics, 2002, Vol. 31, pp. 195-216.

[10] Hu, H.T., Huang, C.S., Wu, M.H. and Wu, Y.M., "Nonlinear Analysis of Axially Loaded Concrete-filled Tube Columns with Confinement Effect", Journal of Structural Engineering, ASCE, 2003, Vol. 129, No. 10, pp.1322-1329.

[11] DIANA User's Manual. Ver. 9.1, 2005.

[12] Nakamura, S., Yasunami, H., Kobayashi, Y., Nakagawa, T. and Mizutani, S., "An Experimental Study on the Seismic Performance of Steel Bridge Piers with Less Stiffened and Compact Sized Section", Proceeding of Nonlinear Numerical Analysis and Seismic Design of Steel Bridge Piers, JSCE, 1997, pp. 331-338.

[13] Nishikawa, K., Yamamoto, S., Natori, T., Terao, O., Yasunami, H. and Terada, M., "An Experimental Study on Improvement of Seismic Performance of Existing Steel Bridge Piers", Journal of Structural Engineering, JSCE, 1996, Vol. 42A, pp. 975-986. (in Japanese)

[14] Chen, W.F. and Ross, D.A., "Test of Fabricated Tubular Columns", Journal of Structural Division, ASCE, 1977, Vol. 103(ST3), pp. 619-634.

[15] Usami, T. and Ge, H.B., "Cyclic Behavior of Thin-walled Steel Structures—Numerical Analysis", Thin Walled Structures, 1998, Vol. 32, No. 1/3, pp. 41-80.

[16] Japan Concrete Standard Specification. Aseismic Performance Verification Part, 2002. (in Japanese)

[17] Mander, J.B., Priestley, M.J.N. and Park, R., "Theoretically Stress-strain Model for Confined Concrete", Journal of Structural Engineering, ASCE, 1988, Vol. 114, No. 8, pp.1804-1826.

[18] Richart, F.E., Brandtzaeg, A. and Brown, R.L., "A Study of the Failure of Concrete under Combined Compressive Stresses", Bulletin 185, University of Illinois Engineering Experimental Station, Champaign, III, 1928.

DYNAMIC STABILITY ANALYSIS OF BEAM STRING STRUCTURES UNDER EARTHQUAKE LOADS

Qinghua Han[1,*], Chenyin Ma[1], Jingyu Zhang[2]

[1]*Department of Civil Engineering, Tianjin University, Tianjin, 300072, China*
[2]*Department of Mechanical Engineering, Tianjin University of Technology, Tianjin, 300191, China*
**(Corresponding author: Email: qhhan@tju.edu.cn)*

Received: 1 July 2005; Revised: 10 April 2007; Accepted: 18 April 2007

ABSTRACT: Beam String Structure (BSS) is composed of an upper structural member, lower strings and struts, which is a new type of long-span hybrid structure. The study on the static behavior is extensive. However, there is still a certain extent of blank in the field of dynamics, especially the dynamic stability. Owing to the limitation of the existing dynamic stability judgment criterion, most of which are based on Lyapunov dynamic stability theory and the highly nonlinear earthquake response of BSS, the nonlinear finite element analysis and time history method (THD) are adopted. THD is effective to the highly nonlinear structures. Based on the displacement time history curves and structural deformation, the critical load of dynamic stability was obtained. The dynamic stability of the plane BSS is analyzed under earthquake loads in respect of the number of struts, height-span ratio, sag-span ratio, moment of inertia, prestressing force of string and restraint type of supports. The results are compared with those of static stability. Some suggestions are put forward to selecting a proper structural model and analysis in project design.

Keywords: Beam string structure; dynamic stability; earthquake loads; non-linear earthquake response; time history method; cable

1. INTRODUCTION

Beam String Structure [1] (BSS) is a new type of space structure, which is composed of an upper structural member, lower steel cables and struts. As shown in Figure 1, the upper structural member may be a beam, an arch, a plane truss or a solid truss and so on [2]. Applying pretension force to lower steel cables [3] causes the structure to deform to an inverted arch, which decreases the deflection of the structuresignificantly. On the other hand, horizontal thrust of the arch springing is offset by steel cables; consequently, both the stress dominance of the arched-type structure and the high tensile performance of the cables are displayed sufficiently. In the past decades, this type of Beam String Structure was accepted extensively all over the world [4]. For example, the steel box beam added with lower cables, a type of BSS, was adopted for the Basketball Arena of Badalona which was built for the Barcelona Olympic Games in 1992. In China, another type of BSS, the internal structure of solid cable-truss of the Guangzhou International Convention and Exhibition Center (GICEC) is shown in Figure 2, the structural span of which is 126.6m. The study on static behavior and the analysis of BSS are extensive [5-9]. However, as a new type of space structure, the domestic and overseas studies in the problem of dynamic stability of BSS are still in the initial stage.

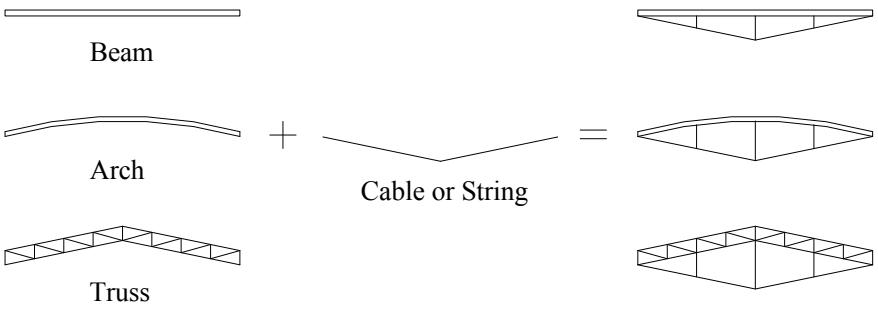

Figure 1. Forming Sketch of BSS

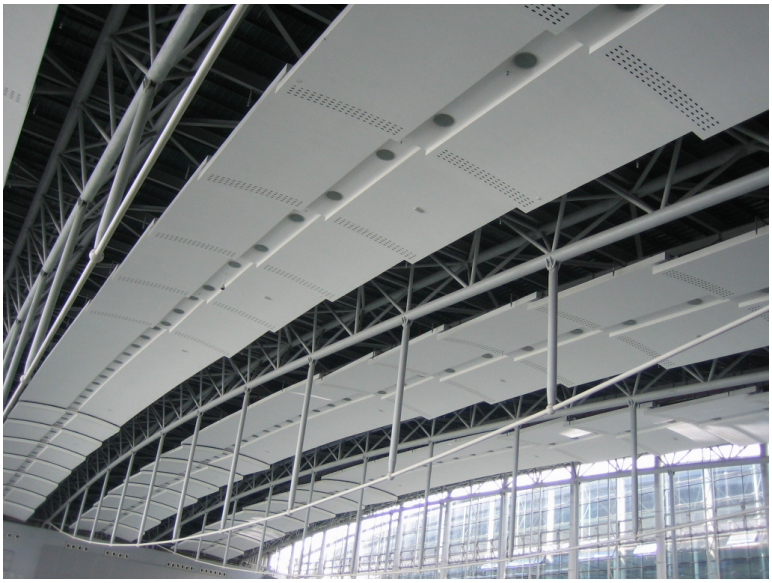

Figure 2. Structure of solid cable-truss of GICEC

This structure is of high nonlinearity. Based on well-established mathematical definition, the Lyapunov dynamic stability theory, in essence, is the study of the effect of the initial condition on the general equation of motion [10]. In other words, we adopted the definition that the structure subjected to a certain input is stable if small increases in the magnitude of excitation result in the small changes in the response [11,12]. The load that causes the loss of stability is identified as the critical load. In consideration of the high nonlinearity of dynamic stability and the multiple-degree-of-freedom system under time-varying loads, the effective dynamic stability judgment criterion is not available at present. This situation is a result of both the complexity of problem itself and the limitation of the Lyapunov theory. The dynamic stability analysis is predominant for some specific structures, which are initially studied in these references [13-18]. In some structures, there may be multiple equilibrium positions, the structure could swap among these positions under dynamic loads. Local dynamic buckling may occur in the structure under certain dynamic loads; however, after reaching new equilibrium position, the structure can still carry load or it may lose the entire dynamic stability. For this reason, the definition of dynamic stability based on mathematical definition is not indiscriminately imitated. Therefore, time history method is visualized and effective.

In this paper, nonlinear finite element method is used to study the dynamic stability of planar Beam String Structures under earthquake loads in respect of the number of struts, height-span ratio, sag-span ratio, moment of inertia, prestressing force of string and restraint type of supports.

2. ANALYSIS METHOD

This Beam String Structure, a type of hybrid structure, is composed of an upper arch, lower cables and struts. When analyzing the stability, upper chords are regarded as discrete plane straight beam elements, lower cables are treated as plane drag link elements which do not have the capacity to carry compression force, and struts are identified as plane links. Iterative algorithm is utilized in the geometric nonlinear finite element analysis.

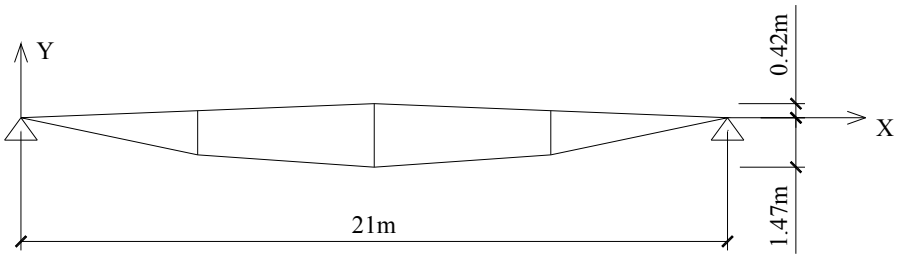

Figure 3. Elementary Model

Elementary model is single Beam String Structure, whose span is 21m, height-span ratio is 0.02 and sag-span ratio is 0.07. Its model is shown in Figure 3. The sectional dimension of upper beam and struts are Φ259×12 and Φ140×10 respectively. And lower cables used seven steel wires with a diameter of 5mm (7Φ5). Fixed hinged supports are accepted. In addition, the prestressing force of the lower strings is 20kN. The current general finite element analysis software ANSYS is applied to the time history method under earthquake loads. Upper chords, lower cables and struts employ BEAM3, LINK10 and LINK1 element respectively. During the process of calculation and analysis, large-deflection effects and damping are included. The damping ratio is 0.02.

Firstly, the characteristics of self-excited oscillation of the structure is studied, which is calculated using modal analysis. Natural vibration frequency of elementary model is shown in the Table 1. And Figure 4 illustrated the first eight modes.

Table 1. Natural Vibration Frequency

Modal exponent number	1	2	3	4	5	6	7	8
Natural vibration frequency /Hz	3.1	4.4	10.6	20.2	23.0	31.2	47.5	49.5

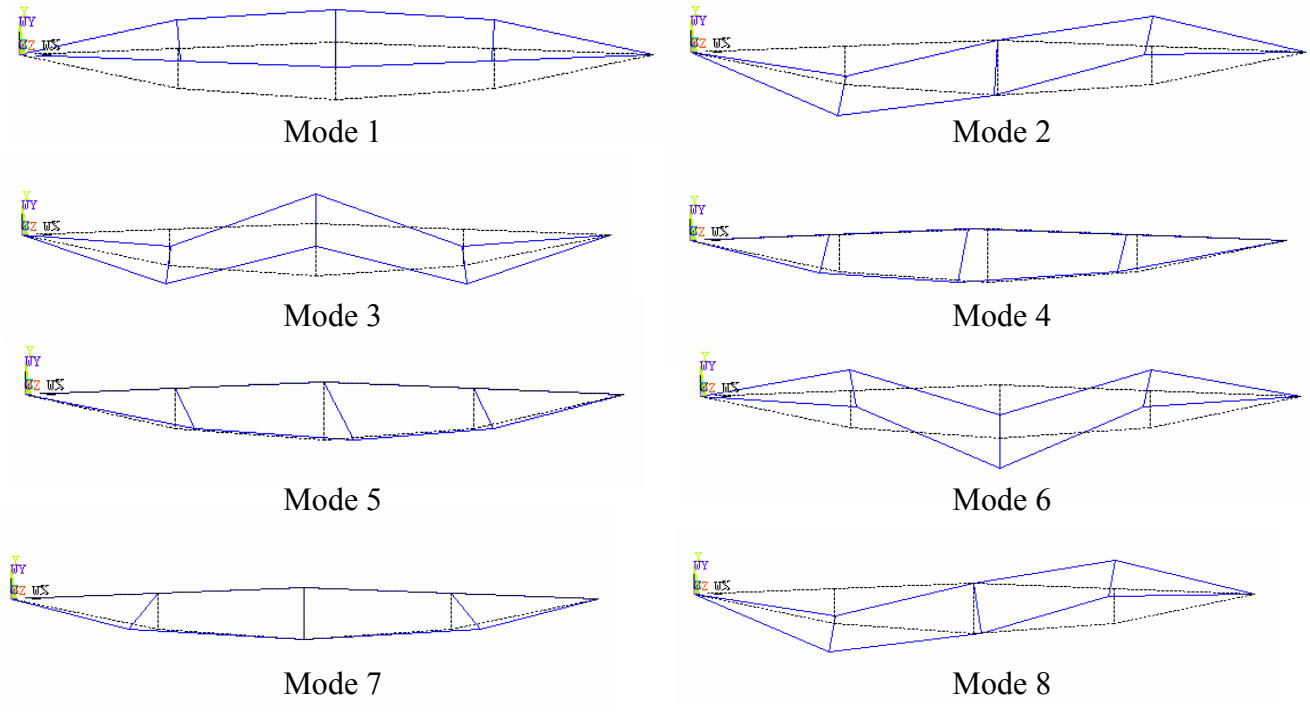

Figure 4. Mode Shape

When it comes to the research of the earthquake response of this structure, loads by way of acceleration are applied, and the earthquake wave El-Centro spectrum is preferred. Its recording time-interval is 0.02s, and its duration is compressed to 8s in the y direction, which is the direction of vertical earthquake loads.

According to former studies, it is proposed that if small load increment results in great changes in the characteristic response parameter, the situation can be regarded as dynamic instability, and this corresponding load is defined as the critical load of structural dynamic stability. Based on dynamic response of BBS, the node possesses the maximum structural displacement under seismic loads is specified as the structural characteristic response parameter.

Therefore, the time history curve of midspan nodal displacement response under the acceleration peak value of 341.7gal (1gal=0.01m/s^2) is shown in Figure 5 and Figure 6. The response of midspan upper chord nodal vertical displacement is shown in Figure 7. It is indicated that the response of the nodal vertical displacement remains stable under the acceleration peak value that lies between 200gal to 1400gal. The dynamic characteristics of the structure does not change obviously. When reaching the acceleration of 1400gal, the nodal vertical displacement increases significantly and drives to damage. At this instance, it is shown that the dynamic stability critical load of this structure is between 1200gal and 1400gal.

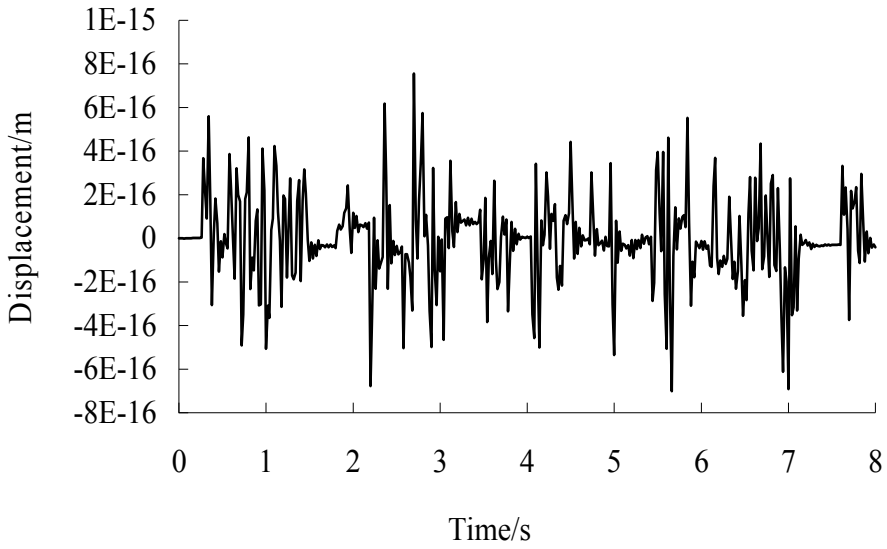

Figure 5. Time History Curve of Midspan Nodal Displacement in x Direction

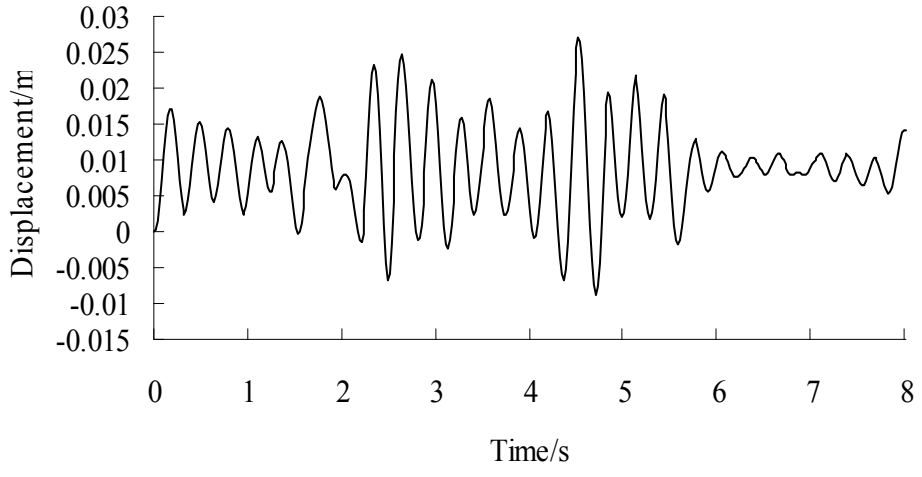

Figure 6. Time History Curve of Midspan Nodal Displacement in y Direction

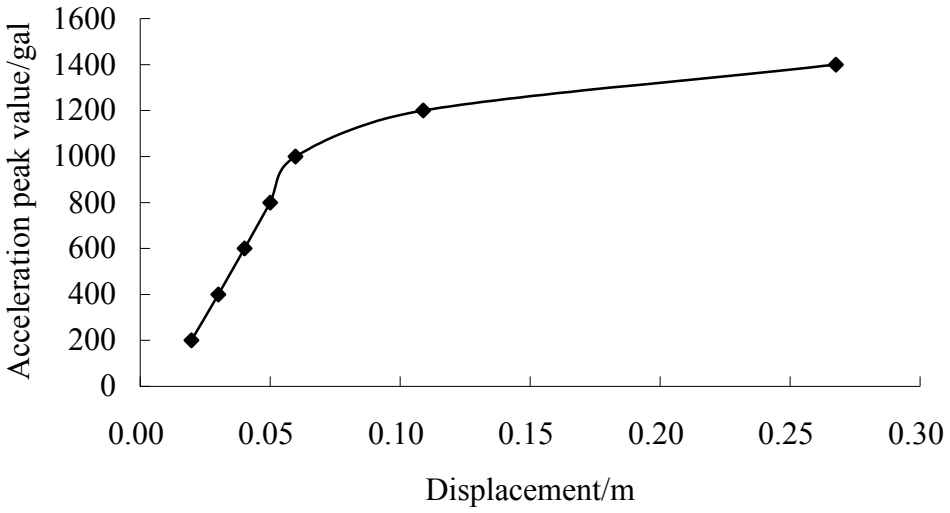

Figure 7. Maximum Vertical Displacements under Different Acceleration Peak Value

3. INFLUENCES OF VARIOUS FACTORS

When supports are both fixed hinged, the dynamic response of the structure under earthquake loads is mild. The orders of magnitude of the horizontal displacements are approximately 10^{-16}m or 10^{-15}m. More attention is paid to the responses of vertical displacements in the following work.

3.1 The Number of Struts

Struts are elastic supports to the upper arch in the structure. The improvement of struts to the stabilization of the structure under earthquake loads is studied, and models composed of 1, 3, 5, 7 and 9 struts are adopted. Other calculated parameters of these five models are identical. From Figure 8, according to the increase in the number of struts, midspan upper chord nodal vertical displacement increases initially, and after the number of struts reaches 5, its value begins to drop. Thus, the proper number of struts needs to be studied and then adopted. In general, the order of magnitude of the displacement is 10^{-2}m, so the influences of number of struts are not significant.

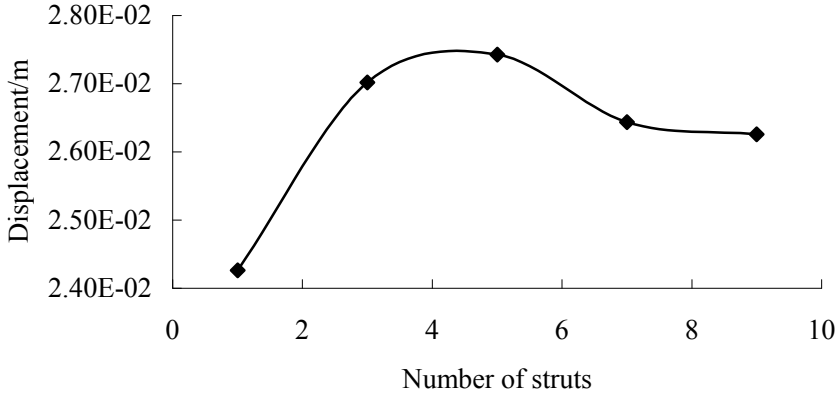

Figure 8. Maximum Vertical Displacements of Midspan Node under Different Numbers of Struts

3.2 The Ratio of High-span

Six models with different high-span ratios are analyzed to study the effect of high-span ratio on load-carrying performance of BSS. Three struts are taken. Besides the different high-span ratios, other parameters are identical. As shown in Figure 9, midspan upper chord nodal vertical displacement declined considerably as the high-span ratio increased. In this case, it illustrates that the increase of high-span ratio is decisive to resisting integral deformation. Meanwhile, what should be noted is that the displacement dropped slightly when the high-span ratio is over 0.07, compared with that of its ratio under 0.07, which has a significant reduction. It elucidates that increasing high-span ratio can lessen the response of this structure under earthquake loads.

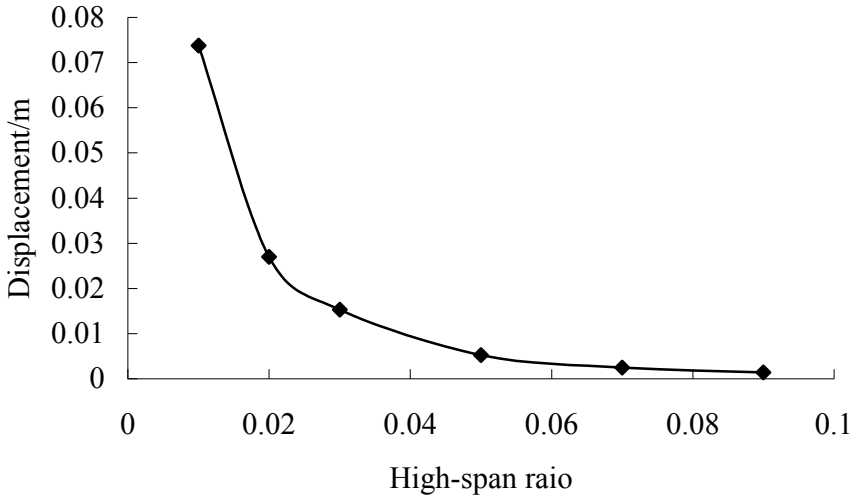

Figure 9. Maximum Vertical Displacements of Midspan Node under Different High-span Ratios

3.3 The Ratio of Sag-span

Eight models with different sag-span ratios are analyzed to study its effect on load-carrying performance of BSS. Three struts are also introduced. Besides the diverse sag-span ratios, other parameters are equal. Figure 10 describes that the value of midspan upper chord nodal vertical displacements rises moderately with the growth of sag-span ratio. It clarifies that lessening the sag-span ratio appropriately helps to reduce the vertical displacement response of this structure under earthquake load. In this case, the value of sag-span ratio should be kept in a rational extent.

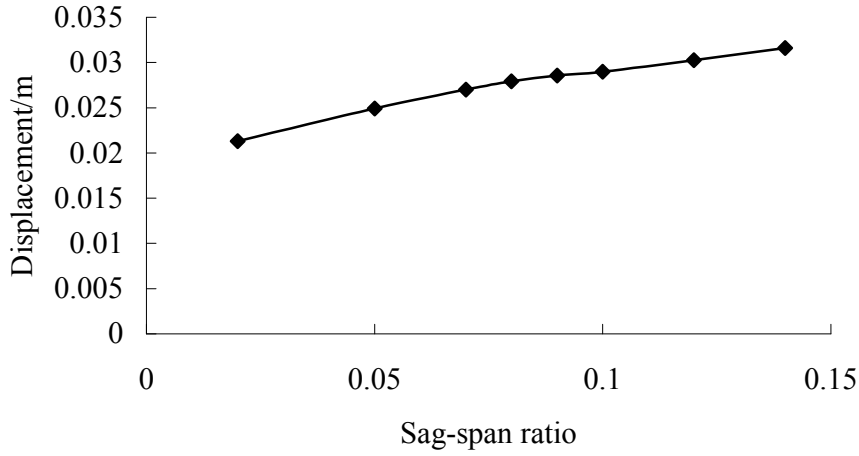

Figure 10. Maximum Vertical Displacements of Midspan Node under Different Sag-span Ratios

3.4 Stiffness of the Upper Beam

Three models with different section inertia moment are analyzed to study its impact on load-carrying performance of BSS. Besides the different sectional situation, other parameters are identical. From Figure 11, there is little change in deflection of the midspan upper chord nodal vertical displacement with the increase of sectional inertia moment. It reveals that the effect of sectional dimension on performance of this structure is little .

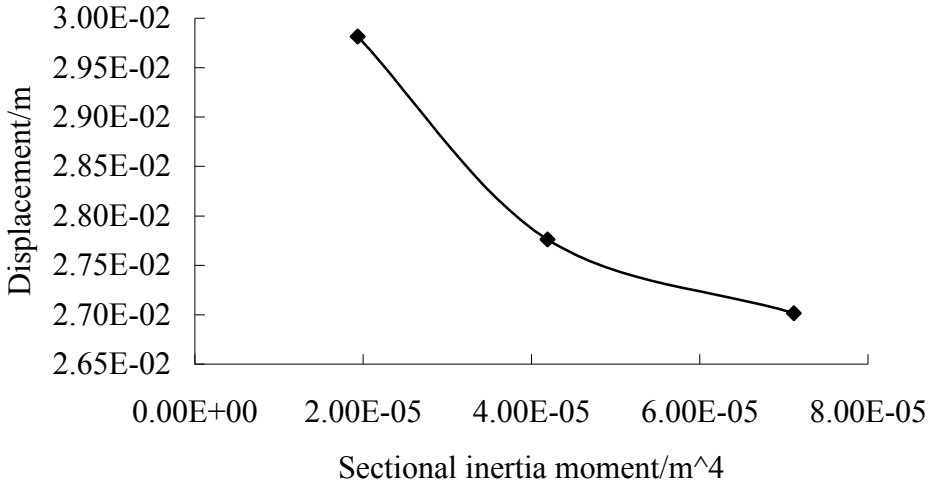

Figure 11. Maximum Vertical Displacements of Midspan Node under Different Sections

3.5 Prestressing Force of Lower Cables

Three models with different prestressing forces in the string are analyzed to study its effect on load-carrying performance of BSS. Besides the prestressing force value applied in the string, other parameters are identical. Figure 12 depicts that there is stable rise in the response of midspan upper chord nodal vertical displacements with the multiplication of prestressing force. It indicates that the increase of prestressing force of string will develop the structure's dynamic response. However, these effects are not significant. Thus, the value of prestressing force of string should be maintained in a reasonable range.

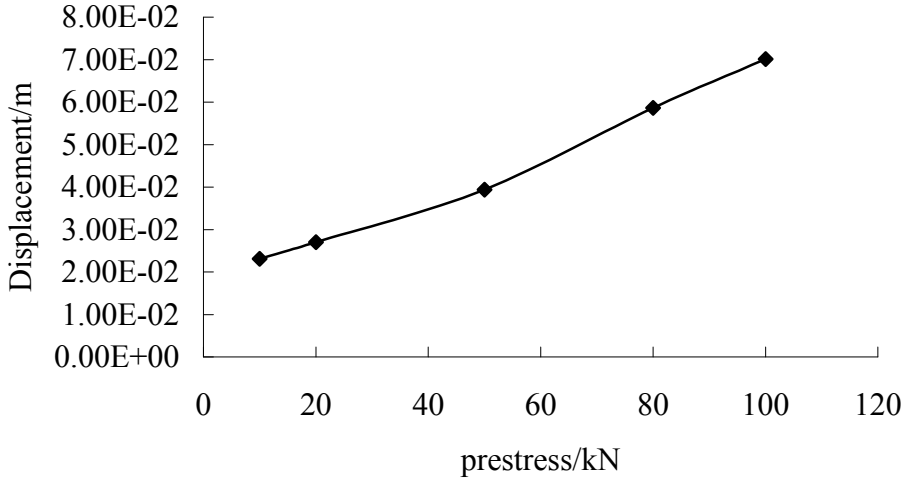

Figure 12. Maximum Vertical Displacements of
Midspan Node under Different Prestressing Force of String

3.6 Restraint Type of the Supports

On the premise of identical other parameters, when one end of the structure is fixed hinged support, while the other end is sliding hinged support, midspan upper chord node of the structure produces larger vertical displacement than that with two hinged supports do. As can be seen in Table 2, in the vertical displacement, the value of former has larger order of magnitude than that of the latter, in contrast, the gap is greater for horizontal displacement. It reveals that the effects of restraint type of the supports on performance of this structure are marked.

Table 2. Maximum Displacements of Midspan Node under Different Restraint Type of the Supports

Restraint type	One fixed hinged support	Both fixed hinged support
UX/m	1.05E-02	7.57E-16
UY/m	2.03E-01	2.70E-02

4. ELASTO-PLASTIC ANALYSIS

The discussions above are limited to the elastic range. However, the plastic yielding will take place and be inevitable on the structure under earthquake loads. During the earthquake, when certain parts of the structure enters into plasticity, which gives rise to the re-distribution of internal force. Thus, the plastic nature of the structure and the material nonlinearity should be taken more cautiously.

When plastic yielding is taken into account, upper chords, lower cables and struts employ BEAM23, LINK10 and LINK1 elements respectively. Figure 13 shows the comparison of the maximum vertical displacements of the structure both in elastic and plastic ranges. Hereinto, Model A and Model C represent the dynamic responses of the structure in the elastic range, Model B and Model D stand for the dynamic responses of structure when elastic-plasticity occurs in the structure. Meanwhile, Model A and Model B are both of fixed hinged supports, and one ends support of Model C and Model D are of single fixed hinged while the other end support are sliding hinged. As clearly shown in Figure 13, the vertical displacement response of the structure (for Model A and B) rises just comparatively less moderately (when considering the influences of elastic-plastic property) than those of the structure (Model C and D) in the perfectly elastic range. It seems that the plasticity helps to improve the critical load of the dynamic stability.

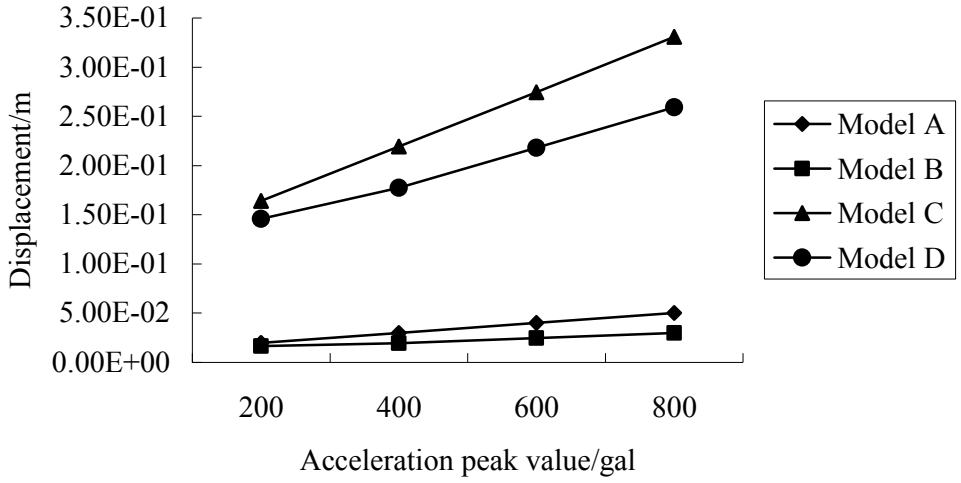

Figure 13. Maximum Vertical Displacement of Different Models

5. CONCLUSIONS

Based on the discussion above, it can be concluded as follows.

1. Effect of various parameters on the dynamic response in x direction under vertical earthquake loads is not obvious.

2. Vertical displacement response of the structure changed indistinctively according to the variations in the number of struts. Only five numbers of struts are analyzed in this paper. The structures with more than 9 struts were not considered sufficient and should be further studied.

3. The increase of high-span ratio is conducive to the strengthening of structural stiffness and resisting integral deformation. Moreover, load-carrying performance of the structure under earthquake loads is improved. In contrast, the influences of sag-span ratio are more complicated. Therefore, the value of sag-span ratio should be kept in a rational extent.

4. Although increasing sectional dimension and inertia moment can enhance a certain degree of structural stiffness, the improvement on the dynamic performance of this structure is little.

5. There is larger deformation to inverted arch as the prestressing force increases, which can enhance a certain degree of structural stiffness and also can increase the initial dynamic response of the structure. In this case, the value of prestressing force of strings should be taken reasonably.

6. Compared with the static stability analysis, the effect of section situation on the structure is not obvious. Increasing the prestressing force of string will enhance the earthquake response. In addition, increasing sag-span ratio seems not to take such a positive role in the dynamic analysis. Results of the effects of other parameters on this Beam String Structure are consistent with the results of the static analysis.

7. Under comparatively weak seismic loads, the dynamic responses in the structure, taking the elastic-plastic property into consideration, is less than those in the elastic range. However, dynamic stability of elastic-plasticity should be further studied; more proper model should be strictly employed.

8. As discussed above, in terms of BSS with comparatively small span, the dynamic response is not strong. Small span has advantage to resist destabilization and to enhance the structural stability. When it comes to the longer span BSS, the stiffness of the structure will diminish rapidly, the potential probability of dynamic instability is increased. Furthermore, more and more larger span Beam String Structures are employed in the practical project, in this case, BSS with long span should be exactly researched for further development.

ACKNOWLEDGEMENTS

Funding for the project was provided by the National Natural Science Foundation of China (No.50608054) and the High Education Development Foundation of Tianjin (No.20031105). The support is gratefully acknowledged. The technical consultation provided by Professor Xingye Liu throughout the whole process is appreciated.

REFERENCES

[1] Saitoh, M., "Role of String-aesthetics and Technology of the Beam String Structures", Proceeding of the LSA98 Conference-Light Structure in Architecture Engineering and Construction, 1998, pp. 692-701.

[2] Huang, M.X., "Design and Construction of Long-span Beam String Structures" (in Chinese), Shandong Science and Technology Publishing Company, 2005, pp. 1-9.

[3] Saitoh, M. and Okada, A., "The Role of String in Hybrid String Structure", Engineering Structures, 1999, Vol. 21, pp. 756-769.

[4] Zhang, Y.G. and Xue, S.D., "Long-span Space Structure" (in Chinese), Beijing Mechanical Industry Publishing Company, 2005, pp. 355-359.

[5] Chen, R.Y., Dong, S.L. and Sun, W.B., "Design and Analysis of a Long-span Prestressed Truss String Structure" (in Chinese), Spacial Structures, 2003, Vol. 9, No. 1, pp. 45-47.

[6] Shi, G.P., Chan, S.L. and Lu, Z.T., "Second-order Analysis and Design of Cables and Cable-frames", International Journal of Structural Stability and Dynamics, 2005, Vol. 5, No. 4, pp. 521-537.

[7] Bai, Z.X., Liu, X.L. and Li, Y.S., "Influence Analysis of Factors of Beam String Structure" (in Chinese), Steel Structures, 2001, Vol.3, No. 16, pp. 42-46.

[8] Bai, Z.X. and Liu, X.L., "Mechanics and Programming of Beam String Structure" (in Chinese), Engineering Mechanics Supplement, 1998, pp. 157-162.

[9] Liu, K.G., "Analysis of Large-span Beam String Structure" (in Chinese), Spacial Structures, 2001, Vol. 7, No. 2, pp. 39-43.

[10] Shu, Z.Z. and Zhang, J.Y., "Stability of Movement" (in Chinese), China Railway Publishing Company, 2001, pp. 12-13.

[11] Goldhirsch, I., Sulem, P.L. and Orszag, S.A., "Stability and Lyapunov Stability of Dynamical Systems-a Differential Approach and a Numerical Method", Physics, 1987, Vol. 27, pp. 311-337.

[12] Gilat, R. and Aboudi, J., "The Lyapunov Exponents as a Quantitative Criterion for the Dynamic Buckling of Composite Plates", International Journal of Solids and Structures, 2002, Vol. 39, pp. 461-481.

[13] Bernal, D., "Instability of Buildings During Seismic Response", Engineering Structures, 1998, Vol. 20, No. 4-6, pp. 496-502.

[14] Gui, G.Q. and Lin, Z.B., "Dynamic Stability of Single-layer Reticulated Spherical Domes" (in Chinese), Journal of Nanchang University (Engineering & Technology), 2003, Vol. 25, No. 1, pp. 43-47.

[15] Guo, H.S., Qian, H.L. and Shen, S.Z., "Dynamic Stability of Single-layer Reticulated Domes under Earthquake Excitation" (in Chinese), Earthquake Engineering and Engineering Vibration, 2003, Vol. 23, No. 1, pp. 31-37.

[16] Guo, H.S. and Shen, S.Z., "Analysis Method of Dynamic Stability of Single-layer Reticulated Domes" (in Chinese), Journal of Building Structures, 2003, Vol. 24, No. 3, pp.1-9.

[17] Ye, J.H. and Shen, Z.Y., "Dynamic Stability of Single-layer Spherical Domes under Earthquake Action" (in Chinese), Engineering Mechanics Supplement, 1998, pp. 6-10.

[18] Xia, K.Q., Yao, W.X. and Dong, S.L., "Dynamic Behavior of Snap-through Buckling in Reticulated Domes" (in Chinese), Engineering Mechanics, 2002, Vol. 19, No. 1, pp. 9-13.

MINLP OPTIMIZATION OF STEEL FRAMES

Uroš Klanšek[1], Tomaž Žula[2], Zdravko Kravanja[3] and Stojan Kravanja[4,*]

[1] *DSc, University of Maribor, Faculty of Civil Engineering, Maribor, Slovenia*
[2] *BSc, University of Maribor, Faculty of Civil Engineering, Maribor, Slovenia*
[3] *Professor, University of Maribor, Faculty of Chemistry and Chemical Engineering, Maribor, Slovenia*
[4] *Professor, University of Maribor, Faculty of Civil Engineering, Maribor, Slovenia*
[*] *(Corresponding author: E-mail: stojan.kravanja@uni-mb.si)*

Received: 22 September 2006; Revised: 26 April 2007; Accepted: 13 June 2007

ABSTRACT: The paper presents the discrete dimension optimization of unbraced rigid steel plane frames. The optimization of steel frames was carried out by the Mixed-Integer Non-linear Programming (MINLP) approach. The MINLP is a combined discrete-continuous optimization technique. It performs the discrete optimization of discrete decisions simultaneously with the continuous optimization of continuous parameters. The task of the optimization is to minimize the mass of the frame structure and to find the optimal discrete sizes of standard steel sections for frame members. The finite element equations are defined as the equality constraints for the second-order elastic structural analysis. The design constraints for the steel members were formulated according to Eurocode 3. The Modified Outer-Approximation/ Equality-Relaxation algorithm and a two-phase MINLP optimization approach were applied for the optimization. The latter starts with the continuous optimization of the frame, while the standard dimensions are temporarily relaxed into continuous parameters. When the optimal continuous solution is found, standard sizes of cross-sections are re-established and the simultaneous continuous and discrete dimension optimization by MINLP is then continued until the optimal solution is found. A numerical example of the optimization of a steel frame is presented at the end of the paper to show the suitability of the proposed approach.

Keywords: Optimization; mixed-integer non-linear programming; MINLP; steel structures; frames; Eurocode 3

1. INTRODUCTION

Traditional engineering methods for the structural design of steel frames are based on a trial-and-error procedure. The effective design is achieved in a time-consuming procedure of analyzing different structural alternatives by varying the sizes of the steel members. However, doubt always exists as to whether or not the obtained structural design is optimal.

To surmount the mentioned disadvantages, various different techniques, suited either for the continuous or the discrete structural optimization, have been proposed over the last three decades. These modern optimization methods may be partitioned into mathematical programming methods and heuristic methods.

As regards the mathematical programming, the non-convex and non-linear optimization problem of steel frames has in most cases been solved by using different continuous Nonlinear Programming (NLP) methods based on the well known Karush-Kuhn-Tucker optimality conditions, Kuhn HW and Tucker [1]. In this field, the Optimality Criteria methods (OC) are one of the most frequently used approaches. The OC methods were developed on the basis of the contributions by several researchers in the 1960s and early 1970s such as Barnett [2], Prager and Shield [3] and Venkayya et al. [4]. In the recent years, the OC approach to the optimization of steel frames was proposed by Chan et al. [5], Soegiarso and Adeli [6], Saka and Kameshki [7]. While the Karush-Kuhn-Tucker conditions ensure the requirements for the optimal solution, the Lagrange multipliers are applied to comprise the constraints. The OC methods handle continuous design variables. In cases when discrete variables are required, an optimum solution is commonly obtained in two steps. In the first step, the optimization problem is solved using the continuous variables. In the second step the discrete values are estimated by matching or rounding the values obtained from the continuous solution.

Since the nature of the optimization problem of steel frames is discrete, meaning that the structural design of steel frame members is determined by the discrete standard sizes, the nonlinear discrete optimization must be applied to handle discrete variables explicitly. In this way, various heuristic methods have been developed and mainly used: e.g. Direct Search (DS), Hook and Jeeves [8], Genetic Algorithms (GA), Holland [9], Simulated Annealing (SA), Kirkpatrick et al. [10], Tabu Search (TS), Glover [11], Neural Networks (NN), Rumelhart et al. [12], Ant Colony Optimization (ACO), Dorigo et al. [13], etc. In the class of heuristic methods, the GA are probably the most frequently applied approaches. GA are search algorithms based on the principles of natural selection and mutation. Not to go into too many details concerning the GA, some of their basic characteristic should be described: GA work with an encoded set of variables and operate on a population of potential solutions. They use a transition scheme that is probabilistic and an objective function information without any gradient information, and are able to deal with discrete optimum design problems without the derivates of functions. Only few of the numerous contributions of the frame optimization based on the GA, are brought to attention here: Camp et al. [14], Erbatur et al. [15], Kameshki and Saka [16], Jármai et al. [17], Hayalioglu and Degertekin [18], Kim et al. [19], Kaveh and Abdietehrani [20], Sarma and Adeli [21].

In recent years, some research contributions were presented on the optimization of steel frames with the Eurocode 3 design constraints for the dimensioning. In most of the published research works, different optimization methods were combined with the elastic first-order structural analysis. Guerlement et al. [22] have presented a practical sequential optimization algorithm which was used for discrete optimization of steel portal frames. Uys et al. [23] have used the leap-frog gradient method for the optimal design of the steel hoist structure frame. A gradient based optimization algorithm was used to obtain a continuous solution, which was then utilized as the starting point for a neighbourhood search within the discrete set of profiles available to attain the discrete optimal design. Jármai et al. [17] have investigated the suitability of four different optimization algorithms (i.e. genetic algorithm, the leap-frog gradient method, the method of Rosenbrock and the differential evolution algorithm) for the optimal design of the welded steel I-section frame. Further, Jármai et al. [24] have presented the optimum seismic design of a three-storey steel frame, obtained by the particle swarm optimization algorithm. Krajnc and Beg [25] have performed the weight optimization of welded frame structures, where the optimization was carried out by the genetic algorithm combined with elastic second-order structural analysis. The elastic second-order structural analysis was based on the approximate stiffness equation, which is the most commonly used method in the engineering practice. The research was then extended to cost optimization of welded steel frames by Pavlovčič et al. [26].

On the other hand, this paper presents the discrete dimension optimization of unbraced rigid steel plane frames performed by the Mixed-Integer Non-linear Programming (MINLP) approach. The MINLP is a type of mathematical programming method which handles both the continuous and the discrete variables simultaneously. Since the MINLP denotes combined discrete-continuous optimization techniques, it performs the discrete optimization of discrete dimensions (i.e. standard cross-section sizes of columns and beams) simultaneously with the continuous optimization of continuous parameters (e.g. internal forces, deflections, the structure mass).

The methodology and the applicability of the proposed MINLP approach to structural optimization problems may be found in the following contributions. Kravanja et al. [27] have presented a general view of the MINLP approach to simultaneous topology and continuous parameter optimization. The development of suitable strategies to solve comprehensive, non-convex and highly combinatorial MINLP problems for the simultaneous topology, material, standard and rounded dimension optimization was introduced by Kravanja et al. [28, 29]. The applicability of the proposed MINLP optimization approach was supported by the examples such as the MINLP

optimization of roller hydraulic steel gate Intake Gate of Aswan II for Egypt by Kravanja et al. [30], the optimization of steel gates for Sultartangi project in Iceland [31] as well as the MINLP optimization of steel trusses and composite I beams by Kravanja et al. [29].

The MINLP discrete-continuous optimization problems of steel frames are comprehensive, non-convex and highly non-linear. The Modified Outer-Approximation/Equality-Relaxation algorithm is applied to carry out the structural optimization, Kravanja and Grossmann [32], Kravanja et al. [28, 29]. A two-phase MINLP optimization approach is proposed. It starts with the continuous Non-linear Programming (NLP) optimization of the frame structure, while the standard dimensions are temporarily relaxed into continuous parameters. When the continuous NLP result is found, the standard sizes of the cross-sections are re-established and the simultaneous continuous and discrete dimension optimization by MINLP then continues until the optimal solution is found.

The mass objective function of the frame structure is subjected to the design, material, resistance and deflection constraints taken from the structural analysis. The finite element equations are defined as the equality constraints for the calculation of the internal forces and the deflections of the structure. The second-order elastic structural analysis is performed by considering the geometric nonlinearity due to the P-δ and the P-Δ effect. Both effects are included in the non-linear stiffness matrix of the individual frame member using the stability function approach, Chen and Lui [33]. Design constraints of the steel members are formulated according to Eurocode 3 [34]. Alongside the theoretical basis, a numerical example of the optimization of a steel frame is presented at the end of the paper in order to show the suitability of the proposed approach.

2. STEEL FRAMES

The considered steel frames are proposed to be built as unbraced rigid plane frames from standard hot rolled steel sections, see Figure 1. The discrete dimension optimization of the steel frames is performed under the combined effects of the self-weight of the frame members, the horizontal concentrated variable loads at the left exterior joints, the vertical uniformly distributed variable load at each storey and an initial frame imperfection.

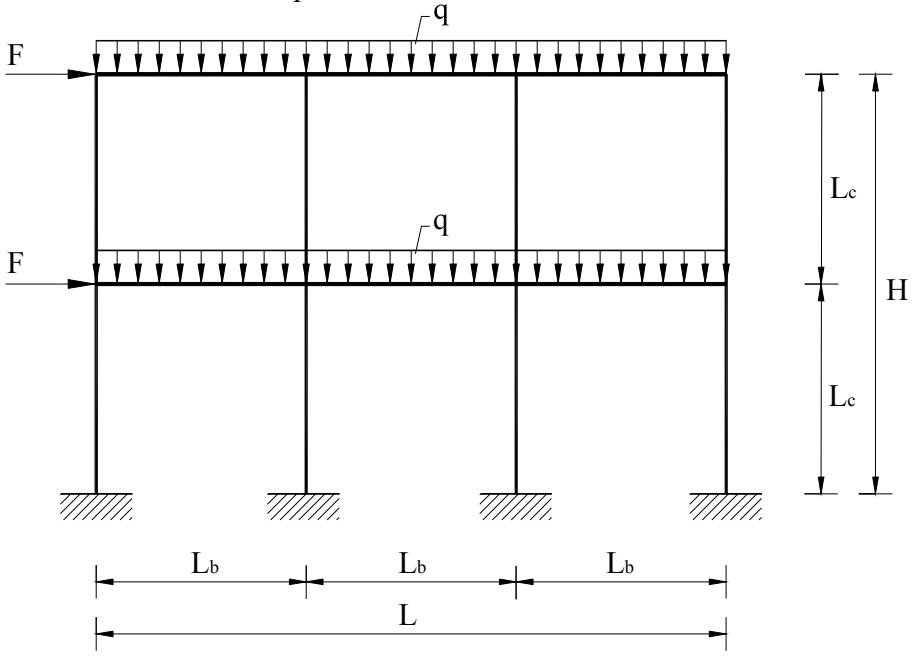

Figure 1. Unbraced Plane Steel Frame

The finite element equations are defined as the equality constraints for the second-order elastic structural analysis. Both the P-δ and the P-Δ effect are included in the non-linear stiffness matrix of the individual frame member using the stability function approach, Chen and Lui [33]. The stability function approach to elastic second-order analysis of steel frames was presented in details by Chen and Lui [35], Chen et al. [36]. While the P-δ effect is associated with the influence of the axial force on the beam-column member flexure, the P-Δ effect denotes the influence of the axial force acting through the relative side sway displacements of the element ends. The stability functions s_{ii} and s_{ij} proposed by Chen WF and Lui [33] are different for tensile and compressive axial forces. Moreover, they give an indeterminate numerical solution when the axial force is zero. To circumvent these problems, Kim et al. [37] have used simplified expressions for the stability functions S_1 and S_2. These expressions are involved in the optimization. Note that the shear deformation effect was neglected considering the fact that only the slender structural members are subjected to buckling for which shear deformation becomes insignificant.

Steel frames are designed in accordance with Eurocode 3 [34] for the conditions of both the ultimate limit and the serviceability limit states. Since the out-of-plane characteristics of the plane structure are unknown, the steel frames are calculated as laterally and torsionally supported frames. Hereby, the steel members are checked only for in-plane instability, i.e. for the compression/buckling resistance of the members.

When the ultimate limit states of the beam-column members are considered, the elements are checked for a required resistance of the cross-section related to local buckling, to the interaction between bending and axial force, to the interaction between bending and axial in-plane compression/buckling, to the effect of both, i.e. the shear and axial forces, on the reduced plastic resistance moment of the cross-section and to shear buckling. The ultimate moment capacity is calculated by the elastic method. Since the second-order elastic global analysis is used, the in-plane buckling lengths of compression members are calculated to be equal to the member's lengths.

When it comes to the serviceability limit states, the vertical deflections of the beams in the individual storey are calculated by the elastic method. The deflections δ_2, resulting from the variable imposed load, and the total deflections δ_{max}, resulting from the overall load, are defined under the limited maximum values: span/300 and span/250, respectively. The horizontal deflections are also checked for each individual storey and for the structure as a whole. Both types of horizontal deflections are checked for the recommended limits: the relative horizontal deflection of each storey required to be smaller than each storey height/300 and the horizontal deflection of the top of the frame must be smaller than the overall frame height/500. Some important ultimate limit state constraints and serviceability limit state constraints are defined in the following sections.

2.1 Ultimate Limit State Constraints

Constraints relating to the steel cross-section requirements for the elastic global analysis and local buckling are given by:

$$d/t_w \leq 42\,\varepsilon / (0.67 + 0.33\,\psi) \quad \text{for} \quad \psi > -1 \tag{1}$$

$$d/t_w \leq 62\,\varepsilon\,(1 - \psi)\,(-\psi)^{0.5} \quad \text{for} \quad \psi \leq -1 \tag{2}$$

$$b/t_f \leq 30\,\varepsilon \tag{3}$$

where:

$$\varepsilon = (235/f_y\ [\mathrm{N/mm^2}])^{0.5}, \qquad \psi = (-M_{y,Sd}/W_{el,y} + N_{x,Sd}/A) \,/\, (M_{y,Sd}/W_{el,y} + N_{x,Sd}/A) \tag{4}$$

where d and t_w are the clear depth and the thickness of the web; b and t_f are the width and the thickness of the flange; f_y is the yield strength of the structural steel; ψ is the stress ratio; $M_{y,Sd}$ is the design bending moment about the y axis; $W_{el,y}$ is the elastic section modulus; $N_{x,Sd}$ is the design axial force and A is the cross-section area.

The constraint concerning the resistance of the steel cross-section subjected to the bending moment and axial force is defined as follows:

$$N_{x,Sd}/(A\, f_y/\gamma_{M0}) + M_{y,Sd}/(W_{el,y}\, f_y/\gamma_{M0}) \leq 1 \tag{5}$$

where γ_{M0} is the partial safety coefficient for the plastic, compact and semi-compact sections.

Constraints concerning the resistance of the laterally and torsionally supported beam-column subjected to the bending and axial in-plane compression/buckling may be expressed as follows:

$$N_{x,Sd}/(\chi_y\, A\, f_y/\gamma_{M1}) + k_y\, M_{y,Sd}/(W_{el,y}\, f_y/\gamma_{M1}) \leq 1 \tag{6}$$

where:

$$\chi_y = 1/[\Phi_y + (\Phi_y^2 + \overline{\lambda_y}^2)^{0.5}], \qquad \Phi_y = 0.5[1 + \alpha\,(\overline{\lambda_y} - 0.2) + \overline{\lambda_y}^2], \qquad \overline{\lambda_y} = K\,L\,/[93.9\,\varepsilon\, i_y] \tag{7}$$

$$k_y = 1 - \mu_y\, N_{x,Sd}/(\chi_y\, A\, f_y), \qquad k_y \leq 1.5, \qquad \mu_y = \overline{\lambda_y}(2\,\beta_{My} - 4) + (W_{pl,y} - W_{el,y})/W_{el,y}, \qquad \mu_y \leq 0.9 \tag{8}$$

where χ_y is the reduction factor for the relevant buckling mode about the y axis; γ_{M1} is the partial coefficient for element instability; α is the imperfection factor; $\overline{\lambda_y}$ is the relative slenderness of the beam-column; K is the buckling length ratio; L is the length of the beam-column; i_y is the radius of gyration; β_{My} is the equivalent uniform moment factor and $W_{pl,y}$ is the plastic section modulus.

Constraints concerning the effect of both shear force and axial force on the reduced plastic resistance moment of the cross-section are written in the following form:

$$V_{z,Sd} \leq 0.5\ V_{z,pl,Rd} \tag{9}$$

where:

$$V_{z,pl,Rd} = A_{v,z}\, f_y\, /(\sqrt{3}\ \gamma_{M0}), \qquad A_{v,z} = 1.04\ h\ t_w \tag{10}$$

where $V_{z,Sd}$ is the design shear force; $V_{z,pl,Rd}$ is the design plastic shear resistance; $A_{v,z}$ is the steel cross-section shear area and h is the depth of the steel cross-section.

The constraint concerning the resistance to shear buckling is expressed as:

$$d/t_w \leq 69\ \varepsilon \tag{11}$$

2.2 Serviceability Limit State Constraints

The constraint concerning the vertical deflections of the beams in each individual storey due to the variable imposed load is determined as:

$$\delta_2 \leq L / 300 \tag{12}$$

where δ_2 is the deflection subjected to the variable imposed load and L is the length of the beam.

The constraint concerning the vertical deflections of the beams in each individual storey due to overall load is written as:

$$\delta_{max} \leq L / 250 \tag{13}$$

where δ_{max} is the total deflection due to overall load.

The constraint concerning the relative horizontal deflection of each storey is stated as:

$$\delta_{hs} \leq h_s / 300 \tag{14}$$

where δ_h is the relative horizontal deflection of the individual storey and h_s is the height of the storey.

The constraint concerning the horizontal deflection of the top of the frame is defined by:

$$\delta_{h0} \leq h_0 / 500 \tag{15}$$

where δ_{h0} is the horizontal deflection of the top of the frame and h_0 is the overall height of the frame.

3. THE MINLP MODEL FORMULATION FOR STEEL FRAMES

The MINLP optimization approach is proposed to be performed through three steps. The first one includes the generation of a mechanical structure with a fixed topology and different standard dimension alternatives, the second one involves the development of an MINLP model formulation and the last one consists of a solution for the defined MINLP optimization problem.

The MINLP structure is proposed to be generated as a mechanical structure consisting of various standard dimension alternatives (e.g. standard hot rolled steel sections) from which an optimal frame structure is obtained within all variations. The selection of the standard dimensions of the alternatives requires a discrete decision optimization.

As soon as the mechanical structure is generated, the MINLP optimization is followed by the development of a MINLP model formulation for steel frames. The proposed MINLP model formulation of frames includes the mass objective function subjected to various constraints with continuous and binary variables. While continuous variables are used for continuous parameter optimization, discrete binary 0-1 variables are used for discrete optimization. They represent the potential selection of standard dimension alternatives which are defined in the mechanical structure.

The non-linear and non-convex discrete/continuous optimization problem of steel frames may be formulated as an MINLP problem in the following form:

$$\begin{aligned} \min \quad & z = \sum_{i \in I} \rho\, A_i\, L_i \\ \text{s.t.} \quad & \boldsymbol{h}(\boldsymbol{x}) = \boldsymbol{0} \\ & \boldsymbol{g}(\boldsymbol{x}) \le \boldsymbol{0} \\ & \boldsymbol{A}(\boldsymbol{x}) \le \boldsymbol{a} \\ & \boldsymbol{S}(\boldsymbol{d}^{st}) \le \boldsymbol{s} \end{aligned} \qquad \text{(MINLP)}$$

$$\boldsymbol{x} \in X = \{\boldsymbol{x} \in R^n : \ \boldsymbol{x}^{\mathrm{LO}} \le \boldsymbol{x} \le \boldsymbol{x}^{\mathrm{UP}}\}$$
$$\boldsymbol{y} \in Y = \{0,1\}^m$$

where z is an objective function; ρ represents the steel density; A_i is a cross-section area of the i-th structural element; L_i stands for a length of the i-th structural element; I represents a set of structural elements; $\boldsymbol{x}$ is a vector of continuous variables specified in the compact set X; and $\boldsymbol{y}$ denotes a vector of 0-1 discrete binary variables defined inside the set Y. The functions $\boldsymbol{h}(\boldsymbol{x})$ and $\boldsymbol{g}(\boldsymbol{x})$ are non-linear functions involved in the equality and inequality constraints, respectively. $\boldsymbol{A}(\boldsymbol{x}) = \boldsymbol{a}$ represent linear constraints and $\boldsymbol{S}(\boldsymbol{d}^{st}) \le \boldsymbol{s}$ are mixed linear equality/inequality constraints.

Both, the vector of continuous variables $\boldsymbol{x} = \{\boldsymbol{d}, \boldsymbol{p}\}$ and the vector of discrete binary variables $\boldsymbol{y}^{st}$ are involved in the MINLP frame model formulation. The continuous variables are partitioned into design variables $\boldsymbol{d} = \{\boldsymbol{d}^{cn}, \boldsymbol{d}^{st}\}$ and into performance (non-design) variables $\boldsymbol{p}$ (e.g. internal forces, deflections), where sub-vectors $\boldsymbol{d}^{cn}$ and $\boldsymbol{d}^{st}$ stand for continuous and standard dimensions, respectively. The vector of binary variables $\boldsymbol{y}^{st}$ denotes the potential selection of standard dimension alternatives.

The objective function z defines the steel frame structure mass including i, $i \in I$, structural elements (beams and columns). Parameter non-linear and linear constraints $\boldsymbol{h}(\boldsymbol{x}) = \boldsymbol{0}$, $\boldsymbol{g}(\boldsymbol{x}) \le \boldsymbol{0}$ and $\boldsymbol{A}(\boldsymbol{x}) \le \boldsymbol{a}$ represent a rigorous system of design, loading, stress, resistance and deflection constraints known from the structural analysis. The finite element equations (second-order elastic structural analysis) are defined in the set of equality constraints for the calculation of internal forces and deflections, while the constraints for the dimensioning are determined in accordance with Eurocode 3 [34].

Mixed linear constraints $\boldsymbol{S}(\boldsymbol{d}^{st}) \le \boldsymbol{s}$ define the standard design variables $\boldsymbol{d}^{st}$. Each standard dimension d^{st} is determined as a scalar product between its vector of standard dimension constants $\boldsymbol{q}$ and its vector of binary variables $\boldsymbol{y}^{st}$. Only one discrete value can be selected for each standard dimension since:

$$d^{st} = \sum_{i \in I} q_i\, y_i^{st} \tag{16}$$

$$\sum_{i \in I} y_i^{st} = 1 \tag{17}$$

Although the variable d^{st} takes a discrete value of standard section, it is from the mathematical point of view defined as the continuous variable, proposed to be calculated between its lower and upper bounds. The continuous variable d^{st} is determined by using of its subjected vector of discrete binary variables $\boldsymbol{y}^{st}$ according to eqs. (16) and (17).

4. OPTIMIZATION

A general MINLP class of optimization problems can in principle be solved by the following algorithms and their extensions: the Nonlinear Branch and Bound (NBB), proposed by Gupta OK and Ravindran [38]; the Sequential Linear Discrete Programming method (SLDP), by Olsen GR and Vanderplaats [39] and Bremicker et al. [40]; the Extended Cutting Plane method (ECP), by Westerlund and Pettersson [41]; Generalized Benders Decomposition (GBD), by Benders [42] and Geoffrion [43]; the Outer-Approximation method (OA), by Duran and Grossmann [44]; the Feasibility Technique (FT) by Mawengkang and Murtagh [45]; and the LP/NLP based Branch and Bound algorithm (LP/NLP BB) by Quesada and Grossmann [46].

The Nonlinear Branch and Bound method is a direct extension of the original Branch and Bound method which was developed to solve mixed-integer linear optimization problems (MILP), see Land and Doig [47], Dakin [48]. Instead of solving LP relaxed problems, it solves NLP relaxed problems at each node. The method, thus, deals with the sequence of generated continuous NLP subproblems which are performed at each node of a tree enumeration where a subset of relaxed 0-1 discrete variables is successively fixed.

The Sequential Linear Discrete Programming (SLDP) method is an extension of the continuous Sequential Linear Programming (SLP). The SLDP method begins with the creation of a mixed-integer linear approximate problem (MILP) from the nonlinear discrete problem (MINLP). Linear programming techniques are then used to solve the approximate problem. A series of approximations and optimizations is carried out, using the Branch and Bound method, until convergence occurs.

The Extended Cutting Plane method (ECP) is suitable for solving large-scale weakly nonlinear MINLP problems (with a high number of linear, but a few or a reasonable number of nonlinear constraints). This method is based on Kelley's Cutting Plane method, Kelley [49]. Instead of solving LP subproblems as the standard method does, it deals with relaxed MILP subproblem optimization at each iteration. The objective function must be defined linearly.

Unlike the SLDP and the ECP method, both the General Benders Decomposition method (GBD) and the Outer-Approximation one (OA) involve solving an alternative sequence of NLP and MILP optimization subproblems. The NLP subproblem corresponds to the optimization of parameters with 0-1 variables, which are temporarily fixed, and yields an upper bound to the MINLP objective function to be minimized. The MILP master problem predicts a lower bound for the MINLP, where new 0-1 variables are identified. The predicted lower bounds increase monotonically as the cycle of major iterations (MILP plus NLP) proceeds. The search is terminated when the predicted lower bound coincides with or exceeds the current best upper bound. The main difference between the GBD method and the OA one lies in the definition of the MILP master problem. In the case of GBD it is given by a dual representation of the continuous space, while in the case of the OA it is given by a primal approximation. Both methods accumulate new constraints as the major iterations proceed. The GBD accumulates one Lagrangian cut in the space of 0-1 variables, while the OA accumulates a set of linear approximations of nonlinear constraints in the space of both the 0-1 variables and the continuous ones. The Outer-Approximation/Equality-Relaxation method (OA/ER) by Kocis and Grossmann [50] was extended from the OA method to provide for explicit handling of the nonlinear equality constraints of MINLP problems.

The main idea of the Feasibility Technique is to round up the relaxed NLP solution into an integer solution with the least local degradation. This is accomplished through the computer code MINOS by Murtagh and Saunders [51] by successively forcing superbasic variables to become nonbasic ones based on the information of the reduced costs.

The LP/NLP based Branch and Bound method (LP/NLP BB) was proposed for solving convex MINLP problems. The method is based on the solution of both LP and NLP subproblems. NLP subproblems are solved at those nodes in which feasible integer solutions are found.

4.1 The Modified OA/ER Algorithm

Since the MINLP discrete/continuous optimization problems of steel frames are in most cases comprehensive, non-convex and highly non-linear, the Outer-Approximation/Equality-Relaxation algorithm (OA/ER) by Kocis and Grossmann [50] was selected to fulfil this optimization task. The OA/ER algorithm consists of an alternative sequence of solving Non-linear Programming (NLP) optimization subproblems and Mixed-Integer Linear Programming (MILP) optimization master problems, see Figure 2.

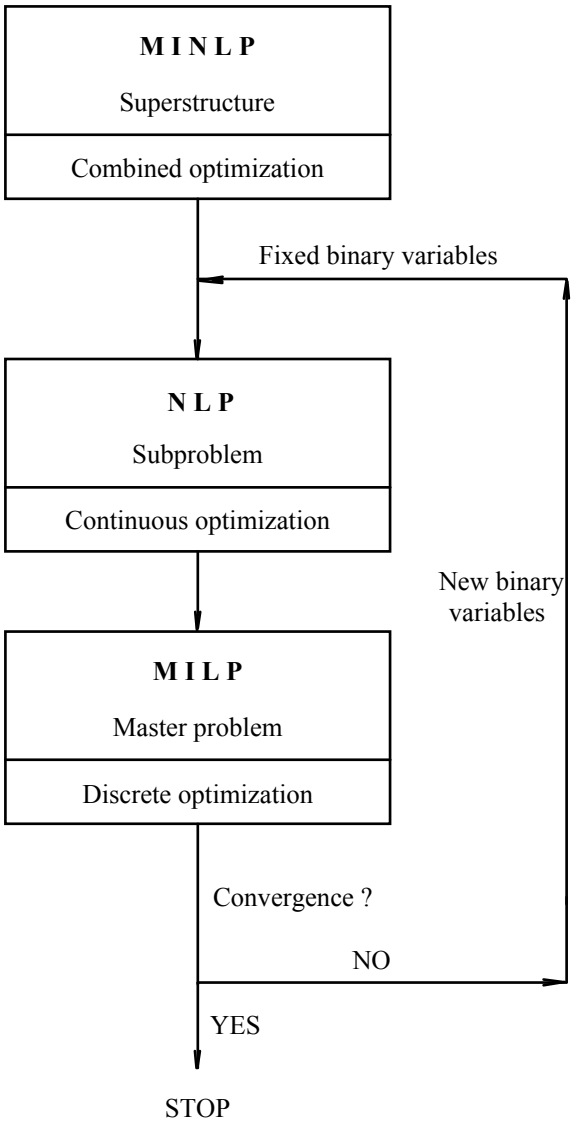

Figure 2. Steps of the OA/ER Algorithm

The NLP optimization subproblem comprises the continuous optimization of the parameters of the frame structure with fixed standard dimensions and yields an upper bound to the objective to be minimized. The MILP optimization master problem predicts a new vector of binary variables. A global linear approximation to the structure of standard dimension alternatives is constructed for the MILP master problem in which new standard sizes (i.e. the standard hot rolled steel sections) are identified in such a way that MILP's lower bound does not exceed the current best NLP's upper bound.

The NLP subproblems and the MILP master problems are sequentially solved until the convergence is satisfied. The search for the optimal solution is terminated when the predicted MILP's lower bound exceeds the current best NLP's upper bound. The convergence is usually achieved in a few MINLP iterations (up to 10). The OA/ER algorithm guarantees the global optimality of solutions for convex and quasi-convex optimization problems.

The OA/ER algorithm as well as all other mentioned MINLP algorithms does not generally guarantee that the obtained solution is the global optimum. This is due to the presence of non-convex functions in the models that may cut off the global optimum. In order to reduce the undesirable effects of non-convexities the Modified OA/ER algorithm was proposed by Kravanja and Grossmann [32] by which the following modifications are applied to the master problem: deactivation of the linearizations, decomposition and deactivation of the objective function linearization, use of the penalty function, use of the upper bound on the objective function to be minimized as well as a global convexity test and a validation of the outer approximations.

Deactivation of the linearizations is a modification procedure proposed by Kocis and Grossmann [52] which establishes the feasibility of the linearizations at zero conditions when the structural element does not exist. An extra existence binary variable y is assigned for each structural element and the set of linear approximations can then be potentially deactivated. The objective here is to enforce linearizations for $y = 1$ (i.e. the structural element is selected), while they become redundant for $y = 0$.

The objective function is usually given in the composite nonlinear form $\boldsymbol{c}^{\mathrm{T}}\boldsymbol{y} + f(\boldsymbol{x})$. Consequently, its linearization also has a composite form, which prevents the above mentioned deactivation procedure from being applied. The objective function is proposed to be decomposed into the mixed linear part $\boldsymbol{c}^{\mathrm{T}}\boldsymbol{y} + f^{\mathrm{lin}}(\boldsymbol{x})$ and into the nonlinear part $f^{\mathrm{nl}}(\boldsymbol{x})$. The nonlinear part $f^{\mathrm{nl}}(\boldsymbol{x})$ of the composite objective function is then further decomposed and represented as a sum of nonlinear terms for each structural element. Since an extra existence variable y is assigned to each nonlinear term, the linearization of each term can be performed separately and the corresponding set of linearizations can potentially be deactivated.

The OA/ER algorithm has been improved by the use of the penalty function which allows violations of the linearizations of nonconvex constraints in the infeasible region despite the nonconvexities and thus makes the obtaining of a feasible solution possible. This can be accomplished by introducing slack variables into any linearization and by including the violations of linearizations with the corresponding weights for slack variables in the penalty function.

Although the shifting of the linearizations into the infeasible region may due to the procedure mentioned above prevent the nonconvexities from cutting off the global optimum, this solution may not be "seen" because of the very high penalties which may be assigned to it. In order to encourage a search into the (in)feasible region, the upper bound UB on the objective function of the MILP master problem is introduced, where the UB is usually set to the currently best NLP solution.

The troublesome impacts of highly nonconvex constraints or terms in the objective function are usually so strong that the original master problem of the OA/ER algorithm fails to predict a good starting point for the next NLP stage. The values of variables are usually shifted either to their upper or to their lower bounds which prevents the next NLP subproblem from converging into its feasible solution. In order to overcome such difficulties, a special global convexity test is applied to the linearizations before each MILP step and then all linearizations that violate the convexity test are made temporarily redundant. Thus, the proposed procedure may accumulate much fewer nonconvexities and prevent violating linearizations from cutting off the feasible region. The convexity conditions must be verified for linearizations for the last point $\boldsymbol{x}^K$. The linearizations which do not satisfy the above conditions are then made currently redundant by simply setting their weights on the slack variables to zero value.

4.2 The Two-phased MINLP Approach

The optimal solution of a complex non-convex and non-linear MINLP problem with a high number of discrete decisions is in general very difficult to obtain. The optimization is thus performed sequentially in two different phases to accelerate the convergence of the Modified OA/ER algorithm. The optimization is proposed to start with the continuous NLP optimization of the frame, while standard dimensions are temporarily relaxed into continuous parameters. When the optimal result is found, the standard sizes of the cross-sections are re-established and the standard dimension optimization of the beams and columns is then continued until the optimal solution is found.

The task of the first phase (the continuous NLP) is to find a good starting point for the MINLP optimization. All linearizations of the nonlinear (in)equality constraints derived at this level, together with the original linear constraints, are valid outer-approximations for the second phase. In this way, each feasible NLP solution of each MINLP iteration (NLP plus MILP) of the second phase accumulates (adds new linearizations) a global linear approximation of the structure model representation to be used at the next MINLP iteration, thus enabling the second phase to be solved much more efficiently, see also Kravanja et al. [27].

The optimization model may contain up to some thousand binary 0-1 variables of standard dimension alternatives. Since this number of 0-1 variables is too high for a normal solution of the MINLP, a special pre-screening and a reduction procedure have been developed, which automatically reduce the binary variables for standard dimension alternatives into a reasonable number. The discrete optimization includes only those 0-1 variables which determine the standard dimension alternatives close to the continuous dimensions obtained at the first NLP.

5. THE EXAMPLE

In order to present the advantages of the proposed MINLP optimization approach, the paper introduces an example of the optimization of a three-storey, three-bay rigid steel plane frame, see Figure 3. The frame was subjected to the combined effects of the self-weight of frame members, the horizontal concentrated variable load of 10 kN at the left exterior joints, the vertical uniformly distributed variable load of 50 kN/m at each storey and the initial frame imperfection. The material used was standard structural steel S 355. The task of the optimization was to minimize the mass of the frame and to find the optimal sizes of standard hot rolled European wide flange HEA sections for the frame members. The optimization of the frame was performed by the MINLP optimization approach.

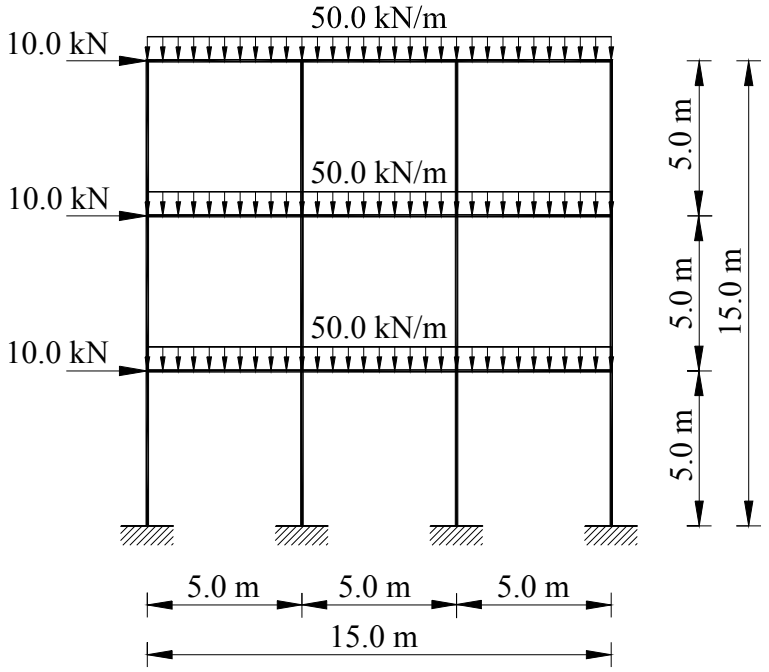

Figure 3. Three-storey, Three-bay Steel Frame

The MINLP optimization model FRAMEOPT for the optimization of steel frames was developed. The model FRAMEOPT was developed on the basis of the proposed MINLP model formulation for steel frames, see paragraph 3. The defined mass objective function of the structure was subjected to the given design, material, resistance, and deflection constraints, checking for both the ultimate and the serviceability limit states according to the Eurocodes, see paragraph 2. As an interface for mathematical modelling and data inputs/outputs GAMS (General Algebraic Modelling System), a high level language was used, see Brooke et al. [53].

A steel frame structure was generated in which all possible variations of different standard sizes were embedded. The structure comprised 17 different standard steel HEA sections (from HEA 100 to HEA 500) for each beam and column separately.

The optimization was carried out by a user-friendly version of the MINLP computer package MIPSYN, the successor of PROSYN Kravanja and Grossmann [32] and TOP Kravanja et al. [54]. The Modified OA/ER algorithm and the two-phased (continuous and then discrete) optimization were applied, where GAMS/CONOPT2 (the Generalized reduced-gradient method) Drudd [55] was used to solve NLP subproblems and GAMS/Cplex 7.0 (Branch and Bound) [56] was used to solve MILP master problems.

The MINLP optimization model of the steel frame contained 1530 (in)equality constraints, 1195 continuous and 357 binary 0-1 variables (61 after the pre-screening). The final optimal solution of 6214 kg was obtained in the 62^{th} main MINLP iteration (the subsequent feasible results were not as good). 30 minutes of overall working time were spent on a 2,13 GHz M and 2 GB of RAM PC to obtain the optimal result. The outline of the optimal frame structure is shown in Figure 4.

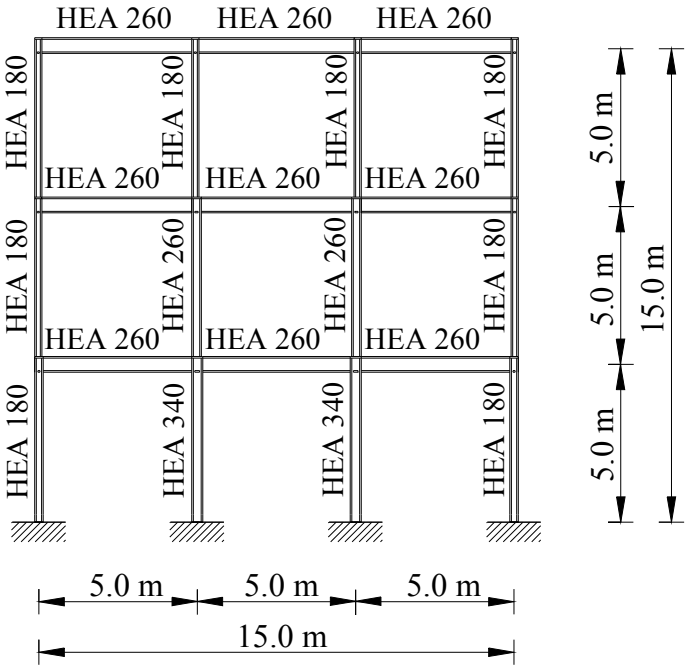

Figure 4. Optimum Design of the Frame

In order to obtain a good starting point for discrete optimization, the optimization of the frame started with the continuous NLP only. All variables and dimensions obtained were the continuous ones. The calculation then proceeded with the discrete optimization of standard sections at the second phase, where 17 different standard section alternatives and thus 17 associated binary 0-1 variables were defined for each structural element separately. In this way, 17×21=357 binary variables were associated with all 21 beams and columns. Since this number of 0-1 variables is high, the pre-screening procedure of alternatives was applied, which automatically reduced the binary variables for standard dimension alternatives into a smaller number. The optimization at the second level included only those 0-1 variables, which determined the standard section alternatives close to the continuous dimensions, obtained at the first NLP. Only 3 binary variables, i.e. 2 variables over and 1 variable under the calculated continuous value, were used for the calculation of each standard section of 19 beams and columns. One variable over and one variable under the continuous value were extra defined for each of two lower inner columns. In this way, only 19×3+2×2=61 binary variables were used at the second level instead of all 357 binary variables, which considerably improved the efficiency of the search.

Alongside the optimal structure mass, the optimal sizes of the standard steel HEA sections of the beams and columns were also obtained. Without the two-phased optimization approach no feasible result was calculated.

6. CONCLUSIONS

The paper presents the Mixed-Integer Non-linear Programming approach (MINLP) to the discrete dimension optimization of unbraced rigid steel plane frames. The optimization is carried out in a single uniform calculating process, where continuous parameters and discrete dimensions are considered simultaneously in order to obtain the minimum mass of a frame structure.

In order to fulfil this task, a frame mechanical structure consisting of various standard dimension cross-section alternatives was generated and the MINLP optimization model FRAMEOPT for steel frames developed. The mass objective function of the frame structure is subjected to a given design, material, resistance, and deflection constraints. The finite element equations (second-order elastic structural analysis) are defined in the set of constraints for the calculation of internal forces and deflections, while the constraints for the dimensioning are determined in accordance with Eurocode 3. The Modified Outer-Approximation/Equality-Relaxation (OA/ER) algorithm is proposed to be used to solve highly combinatorial, non-linear and non-convex optimization problem of frames. The optimization is performed sequentially in two different phases to accelerate the convergence of the Modified OA/ER algorithm and to obtain feasible solutions. In order to achieve a good starting point, the optimization starts with the continuous NLP in the first phase. The MINLP at the re-established discrete dimensions is then performed until the optimal solution is found. Binary variables for standard dimension alternatives are on the basis of the NLP solution pre-screened and reduced into a reasonable number thus enabling a normal solution of the MINLP.

An example of the optimization of a steel frame is presented at the end of the paper in order to interpret the advantages of the proposed MINLP optimization approach. Considering the obtained results, the MINLP was found to be an applicable optimization technique for solving the optimization problems of this type of structures.

REFERENCES

[1] Kuhn, H.W. and Tucker, A.W., “Nonlinear Programming”, Proceedings of the Second Berkeley Symposium on Mathematical Statistics and Probability, Berkeley, 1951, pp. 481–492.

[2] Barnett, R.L., “Minimum Weight of Beams for Deflection”, Journal of Engineering Mechanics Division, 1961, Vol. 87, No. 1, pp. 75–109.

[3] Prager, W. and Shield, R.T., “A General Theory of Optimal Plastic Design”, Journal of Applied Mechanics, 1967, Vol. 34, No. 1, pp. 184–186.

[4] Venkayya, V.B., Khot, N.S. and Berke, L., “Application of Optimality Criteria Approaches to Automated Design of Large Practical Structures”, AGARD Conference Proceedings, Milano, 1973.

[5] Chan, C.M., Grierson, D.E. and Sherbourne, A.N., “Automatic Optimal Design of Tall Steel Building Frameworks”, Journal of Structural Engineering, 1995, Vol. 121, No. 5, pp. 838–847.

[6] Soegiarso, R. and Adeli, H., “Optimum Load and Resistance Factor Design of Steel Space-frame Structures”, Journal of Structural Engineering, 1997, Vol. 123, No. 2, pp. 184–192.

[7] Saka, M.P. and Kameshki, E.S., “Optimum Design of Unbraced Rigid Frames”, Computers and Structures, 1998, Vol. 69, No. 4, pp. 433–442.

[8] Hook, R. and Jeeves, T.A., “Direct Search Solution of Numerical and Statistical Problems”, Journal of the Association of Computing Machinery, 1961, Vol. 8, pp. 212–229.

[9] Holland, J.H., “Adaptation in Natural and Artificial Systems”, University of Michigan Press, 1975.

[10] Kirkpatrick, S., Gelatt, C.D. and Vecchi, M.P., “Optimization by Simulated Annealing”, Science, 1983, Vol. 220, No. 4598, pp. 671–680.

[11] Glover, F., “Heuristic for Integer Programming using Surrogate Constraints”, Decision Sciences, 1977, Vol. 8, pp. 156–166.

[12] Rumelhart, D.E., Hinton, G.E. and Williams, R.J., “Learning Representations by Backpropagating Errors”, Nature, 1986, Vol. 323, pp. 533–536.

[13] Dorigo, M., Maniezzo, V., Colorni, A., "Distributed Optimization by Ant Colonies", Proceedings of the 1st European Conference on Artificial Life, Cambridge, 1991, pp. 134–142.
[14] Camp, C., Pezeshk, S., Cao, G., "Optimized Design of Two-dimensional Structures using a Genetic Algorithm", Journal of Structural Engineering, 1998, Vol. 124, No. 5, pp. 551–559.
[15] Erbatur, F., Hasançebi, O., Tütüncü, İ., Kiliç, H., "Optimal Design of Planar and Space Structures with Genetic Algorithms", Computers and Structures, 2000, Vol. 75, No. 2, pp. 209–224.
[16] Kameshki, E.S. and Saka, M.P., "Genetic Algorithm Based Optimum Design of Nonlinear Planar Steel Frames with Various Semi-rigid Connections", Journal of Constructional Steel Research, 2003, Vol. 59, No. 1, pp. 109–134.
[17] Jármai, K., Snyman, J.A., Farkas, J. and Gondos, G., "Optimal Design of a Welded I-section Frame using Four Conceptually Different Optimization Algorithms", Structural and Multidisciplinary Optimization, 2003, Vol. 25, No. 1, pp. 54–61.
[18] Hayalioglu, M.S. and Degertekin, S.O., "Design of Non-linear Steel Frames for Stress and Displacement Constraints with Semi-rigid Connections via Genetic Optimization", Structural and Multidisciplinary Optimization, 2004, Vol. 27, No. 4, pp. 259–271.
[19] Kim, S.E., Song, W.K. and Ma, S.S., "Optimal Design Using Genetic Algorithm with Nonlinear Elastic Analysis", Structural Engineering and Mechanics, 2004, Vol. 17, No. 5, pp. 707–725.
[20] Kaveh, A. and Abdietehrani, A., "Design of Frames Using Genetic Algorithm, Force Method and Graph Theory", International Journal for Numerical Methods in Engineering, 2004, Vol. 61, No. 14, pp. 2555–2565.
[21] Sarma, K.C. and Adeli, H., "Comparative Study of Optimum Designs of Steel High Rise Building Structures Using Allowable Stress Design and Load and Resistance Factor Codes", Practice Periodical on Structural Design and Construction, 2005, Vol. 10, No. 1, pp. 12–17.
[22] Guerlement, G., Tragowski, R., Gutkowski, W., Zawidzka, J. and Zawidzki, J., "Discrete Minimum Weight Design of Steel Structures using EC3 Code", Structural and Multidisciplinary Optimization, 2001, Vol. 22, No. 4, pp. 322–327.
[23] Uys, P.E., Jármai, K. and Farkas, J., "Optimal Design of a Hoist Structure Frame", Applied Mathematical Modelling, 2003, Vol. 27, No. 12, pp. 963–982.
[24] Jármai, K., Farkas, J. and Kurobane, Y., "Optimum Seismic Design of Multi-storey Steel Frame", Engineering Structures, 2006, Vol. 28, No. 7, pp. 1038–1048.
[25] Krajnc, A. and Beg, D., "Heuristic Approach to Steel Frame Structural Optimisation," Computational Steel Structures Technology, Edinburgh, pp. 155–164, 2000.
[26] Pavlovčič, L., Krajnc, A. and Beg, D., "Cost Function Analysis in the Structural Optimization of Steel Frames", Structural and Multidisciplinary Optimization, 2004, Vol. 28, No. 4, pp. 286–295.
[27] Kravanja, S., Kravanja, Z. and Bedenik, B.S., "The MINLP Optimization Approach to Structural Synthesis. Part I: A General View on Simultaneous Topology and Parameter Optimization", International Journal for Numerical Methods in Engineering, 1998, Vol. 43, No. 2, pp. 263–292.
[28] Kravanja, S., Kravanja, Z. and Bedenik, B.S., "The MINLP Optimization Approach to Structural Synthesis. Part II: Simultaneous Topology, Parameter and Standard Dimension Optimization by the Use of the Linked Two-phase MINLP Strategy", International Journal for Numerical Methods in Engineering, 1998, Vol. 43, No. 2, pp. 293–328.
[29] Kravanja, S., Šilih, S. and Kravanja, Z., "The Multilevel MINLP Optimization Approach to Structural Synthesis: the Simultaneous Topology, Material, Standard and Rounded Dimension Optimization", Advances in Engineering Software, 2005, Vol. 36, No. 9, pp. 568–583.

[30] Kravanja, S., Kravanja, Z. and Bedenik, B.S., "The MINLP Optimization Approach to Structural Synthesis. Part III: Synthesis of Roller and Sliding Hydraulic Steel Gate Structures", International Journal for Numerical Methods in Engineering, 1998, Vol. 43, No. 2, pp. 329–364.

[31] Kravanja, S., »Optimization of the Sultartangi Sliding Gates in Iceland", International Journal on Hydropower & Dams, 2002, Vol. 9, No. 2, pp. 42–45.

[32] Kravanja, Z. and Grossmann, I.E., "New Developments and Capabilities in PROSYN – An Automated Topology and Parameter Process Synthesizer", Computers and Chemical Engineering, 1994, Vol. 18, No. 11/12, pp. 1097–1114.

[33] Chen, W.F. and Lui, E.M., "Structural Stability: Theory and Implementation", Elsevier Science Publishing Co., Inc., 1987.

[34] Eurocode 3, "Design of Steel Structures", European Committee for Standardization, 1992.

[35] Chen, W.F. and Lui, E.M., "Stability Design of Steel Frames", Boca Raton, FL: CRC Press, 1991.

[36] Chen, W.F., Goto, Y. and Liew, R.J.Y., "Stability Design of Semi-Rigid Frames", John Wiley & Sons, Inc., 1996.

[37] Kim, S.E., Lee, J.S., Choi, S.H. and Kim, C.S., "Practical Second-order Inelastic Analysis for Steel Frames Subjected to Distributed Load", Engineering Structures, 2004, Vol. 26, No. 1, pp. 51–61.

[38] Gupta, O.K. and Ravindran, A., "Branch and Bound Experiments in Convex Nonlinear Integer Programming", Management Science, 1985, Vol. 31, No. 12, pp. 1533–1546.

[39] Olsen, G.R. and Vanderplaats, G.N., "Method for Nonlinear Optimization with Discrete Design Variables", AIAA Journal, 1989, Vol. 27, No. 11, pp. 1584–1589.

[40] Bremicker, M., Papalambros, P.Y. and Loh, H.T., "Solution of Mixed-discrete Structural Optimization Problems with a New Sequential Linearization Method", Computers and Structures, 1990, Vol. 37, No. 4, pp. 451–461.

[41] Westerlund, T. and Pettersson, F., "An Extended Cutting Plane Method for Solving Convex MINLP Problems", European Symposium on Computer Aided Process Engineering–5, Supplement to Computers and Chemical Engineering, Bled, S131–S136, 1995.

[42] Benders, J.F., "Partitioning Procedures for Solving Mixed-variables Programming Problems", Numerische Mathematik, 1962, Vol. 4, pp. 238–252.

[43] Geoffrion, A.M., "Generalized Benders Decomposition", Journal of Optimization Theory and Applications, 1972, Vol. 10, No. 4, pp. 237–260.

[44] Duran, M.A. and Grossmann, I.E., "An Outer-approximation Algorithm for a Class of Mixed-integer Nonlinear Programs", Mathematical Programming, 1986, Vol. 36, pp. 307-339.

[45] Mawengkang, H. and Murtagh, B.A., "Solving Nonlinear Integer Programs with Large-scale Optimization Software", Annals of Operations Research, 1986, Vol. 5, No. 1/4, pp. 425–437.

[46] Quesada, I. and Grossmann, I.E., "An LP/NLP Based Branch and Bound Algorithm for Convex MINLP Optimization Problems", Computers and Chemical Engineering, 1992, Vol. 16, No. 10/11, pp. 937–947.

[47] Land, A.H. and Doig, A., "An Automatic Method of Solving Discrete Programming Problems", Econometrica, 1960, Vol. 28, pp. 297–520.

[48] Dakin, J., "A Tree Search Algorithm for Mixed Integer Programming Problems", Computer Journal, 1965, Vol. 8, pp. 250–255.

[49] Kelley, Jr. J.E., "The Cutting-plane Method for Solving Convex Programs", SIAM Journal, 1960, Vol. 8, pp 703–712.

[50] Kocis, G.R. and Grossmann, I.E., "Relaxation Strategy for the Structural Optimization of Process Flow Sheets", Industrial and Engineering Chemistry Research, 1987, Vol. 26, No. 9, pp. 1869–1880.

[51] Murtagh, B.A. and Saunders, M.A., “MINOS User's Guide, Technical Report SOL 83–20”, System Optimization Laboratory, Department of Operations Research, Stanford University, 1985.
[52] Kocis, G.R. and Grossmann, I.E., “A Modelling and Decomposition Strategy for the MINLP Optimization of Process Flowsheets”, Computers and Chemical Engineering, 1989, Vol. 13, No. 7, pp. 797–819.
[53] Brooke, A., Kendrick, D., Meeraus, A. and Ramesh, R., “GAMS–A User's Guide”, GAMS Development Corporation, 1998.
[54] Kravanja, S., Kravanja, Z., Bedenik, B.S. and Faith, S., “Simultaneous Topology and Parameter Optimization of Mechanical Structures”, Proceedings of the First European Conference on Numerical Methods in Engineering, 1992, Brussels, pp. 487–495.
[55] Drudd, A.S., “CONOPT – A Large-scale GRG Code”, ORSA Journal on Computing, 1994, Vol. 6, No. 2, pp. 207–216.
[56] GAMS/CPLEX 7.0 User Notes, ILOG Inc., 2001.